

DOKUZ EYLÜL UNIVERSITY
GRADUATE SCHOOL OF NATURAL AND APPLIED
SCIENCES

INVESTIGATION OF THE HIGH
TEMPERATURE CORROSION BEHAVIOR OF
CERAMIC MATERIALS CONTAINING BORON

by
İlker ÖZKAN

June, 2012
İZMİR

**INVESTIGATION OF THE HIGH
TEMPERATURE CORROSION BEHAVIOR OF
CERAMIC MATERIALS CONTAINING BORON**


**A Thesis Submitted to the
Graduate School of Natural and Applied Sciences of Dokuz Eylül University
In Partial Fulfillment of the Requirements for the Degree of Doctor of
Philosophy in Metallurgical and Materials Engineering, Metallurgical and
Materials Engineering Program**

**by
İlker ÖZKAN**


**June, 2012
İZMİR**

Ph.D. THESIS EXAMINATION RESULT FORM

We have read the thesis entitled “**INVESTIGATION OF THE HIGH TEMPERATURE CORROSION BEHAVIOR OF CERAMIC MATERIALS CONTAINING BORON**” completed by **İLKER ÖZKAN** under supervision of **ASSOC. PROF.DR. ALİ BÜLENT ÖNAY** and we certify that in our opinion it is fully adequate, in scope and in quality, as a thesis for the degree of Doctor of Philosophy.


Assoc. Prof. Dr. Ali Bülent ÖNAY


Supervisor


Prof. Dr. Ali Aydın GÖKTAŞ


Thesis Committee Member


Prof. Dr. Kadir YURDAKOÇ

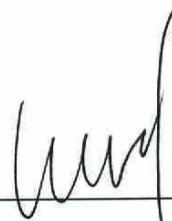
Thesis Committee Member


Prof. Dr. Tayfur ÖZTÜRK

Examining Committee Member


Prof. Dr. Kazım ÖNEL

Examining Committee Member


Prof. Dr. Mustafa SABUNCU
Director
Graduate School of Natural and Applied Sciences

ACKNOWLEDGEMENTS

First and foremost, I would like to thank my advisor Assoc. Prof. Dr. A.Bülent ÖNAY for all his support, patience and guidance.

I would also like to thank my committee members, Prof. Dr. Zeliha YAYLA, Prof. Dr. A.Aydın GÖKTAŞ and also Prof. Dr. İ.Akın ALTUN, for their constructive and valuable comments. I appreciate their time and patience.

I am especially indebted to Esra DOKUMACI for her great self-denying helps. Also I want to thank all the group members at Metallurgical and Materials Engineering Department at Dokuz Eylül University.

I gratefully acknowledge the financial assistance provided by The Scientific and Technological Research Council of Turkey (TUBITAK), under project number 105M362.

Finally, my deepest appreciation goes to my wife Arzu; thank you for all your support, patience, love, and encouragement. This is our accomplishment.

İlker ÖZKAN

INVESTIGATION OF THE HIGH TEMPERATURE CORROSION BEHAVIOR OF CERAMIC MATERIALS CONTAINING BORON

ABSTRACT

In this Thesis work, high temperature oxidation behavior of three boron-containing compounds; titanium diboride, zirconium diboride and boron carbide were studied. Oxidation studies were conducted mostly in air at temperatures between 300 and 1200 Celcius degrees. Additionally, two applications of boron-containing materials were also investigated.

It was observed that solid and protective oxides titanium dioxide and zirconium dioxide formed over titanium diboride and zirconium diboride, respectively, at high temperatures. Weight gains of these two borides changed with changes in both the temperature and the oxidation time. Because boron carbide could not form solid oxidation products, its high temperature oxidation behavior was controlled by the formation and evaporation of boron-containing liquid phase such as boron oxide which was molten at the test temperatures of this study. The presence of a liquid phase was indicated by the agglomeration of the oxidized boride powders and by the weight losses of the boron carbide samples after their long-term oxidaton in both air and water vapor. Formation of the solid, liquid or gasesous oxidation products also affected the kinetic aspects of the boride oxidation.

As an application of boron-containing materials, titanium diboride-based composite production by using the vacuum arc melting method was investigated. Experimental results conducted showed that processing of bulk products by this method will be difficult. However, the process can be applied to modify material surfaces. In the other application, thermochemically formed iron boride layer was observed to decrease the oxidation attack of the steel substrate at 800 Celcius degrees, in air, by forming protective oxidation products containing glassy phases.

Keywords: Borides, high temperature, corrosion

BOR İÇERİKLİ SERAMİK MALZEMELERİN YÜKSEK SICAKLIK KOROZYON DAVRANIŞLARININ İNCELENMESİ

ÖZ

Bu çalışmada, bor içerikli üç bileşiğin (titanyum diborür, zirkonyum diborür ve bor karbür) yüksek sıcaklık oksidasyon davranışları incelenmiştir. Oksidasyon çalışmaları 300 ve 1200 Celcius derece arasındaki sıcaklıklarda çoğunlukla hava ortamında yapılmıştır. Bunlara ek olarak, bor içerikli malzemelerin iki uygulaması da incelenmiştir.

Titanyum diborür ve zirkonyum diborür numunelerinin yüzeylerinde yüksek sıcaklıklarda, titanyum dioksit ve zirkonyum dioksit koruyucu katı oksitlerin oluştuğu gözlenmiştir. Bu iki borürün ağırlık artışları, sıcaklığa ve oksidasyon zamanına göre değişmiştir. Bor karbür katı oksidasyon ürünü oluşturamadığından, bu bileşiğin yüksek sıcaklık oksidasyon davranışı, bu çalışmadaki deney sıcaklıklarında ergiyen sıvı bor oksit fazının oluşumu ve buharlaşması ile kontrol edilmiştir. Oksitlenmiş borür tozlarının topaklaşması ve bor karbür numunelerinin hava su buharı ortamlarında uzun süren oksidasyon deneylerinden sonra ki ağırlık azalmaları, bu sıvı fazın varlığını işaret etmektedir. Oluşan katı, sıvı ve gaz oksidasyon ürünleri de, borürlerin oksidasyonunun kinetiğini etkilemiştir.

Bor içerikli malzemelerin bir uygulaması olarak, vakum ark ergitme metodu kullanarak titanyum diborür bazlı kompozit malzeme üretimi çalışılmıştır. Deneyler, bu metodu kullanarak kütleli ürünlerin üretiminin zor olduğunu göstermiştir. Bununla beraber, bu proses malzeme yüzeylerini iyileştirmek için kullanılabilir. Diğer bir uygulamada, termokimyasal olarak oluşturulan demir borür tabakasının, 800 Celcius derecede camsı fazlar da içeren oksidasyon ürünleri oluşturarak çelik altlığın oksidasyon direncini artırdığı gözlenmiştir.

Anahtar Kelimeler: Borür bileşikleri, yüksek sıcaklık, korozyon.

CONTENTS

	Page
THESIS EXAMINATION RESULT FORM.....	ii
ACKNOWLEDGEMENTS	iii
ABSTRACT	iv
ÖZ	v
CHAPTER ONE - INTRODUCTION	1
1.1 High Temperature Corrosion	1
1.1.1 Kinetics of Oxidation.....	4
1.2.1.1 Linear Kinetics of Oxidation	5
1.2.1.2 Parabolic Kinetics of Oxidation.....	6
1.2.1.3 Logarithmic Kinetics of Oxidation	6
1.1.2 Temperature Dependence of Oxidation	7
1.2. Boron	7
1.3 Applications of Boron	8
1.4 Chemical properties of Boron.....	9
1.5 Properties of the Studied Boron Compounds.....	10
1.5.1 TiB ₂	10
1.5.2 B ₄ C	13
1.5.3 ZrB ₂	16
CHAPTER TWO - EXPERIMENTAL STUDIES	20
2.1 Materials	20
2.2 Method	20
2.2.1 The method of producing pellet samples	20
2.2.2 Oxidation Tests.....	23
2.2.3 Construction of the test furnace with controlled atmosphere.....	23

2.2.4 Corrosion tests	25
2.3 Characterization	25
2.3.1 Particle Size Analysis	25
2.3.2 Specific Surface Area Measurement by Nitrogen Adsorption (BET)....	25
2.3.3 Scanning Electron Microscope (SEM) and Energy Dispersive Spectrometry (EDS) Analyses	27
2.3.4 Differential Thermal Analyses /Thermogravimetric (DTA-TG) Analyses.....	27
2.3.5 X-Ray Diffraction (XRD) Analysis.....	27
CHAPTER THREE - RESULTS AND DISCUSSION.....	29
3.1 Characterization of the Powder Raw Materials	29
3.1.1 Particle Size Analyses Results	29
3.1.2 Specific Surface Area Analyses Results	29
3.1.3 SEM/EDS Analyses Results	30
3.1.3.1 Powder TiB ₂	30
3.1.3.2 Powder ZrB ₂	31
3.1.3.3 Powder B ₄ C	31
3.1.4 XRD Analyses Results	32
3.1.4.1 Powder TiB ₂	32
3.1.4.2 Powder ZrB ₂	32
3.1.4.3 Powder B ₄ C	33
3.1.5 DTA-TG Analyses Results	34
3.1.5.1 Powder TiB ₂	34
3.1.5.2 Powder ZrB ₂	35
3.1.5.3 Powder B ₄ C	35
3.2 Oxidation Test Results for Powder Raw Materials	36
3.2.1 Oxidation Test Results for Powder TiB ₂	36
3.2.2 Oxidation Test Results for Powder ZrB ₂	40
3.2.3 Oxidation Test Results for Powder B ₄ C	42
3.3 Oxidation Test Results for Pellets under Static Air	44

3.3.1 Oxidation Test Results for TiB ₂ pellets	44
3.3.2 Oxidation Test Results for ZrB ₂ pellets.....	51
3.3.3 Oxidation Test Results of the B ₄ C pellets.....	57
3.4 Corrosion Test Results for the Pellets in Water Vapour Environment	59
3.4.1 Mass Changes of the Pellets.....	61
3.4.2 Analyses of the Pellets.....	62
3.5 Kinetic, Thermodynamic and Mechanistic Evaluations of the Oxidation Test Results	65
3.5.1 Thermodynamic Properties of the Boron Compounds and Their Corrosion Products.....	65
3.5.2 Physical Properties of the Corrosion Products.....	66
3.5.3 Kinetic Evaluations of the Oxidation Test Results.....	67
3.6 Applications of Boron Containing Materials.....	77
3.6.1 Production Metal Added TiB ₂ Pellets.....	77
3.6.1.1 Production of the Pellet Samples.....	78
3.6.1.2 Tests conducted on the Samples.....	78
3.6.2 Production and Oxidation of Boron-Containing Ceramic Layers on Metal Substrates	84
3.6.2.1 Boronizing Process	85
3.6.2.2 Formation of Boron Containing Layers	86
3.6.2.3 Test Results	86
CHAPTER FOUR - CONCLUSIONS	92
REFERENCES	94

CHAPTER ONE

INTRODUCTION

1.1 High Temperature Corrosion

Most of the elements and their compounds react chemically when they are exposed to air or other more aggressive gases. They are affected from high temperature exposure because the reaction rate generally increases with temperature. The term high temperature corrosion usually refers to material degradation at temperatures higher than the ambient, when they are exposed to corrosive environments. The most common reactant is oxygen and the oxygen-related reactions are called oxidation. In the oxidation reaction materials react with oxygen to form oxides. In the case of a metal (M) the oxidation reaction may be written as (Moricca, 2009):



When metal is exposed to an oxidizing gas at elevated temperatures, corrosion can occur by direct reaction with the gas. This type of corrosion is referred to as high temperature oxidation or scaling. The oxide layer formed on the surface typically thickens as a result of reaction at scale/gas or metal/scale interface due to cation or anion transport through the scale, which behaves as a solid electrolyte. If continuous nonporous scales are formed, ionic transport through the scale is the rate-controlling process. Determination of the resistance of the material to a specific environment depends on some factors which are the thermodynamic stability, the ionic defect structure, and certain morphological features of the scale formed (Dokumaci, 2006).

An oxidation reaction begins with the adsorption of oxygen on the metal surface. The oxide nucleates at multiple sites that are thermodynamically favorable and grows to form a film. Oxygen and other may also dissolve in the material. The thin oxide layer grows to a thicker scale and forms a protective barrier. If porosity, cavities and

microcracks form, this will modify the oxidation mechanism and may cause the oxide to fail to protect the substrate material. Figure 1.1 shows the various stages and aspects of oxidation in the case of a metal (Kofstad, 1988; Moricca, 2009).

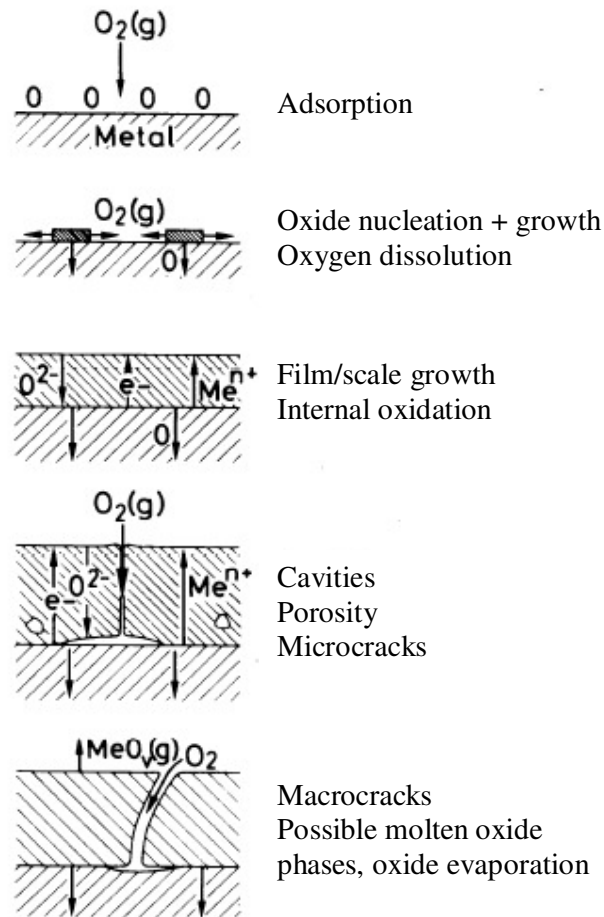


Figure 1.1 Schematic illustration of metal-oxygen reaction (Kofstad, 1988).

Gibbs energy change (ΔG) is the driving force for the oxidation reactions. In high temperature reactions, constant temperature and pressure are the most encountered conditions. Since, ΔG is described as:

$$\Delta G = \Delta H - T\Delta S \quad (1.2)$$

where ΔH is the enthalpy change of reaction, ΔS the entropy change and T the absolute temperature, oxidation reaction will occur spontaneously if $\Delta G < 0$, if $\Delta G = 0$, the system is at equilibrium, and if $\Delta G > 0$ the reaction is thermodynamically unfavorable. The driving force ΔG for the oxidation reaction in Equation 1.1 can be expressed as (Birks & Meier, 1988; Khanna, 2002; Moricca, 2009):

$$\Delta G = \Delta G^o + RT \ln \left[\frac{a_{M_x O_y}}{(a_M)^x (a_{O_2})^{y/2}} \right] \quad (1.3)$$

where “a” shows the activity of each reactant or product, ΔG^o is the standard free energy of formation, and R is the gas constant. In their standard states (pure material), activities of the metal and the oxide are equal to 1. For gases, partial pressure is used as the activity. Therefore, at equilibrium, Equation 1.3 can be written as:

$$\Delta G^o = RT \ln P_{O_2} \quad (1.4)$$

$$P_{O_2}^{equ} = \exp \left[\frac{G}{RT} \right] \quad (1.5)$$

where $P_{O_2}^{equ}$ is the equilibrium partial pressure of oxygen. Thermodynamically the oxide will form only if the oxygen potential in the environment is larger than the oxygen partial pressure in equilibrium with the oxide.

The Ellingham diagram which plots the standard free energies of formation for metal oxides as a function of temperature is shown in Figure 1.2. This diagram can be used to find the equilibrium O_2 partial pressures, directly, at different temperatures. Also, stabilities of oxides can be compared, on this diagram, the lower the position of the line on the diagram, the more thermodynamically stable is the oxide (Moricca, 2009).

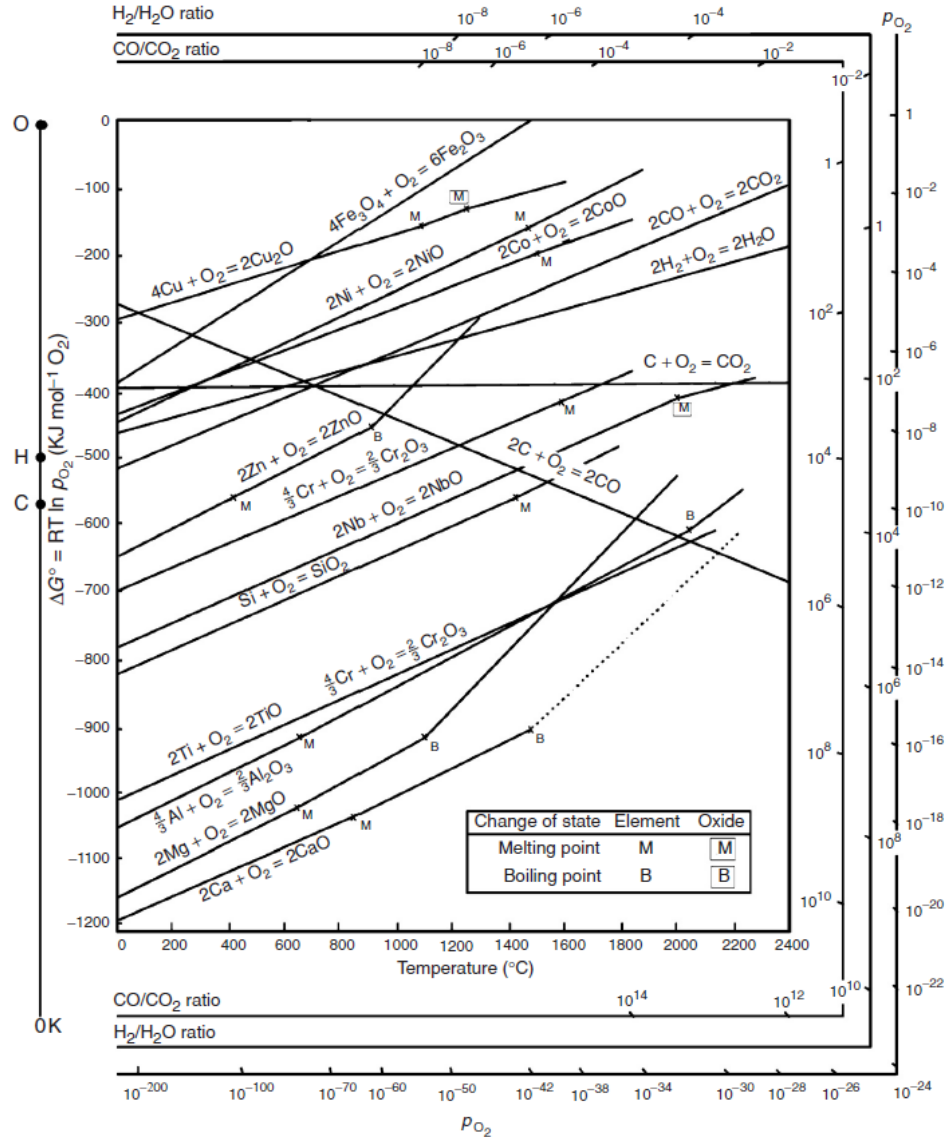


Figure 1.2 Ellingham diagram which shows Standard Gibbs energies of formation of selected oxides as a function of temperature (Birks and Meier, 2006).

1.1.1. Kinetics of oxidation

Besides their Gibbs Free Energies of formation, rates of oxidation reactions are important to understand the nature of these reactions. Based on the rate equations, oxidation reactions can be classified linear, parabolic or logarithmic but some deviations from these reaction rates or combinations are possible. At high

temperatures, combination of linear and parabolic rates can be observed. Since most of the oxidation products stay on the metal surface, the rate of oxidation is usually measured as weight gain per unit area. In Figure 1.3, oxidation rate curves indicating the relationship between weight gain and time are shown. Slopes of these curves determine the oxidation rate (Khanna, 2002).

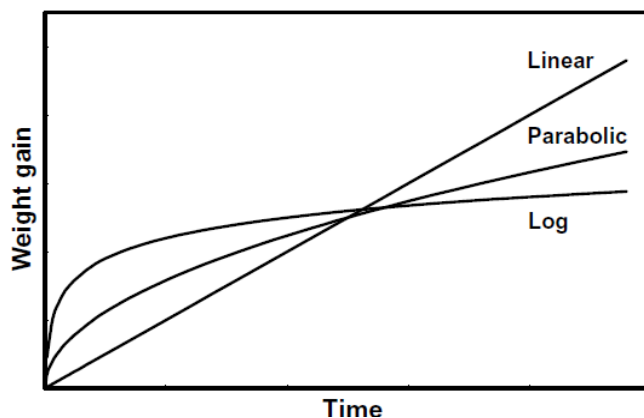


Figure 1.3 Variation of weight gain with time for linear, parabolic and logarithmic oxidation rates.

1.2.1.1. Linear Kinetics of Oxidation

The rate of oxidation remains constant with time and it is independent of the amount of material already consumed in the reaction. The rate of this type of reactions is usually controlled by a surface-reaction step such as dissociation of molecules or by diffusion through the gas phase. The amount of products is directly proportional to the time as suggested by the following equations (Moricca, 2009):

$$\frac{dx}{dt} = k_l \quad (1.6)$$

$$x = k_l t \quad (1.7)$$

where x is the mass or thickness of the product formed, t , the reaction time, and k_l , the linear rate constant. Generally, such products do not provide enough protection

due to processes like oxide cracking or spallation due to internal stresses, porous scales, or the formation of volatile or molten phases (Moricca, 2009).

1.2.1.2. Parabolic Kinetics of Oxidation

At high temperatures, some of the oxidation reactions may follow parabolic kinetics. In this case, the reaction is controlled by the diffusion of ionic species through the product scale. As the scale grows thicker, the diffusion distance increases causing the reaction rate to decrease, thus making the rate inversely proportional to the thickness or the weight of the product formed. This type of kinetics is shown as:

$$\frac{dx}{dt} = \frac{k_p}{x} \quad (1.8)$$

$$x^2 = k_p t \quad (1.9)$$

where k_p is the parabolic rate constant (Khanna, 2002; Moricca, 2009).

1.2.1.3. Logarithmic Kinetics of Oxidation

Reactions obeying this type of kinetics are initially rapid but later slow down to low or negligible rates. Logarithmic oxidation occurs at low temperatures where thin-film type product formation is possible. Although there are different explanations for this type of behavior, most of them involve the transport of either ions or electrons. The logarithmic rate can be expressed by the following equation:

$$x = k_e \log(at + 1) \quad (1.10)$$

where k_e , is the rate constant for logarithmic process and “a” is a constant (Moricca, 2009).

1.2.2. Temperature Dependence of Oxidation

Experimental studies conducted on oxidation reactions have shown that an Arrhenius-type equation (1.11) is valid for the temperature dependence of the reaction rate constants at ambient oxygen pressures.

$$k = k_o \exp(-E_a / RT) \quad (1.11)$$

In Equation 1.11, E_a is the activation energy of the oxidation reaction, R , the gas constant and T , the absolute temperature of the reaction. The rate constant k can be obtained from several isothermal oxidation tests conducted at different temperatures. When the logarithm of k is plotted as a function of $1/T$, the slope of the resulting straight line represents $-Q/R$. Activation energy remains constant as long as the rate determining mechanism does not change. The well-known theory of Wagner for parabolic oxidation stimulates that the rate constant is related to the self diffusion coefficient of the ions in the oxide scale.

1.2 Boron

Boron is a black coloured element and was discovered by Gay-Lussac and Thenard at 1808. Boron percentage is thought to be around between 0.001 and 0.0003, by weight, in the Earth's crust. The borates such as kernite ($\text{Na}_2\text{B}_4\text{O}_7 \cdot 4\text{H}_2\text{O}$), borax ($\text{Na}_2\text{B}_4\text{O}_7 \cdot 10\text{H}_2\text{O}$), colemanite ($\text{Ca}_2\text{B}_6\text{O}_{11} \cdot 5\text{H}_2\text{O}$) and ulexite ($\text{NaCaB}_5\text{O}_9 \cdot 8\text{H}_2\text{O}$) are known as important ores that includes boron element. Amorphous boron was obtained from the electrolysis of boric acid by Davy at 1808. Wöhler and Sainte-Claire Deville determined the crystal form of the boron element at 1856 (Pekin, 1992).

It is hard to give an exact amount on the world's boron reserves but, according to a study the amount of the known reserves and probable reserves are about 170 million tons and 473 million tones, respectively. The main reserves of the boron ores

are in Turkey, Russia and the USA. In Turkey, boron ores are located at Eskişehir-Kırka, Balıkesir-Bigadiç, Bursa-Kestelek and Kütahya-Emet (Roskill, 1999).

1.3 Applications of Boron

Boron is used in many important industrial products and processes in different ways. This includes glass products, ceramic products, cleaning and whitening products, flame-retardant products, pigments, drying products, drugs, metallurgical processes, waste clean-up operations, agricultural operations and nuclear operations (Sekizinci Beş Yıllık Kalkınma Planı, 2001).

For instance, boron compounds are used in metallurgical industry to form a protective layer and as a melting accelerator in non-ferrous metal production. Also it is known that with addition of boron mechanical properties of steels changes. Reduction of the brittleness of some intermetallic compounds was observed with the addition of boron. Boric acid is used in nickel plating, fluoborate and fluoboric acids are used in production of non-ferrous metal such as nickel, tin, lead as an electrolyte.

Boron oxide, which is an important boron compound, is used in traditional ceramic and glass industry to reduce the viscosity and the firing temperature. The enamel coatings on the steel and aluminum prevent the physical and chemical degradation and include 17-32% boron oxide. Boron compounds are also used in the glazes that protect the ceramic materials from the external forces (Sekizinci Beş Yıllık Kalkınma Planı, 2001).

The boron compounds investigated in this thesis have some applications such as abrasives, cutting or friction-reducing products in manufacturing machinery as a refractory material in the metals industry and as a construction material in space transportation vehicles and in energy production systems.

1.4. Chemical Properties of Boron

Boron is placed in III B group of the Periodic Table. The other elements of this group are aluminum, gallium, indium and thallium. Although the other elements exhibit metallic properties, boron has ametallic properties. Table 1.1 lists some important properties of boron (Weast, 1982).

The electronic configuration of the group IIIB elements shows that the most stable oxidation state of these elements is +3. This feature causes the compounds of these elements to have predominantly covalent compounds. On the other hand, IIIB group elements except boron are found as +3 ions in aqueous solution. These ions are present in large amount of water but heat of hydration values of these ions are very high (Pekin, 1992).

Table 1.1 Some characteristic properties of boron

Properties	Values
Density	2.34 g/cm ³
Melting Point	2300°C
Boiling Point	2550°C
Thermal Expansion Coefficient (25-1050°C)	5x10 ⁻⁶ /°C
Hardness (Knoop)	2100-2580
Hardness (Mohs)	9.5
Thermal Conductivity	27.4 W/m.K

Boron has several allotropic forms; one of them is amorphous and six of them have crystalline structures. The most studied crystal structures of boron are the crystal polymorphs of alpha and beta rhombohedral ones. Alpha-rhombohedral structure starts to dissociate over 1200°C and turns into beta-rhombohedral structure at 1500°C. Amorphous structure turns into beta-rhombohedral structure approximately over 1000°C. All types of pure boron turns into beta-rhombohedral

structure after it is heated over its melting point and then recrystallized. The chemical properties of the element changes due to its crystal structure and grain size. While micron-sized amorphous boron can easily and sometimes violently reacts, the crystalline boron does not react easily. At high temperatures boron reacts with water to form boric acid and other products. The reactions of boron with mineral acids can be slow or explosive depending on the concentration and the temperature. Boric acid forms as a major product of such reactions (Sekizinci Beş Yıllık Kalkınma Planı, 2001).

Boron element reacts with several metals to form borides at high temperatures. The geometric arrangements of boron atoms in the crystal structure of the metal borides are different from each other. For example, boron reacts with ammonia or nitrogen at high temperatures and forms boron nitride (BN) compound. This material is isoelectronic with carbon and its structure (hexagonal) is similar to that of graphite. But under high temperature and pressure, this structure of BN turns into the diamond type cubic structure and its hardness increases very much (Pekin, 1992).

1.5 Properties of the Studied Boron Compounds

1.5.1. TiB₂

TiB₂ can be prepared by the carbothermic reduction of mixed oxides of boron and titanium as well as the reduction of titanium oxide by boron carbide and carbon. Reduction of mixed oxides by metals like aluminium, silicon, magnesium, etc. is another preparation method. Also, processes like mechanical alloying and self-propagating high temperature synthesis have also been used for the preparation of this compound (Barin, 1995). Table 1.2 shows some important physical properties of TiB₂.

Hardness of this compound is almost the same as diamond when it is sintered. But it is very hard to sinter TiB₂. Low diffusion rate, rapid grain growth and oxide layer formation on the surface of the grains at high temperatures are the main reasons for

reduced sinterability (Baik& Becher, 1987). The density of the compound can be increased at high temperatures with the help of pressure without any binder. Wang et al. produced high density TiB₂ at 1900°C and under 30 MPa pressure (Wang, 2002). Konigshofer et al. reported that high density TiB₂ can be produced by the hot pressing method at 1800°C and under 45 MPa pressure (Konigshofer et al., 2005).

Table 1.2 Physical properties of TiB₂ (depend on the production method) (Weast, 1982)

Properties	Values
Density	4.50 g/cm ³
Melting Point	2900°C
Thermal Expansion Coefficient	8.1 x 10 ⁻⁶ /°C
Hardness (Knoop)	3400
Hardness (Mohs)	9.5
Electrical Resistance	10-30 mikro-ohm.cm
Thermal Conductivity	26 W/m.K (sample with 15% porosity)

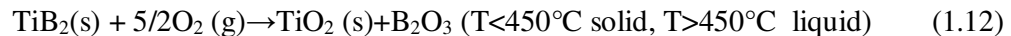
Liquid phase sintering is used to increase the density of TiB₂. Metallic additives such as Ni, Cr and Fe are used for this purpose (Barandika et al., 1998; Subramanian et al., 2006; Kang et al., 1989; Matkovich, 1977). These additives help to sinter the grains but at high temperatures, they cause reduction in the material properties. To increase the sinterability of the material, additives that are in the compound form are used. These include AlN, ZrO₂, SiC, Si₃N₄, CrB₂, B₄C, TaC, TiC, WC, TiN, ZrN, ZrB₂ and MoSi₂ (Li et al., 2002; Matkovich, 1977; Murthy et al., 2006).

TiB₂ can be used to manufacture some electronic materials due to its appropriate electrical and thermal conductivity. In composite materials with polymeric matrix, TiB₂ is used as an additive to increase thermal conductivity. Because of this property, it is possible to form TiB₂ pieces by the Electrical Discharge Machining (EDM) method.

Titanium diboride does not react with some non-ferrous metals such as Cu, Zn and Al thus can be used as an electrode, refractory material and crucible material in the production of these metals. It is also reported that TiB₂ can be used as a control rod at high temperature nuclear reactors. Some research showed that TiB₂ has an acceptable oxidation resistance up to 1000°C.

Besides application-oriented R&D activities, studies on the properties and behavior of this compound are still being done. For example, Murthy et al. recently studied the oxidation of TiB₂ and TiB₂-20 wt.% MoSi₂ composite at 850°C in air. The monolithic TiB₂ exhibited continuous weight gain with increasing time. The TiB₂-MoSi₂ composite showed continuous weight gain up to 16 hours and afterwards the weight gain decreased markedly. The weight loss observed in the composite after 16 hours has been related to the formation and subsequent vaporization of MoO₃ (Murthy et al., 2006).

The oxidation behavior of TiB₂ is an important factor for commercial applications. There are many reports on the oxidation of TiB₂ ceramics, but more-detailed studies are still needed. It is well known that TiB₂ oxidizes to TiO₂ and B₂O₃, according to the following reaction:



Titania is a semiprotective product at high temperatures. Depending on the defect concentration, the growth of TiO₂ is governed by either outward diffusion of interstitial Ti ions or inward diffusion of oxygen ions via vacancies. On the other hand, B₂O₃ has little protectiveness at high temperature, because of its high vapor pressure. During oxidation above 450°C, B₂O₃ is liquid but it solidifies during cooling. There are conflicting reports on the structure of solidified B₂O₃. From the XRD results taken at room temperature for TiB₂, which had been oxidized at 700 and 800°C, Bellosi et al. claimed that B₂O₃ formed was crystalline. They further suggested that B₂O₃ evaporated extensively above 1000°C so that the scale consisted of only highly textured TiO₂ crystals. However, other workers suggested that B₂O₃

formed after oxidation was amorphous, so that it could not be detected by XRD. It may be further noted that most previous workers interpreted oxidation kinetics or the oxidation resistance of TiB₂-base ceramics only from the weight-gain vs. oxidation-time curves. Thickness measurements of the oxide scales formed should be reported for all oxidizing condition to evaluate the actual kinetics of B₂O₃-forming TiB₂ (Lee et al., 2001).

1.5.2 B₄C

Boron carbide (B₄C) is generally produced by the reduction of boron oxide or boric acid with a metal which has affinity for oxygen such as magnesium. Carbothermal or SHS (Self-propagating High temperature Synthesis) methods are used for the production of B₄C. Arc furnaces or resistance furnaces are used for carbothermal processes of an industrial scale. Therefore, energy use in the production of this material is very high. Energy consumption for the production of boron carbide is approximately 1.4 times more than that for the production of aluminum (Kuşoğlu, 2004). Table 1.3 lists some important physical properties of B₄C.

Table 1.3 Physical properties of B₄C (Pierson, 1996), (Töre & Ay, 2002), (Weast, 1982)

Properties	Values
Density	2.52 g/cm ³
Boiling Point	> 3500°C
Melting Point	2350°C
Thermal Expansion Coefficient	4.3 x 10 ⁻⁶ /°C
Hardness (Mohs) (diamond 15)	14
Hardness (Knoop)	2750
Electrical Resistivity	0.1-1.0 mikro ohm.cm
Thermal Conductivity	21 W/m.K

Boron carbide has a low density of 2.52 g/cm³, because it consists of light weight atoms; as boron and carbon. But this density value can increase if it has some heavier

metal impurities such as iron and aluminum. Boron carbide is the third hardest material after diamond and cubic boron nitride (BN). At the hardness test performed under a 200 gr. load, pressureless sintered samples show an average hardness of 25.5 GPa whereas, hot pressed samples have an average hardness value of 29 GPa. Electrical resistance of boron carbide is similar to those of graphite and SiC. Band gap energy of boron carbide is 1 eV so it can be used as a semiconductor material at high temperatures.

B₄C is used as an antioxidant in the refractory industry, a low density additive to metal-matrix composites and a raw material in the production of some boron compounds; TiB₂, SiB₂ and MoB₂. It is also used in the defense industry related products due to its high hardness (Pierson, 1996).

Boron carbide does not react easily with most acids and bases because of its stable chemical structure. But it dissolves slightly in HF-H₂SO₄ and HF-HNO₃ solutions and oxidized by hot and mixed acids such as HNO₃-H₂SO₄-HClO₄. Under ambient air or oxygen gas pressures reaction layers that contain B₂O₃, HBO₃ or H₃BO₃ form on the surface of especially small grain sized B₄C powder. Oxidation starts at 450^oC in dry conditions and at 250^oC in water vapor containing conditions. This shows the importance of water vapor for its oxidation. B₄C reacts with metals such as Fe, Ti, Zr, Ni, Al, Si and forms borides or carbides of these metals at temperatures higher than 1000^oC (Kuşoğlu, 2004).

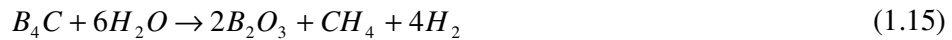
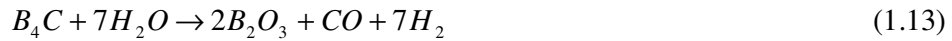
Besides high hardness and high melting point, boron carbide has high strength/density ratio which makes it useful in different applications. Mechanical properties of boron carbide vary depending on the production conditions. For example, hot pressed samples have 300-500 MPa bending strength. Samples that are exposed to HIP process after sintering have 150-350 MPa bending strength. This shows the effects of temperature and testing time on mechanical properties of the material.

Thevenot (1990) reported that the strength of the material did not significantly change under nitrogen gas at temperatures up to 1500°C. But under ambient air conditions decrease in the bending strength of the material was observed between 600-1000°C. The author also noted that oxidation of the material caused a decrease in its bending strength.

Several investigations on the oxidation behaviour of boron carbide ceramic and powder have been reported. Efimenko et al. reported that oxidation of hot-pressed B₄C in air at 1200 K was near-parabolic with an activation energy of 108 kJ mol⁻¹. The oxidation rate increased with temperature and was limited by the diffusion of B and C from the bulk to the surface. Gogotsi and Lavrenko et al. found that oxidation of sintered and hot-pressed boron carbide started at about 550°C in oxygen atmosphere and resulted in the formation of a thin transparent B₂O₃ film that was cracked after cooling. At ≤1200°C, the oxidation process is limited by the diffusion of reagents (O, B and C) through the oxide layer. But, at higher temperatures (>1200°C) the evaporation rate of B₂O₃ exceeds the oxidation rate of B₄C and determines the rate of chemical reaction of carbide with oxygen in air. Sato et al. working on the oxidation of boron carbide ceramics by water vapour at high temperatures, arrived at the conclusion that the oxidation of hot pressed B₄C by water vapour and dry air above 900°C resulted in weight loss, and the formation of BO or HBO₂ seemed to be the main reaction. Oxidation rate of B₄C by water vapour can be expressed by the surface chemical reaction controlled kinetics with the apparent activation energy of 200 kJ mol⁻¹. Unlike the monolithic ceramics, the powdered sample having a higher surface area exhibits a high rate of oxidation. Litz and Mercuri studied the oxidation of boron carbide powder by dry air and/or wet air at elevated temperatures. Their investigation demonstrated that the initial oxidation temperature for water vapour was lower than that for dry air. In low temperature ranges, B₄C was oxidized more rapidly with water vapour than with dry air. At higher temperatures (≥700°C), the oxidation rate with dry air exceeded that with water vapour–air mixtures. The presence of B₂O₃ on the B₄C surface was found to inhibit oxidation by water but not by air. Linear oxidation kinetics in dry air and non-linear oxidation kinetics in water vapour were observed. The activation energy was

found to be 11 and 45 kCal mol⁻¹ for the case of oxidation in water and in air, respectively. Matje and Schwetz investigated the oxidation of submicron B₄C powders at room temperature and found that the fine B₄C powders were slowly oxidized in wet air. The oxidation film formed at the surface contained species like B₂O₃, HBO₂ or H₃BO₃ (Li & Qiu, 2007).

Oxidation of B₄C by steam is highly exothermic forming gaseous carbon and boron containing species. For instance, methane release is of considerable interest because of its potential to produce volatile organic iodine compounds. The following chemical reactions play a role during oxidation of boron carbide:



Excess steam then reacts with liquid boron oxide to form volatile boric acids:



Additionally, boron oxide directly evaporates at high temperatures above 1770 K (Steinbrück, 2005; Steinbrück et al., 2007).

1.5.3 ZrB₂

Ceramic compounds such as ZrB₂ belong to a group of materials known as ultra high temperature ceramics (UHTCs). Interest in UHTCs has increased substantially in recent years due to growing interest in hypersonic vehicles and re-usable atmospheric re-entry vehicles. For these vehicles, materials that are resistant to oxidation at 1500°C and above are needed for a variety of components such as nose cones, wing leading edges and engine cowls. Currently, UHTCs are among the

candidates for these applications as well as other applications that require stability in extreme environments (Rezaie, 2007).

Traditionally, ZrB_2 powder was synthesized by various high temperature methods, such as the carbothermal reduction of ZrO_2 and B_4C ($1400^\circ C$) and the mechano-chemical treatment of a mixture of zirconia powder and amorphous boron followed by a relatively low temperature annealing ($1100^\circ C$). In addition, other methods have been developed to prepare zirconium diboride. Berthon et al. synthesized ZrB_2 by CVD from a mixture of $ZrCl_4$, BCl_3 and H_2 . Devyatkin investigated electrosynthesis from cryolite-alumina melts containing zirconium and boron oxides. Reich et al. prepared zirconium boride by plasma enhanced chemical vapor deposition and Andrievskii et al. obtained amorphous powder of $ZrB_{2.76}$ with mean particle size 40 nm by thermolysis of $Zr(BH_4)_4$ at $573\text{--}623^\circ C$ (Chen et al., 2004).

Table 1.4 Physical properties of ZrB_2 (Weast, 1982).

Properties	Values
Density (theoretical)	6.09 g/cm^3
Melting Point	$3040^\circ C$
Hardness (Mohs)	8-9
Hardness (Knoop)	1550
Electrical resistivity	9.2 mikro ohm.cm
Thermal Conductivity	23 W/m.K

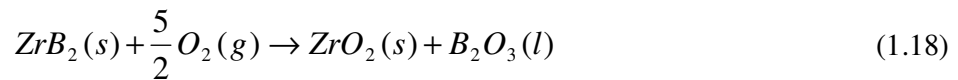
Zirconium diboride (ZrB_2) is a material of particular interest because of the excellent and unique combination of high melting point, high electrical and thermal conductivity, chemical inertness against molten metals or non basic slags, and high thermal shock resistance (Table 1.4). These properties make it an attractive candidate for high temperature applications where corrosion-wear-oxidation resistance is demanded. For the most severe applications, unsatisfactory values of strength and toughness of ZrB_2 are still obstacles to a wider range of use. In order to improve its performance, control of the processing parameters and of the final microstructure are mandatory because residual porosity and microstructural features such as grain size,

chemistry and distribution of the secondary phases are key factors determining the functional properties of ZrB₂-based ceramics (Monteverde et al., 2003; Muolo et al., 2003).

Generally, pressure assisted sintering techniques at temperatures higher than 1850°C are required to achieve complete densification of pure ZrB₂ material. Recently, the use of a ceramic-like additive (i.e. silicon nitride) notably improved both sinterability and strength of ZrB₂ and TiB₂ ceramics. Another strategy to enhance the properties of monolithic ZrB₂ is the addition of second phase(s) with strengthening/toughening capabilities (Monteverde et al., 2003).

Exposure of ZrB₂(s) to air results in the stoichiometric oxidation to ZrO₂(s) and B₂O₃(l) by reaction (1.18). Below about 1100°C, the B₂O₃ (l) forms a continuous layer. In this temperature regime, parabolic (diffusion controlled) kinetics are observed with reported activation energies in the range of 80– 120 kJ/mole, which are consistent with reported values for oxygen diffusion in B₂O₃(l). Based on the activation energy and the dependence of oxidation rate on the partial pressure of oxygen (P_{O₂}), the rate of oxidation below 1100°C appears to be controlled by the transport of oxygen through B₂O₃(l).

The ZrO₂ appears to form a porous skeleton that does not enhance the oxidation protection, but may provide mechanical integrity to the liquid B₂O₃ scale.



Above 1100°C, the oxidation rate increases compared with what would be predicted from the diffusion-controlled (parabolic) behavior observed at lower temperatures. Between 1100°C and 1400°C, so-called para-linear kinetics are observed in which the overall rate of mass change is a combination of weight gain due to formation of B₂O₃(l) and ZrO₂(s) and weight loss due to volatilization of B₂O₃(l). Above 1400°C, the rate of evaporation of B₂O₃(l) is greater than its rate of

production, leaving a non-protective porous $\text{ZrO}_2(\text{s})$ scale. At these temperatures, $\text{ZrB}_2(\text{s})$ oxidation in air exhibits rapid linear kinetics. Despite the evaporation of B_2O_3 , oxidation of $\text{ZrB}_2(\text{s})$ above 1100°C results in mass gain as the mass of ZrO_2 formed is greater than the mass of ZrB_2 consumed (Fahrenholt, 2007).

Recently, SiC addition to ZrB_2 is one of the most interested research areas to improve the oxidation resistance of ZrB_2 . In an earlier study the oxidation mechanism and resistance to oxidation of ZrB_2 -SiC composites were investigated. The temperature limit for ZrB_2 -SiC composites is strongly dependent on the vapor pressure of the gaseous products and volume content of ZrB_2 (Hu et al., 2009). Another study was focused on the effect of SiC content on the oxidation behavior of ZrB_2 -SiC composites. According to this study, ZrB_2 -SiC composites with 20 and 30 vol% SiC oxidized at 1550°C show oxide scale features similar to those formed on an oxidized ZrB_2 -15 vol% SiC composite. Oxide scale density decreases with increased oxidation time and SiC concentration in ZrB_2 -SiC composites. The effect of SiC concentration on oxide scale density can be correlated to the liquid and solid-phase assemblage where composites with more SiC have a larger $\text{SiO}_2/\text{B}_2\text{O}_3$ ratio, which dissolves less ZrO_2 , and thus results in a smaller scale density (Karlsdottir & Halloran, 2009). Han et al. reported that ZrB_2 -20 vol%SiC composites exhibited excellent oxidation resistance at 2200°C (Han et al., 2008). Also other researchers investigated oxidation resistance of ZrB_2 with TaB_2 , TaSi_2 , Ta_5Si_3 , Si_3N_4 , MoSi_2 additives (Talmy et al., 2008; Guo et al., 2011; Peng & Speyer, 2008).

Purpose of this study is to investigate high temperature oxidation behavior of three boron-containing compounds; titanium diboride, zirconium diboride and boron carbide. Oxidation studies were conducted mostly in air at temperatures between 300 and 1200°C . Additionally, two applications of boron-containing materials were also investigated.

CHAPTER TWO

EXPERIMENTAL STUDIES

2.1 Materials

In this thesis TiB_2 , ZrB_2 and B_4C powders were used. TiB_2 , ZrB_2 and B_4C were commercially obtained from Alfa Aesar. According to the information received from this company, B_4C powder has particle sizes between 22 - 59 μm and ZrB_2 and TiB_2 powder was said to have -325 mesh (approximately lower than 44 μm) size.

2.2 Method

2.2.1 The method of producing pellet samples

In the tests, besides powders of compound, circular pellet samples prepared from the powders were also used. Due to the high cost of boron containing ceramic materials and in order to ensure large enough surface area to interact with the corrosive environment, it is thought that pellets should have a diameter of 10 to 20 mm and a thickness of 1 to 4 mm. Table 2.1 and Table 2.2 show the theoretical weight of a circular pellet of a given diameter (10 mm) and varying thickness based on the density values reported in the literature.

Table 2.1 Calculated weights of the pellets with 1 - 4 mm thickness and 10 mm diameter.

	t=0.1 cm	t=0.2 cm	t=0.3 cm	t=0.4 cm
B_4C	0.197 g	0.395 g	0.593 g	0.791 g
TiB_2	0.353 g	0.706 g	1.059 g	1.413 g
ZrB_2	0.478 g	0.956 g	1.434 g	1.912 g

Table 2.2 Calculated weights of the pellets with 1 - 4 mm thickness and 20 mm diameter

	t=0.1 cm	t=0.2 cm	t=0.3 cm	t=0.4 cm
B_4C	0.791 g	1.582 g	2.373 g	3.165 g
TiB_2	1.413 g	2.826 g	4.239 g	5.652 g
ZrB_2	1.912 g	3.824 g	5.736 g	7.649 g

A 20 mm diameter mold is used to prepare the samples as pellets (Figure 2.1). Mold is manufactured from stainless steel and has four pieces (Figure 2.1a). The cylindrical powder holder is placed on the base part, powder is put inside and the punch is used to close the holder (Figure 2.1b). During the forming process, pressure is applied to the punch in two stages. At first, low pressure is applied to remove the air remaining between the powders for better compaction. Then, pressure is applied to form the pellet. After shaping, the base is removed and punch is used to push the pellet out of the mold (Figure 2.1c).

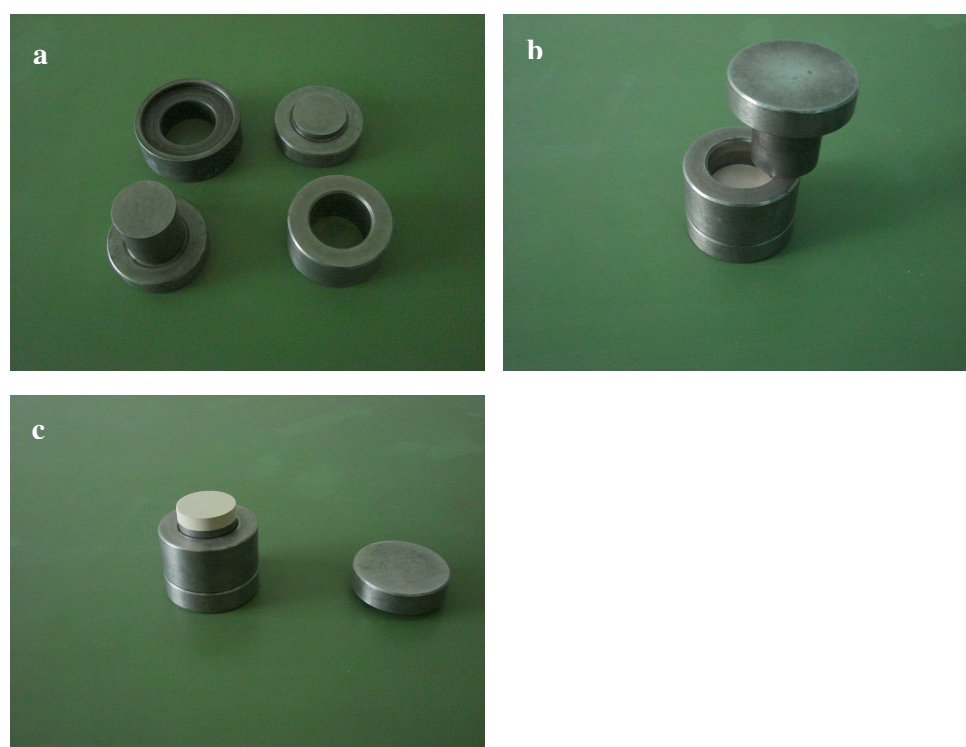


Figure 2.1 Parts used for producing pellet samples.

Small amount of water was added to the powders to increase their plasticity. It was observed that TiB_2 and ZrB_2 pellets could be shaped by this method. In the case of B_4C powder, carboxymethyl cellulose (CMC) was added as an aqueous solution to the powder improve their plasticity and mechanical strength of the pellets. It was observed that, after drying at 110°C , pellets became harder and therefore were suitable to use for the corrosion tests.

To be able to measure properly, weight changes of the pellets after the corrosion tests, it was necessary to drill a hole through the pellets. For this reason, tests were conducted to find out the minimum CMC amount in the aqueous solution to shape pellets with enough plasticity for drilling holes. Best results were obtained for the 4% CMC (by weight) solution.

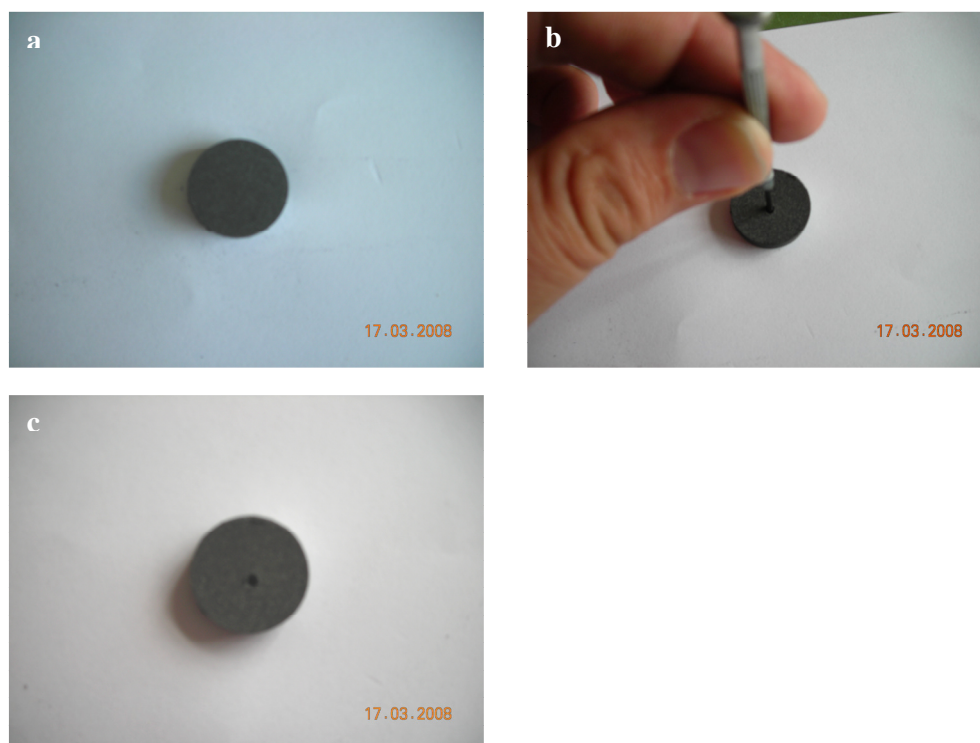


Figure 2.2 (a)-(c) Preparing the pellet for the oxidation tests

After preparing and drying at 110°C some weight loss was observed for the pellets as shown in Table 2.3. It was reasonable to think that evaporation of the water also caused a small decrease in pellet weight. The amount of weight loss seemed to depend on the nature of the powder. These observations can be related to the fact that the studied boride compound has different chemical and physical properties.

Table 2.3 Weight changes measured for boride pellets

	TiB ₂	ZrB ₂	B ₄ C
Green weight (g)	2.94	2.70	2.32
Dried weight (g)	2.70	2.40	2.03
Weight change (%)	8.16	11.11	12.50

2.2.2 Oxidation Tests

Oxidation tests were performed by using both powders and pellets. The ambient air environment was used as the oxidizing agent in the tests conducted between the temperatures 300°C and 1000°C for TiB₂, 550 and 1000°C for ZrB₂, 300 and 800°C for B₄C powders. Powder samples were oxidized in alumina boats. In these oxidation tests a high temperature furnace (HERAEUS- Baseloader BL 1801) and a box furnace were used.

In the first group of experiments a single pellet sample from each compound was placed on a ceramic plate. The plate was placed inside a furnace for oxidation tests at 1000°C for 1 hour in air. Then new samples were prepared by the same way and exposed to oxidation test at 1000°C for 2 hours under ambient air condition. Addition to these tests, oxidation tests were done for TiB₂ pellets at 300°C for 4 hours and at 500°C for 5 hours.

In the second group of tests, pellet samples were suspended inside a quartz crucible. These tests were performed for all boron containing compounds at 800°C for 1, 3, 5 and 10 hours and at 1000°C for 5, 10, 15 and 20 hours in air. Also for TiB₂ and ZrB₂ pellets similar oxidation tests were done at 1200°C for 5, 10, 15 and 20 hours.

Before and after each oxidation test, sample mass changes and dimensions of the samples were measured and mass change-time graphics were drawn.

2.2.3 Construction of the test furnace with controlled atmosphere

This system consists of three parts. In the first part, test gases are supplied from the gas tanks by using pressure regulators. To remove any moisture in the gas, cleaning tubes containing silica gel are used. After cleaning, the gas is sent to a flowmeter. If desired, mixed gases can also be prepared and sent to the furnace. For this purpose, a mixing tube is placed just before the furnace tube entrance.

In the second part, a 3-way flask is placed inside a beaker which is put on a heater. The flask is filled with the desired test fluid (distilled water). The beaker is filled with water and covered with glass wool in order to prevent heat loss from the water inside. Argon gas or air is used as a carrier gas for the vapor of the liquid inside the flask. Glass beads were put inside the flask to prevent moving of the flask and also to provide large surface area for the vapor and the carrier gas to mix with each other.

In the third part of the system, there is a furnace containing a reaction tube made of quartz. At both ends of the reaction tube, multi-way lids were used for gas inlet, gas outlet and a thermocouple. This system is shown schematically in Figure 2.3.

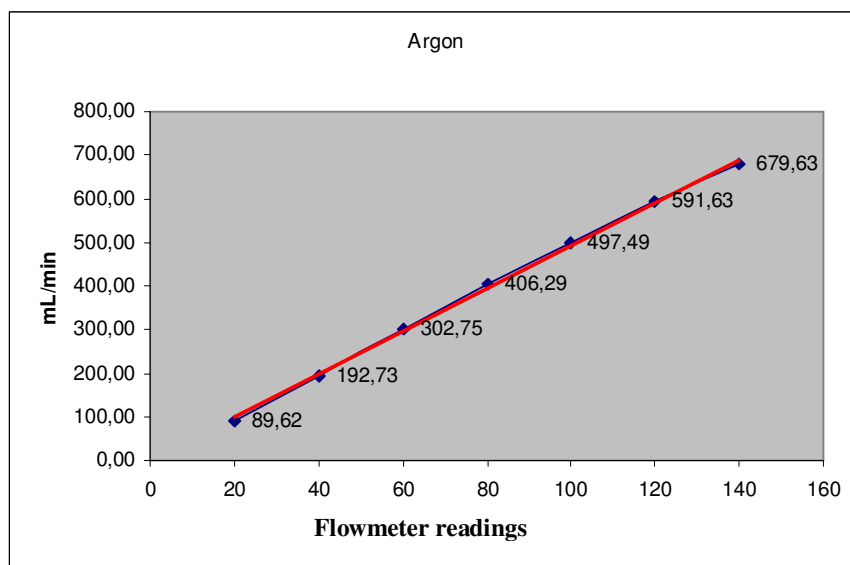


Figure 2.4 Calibration graph for the flow rate of Ar gas.

In Figure 2.3 “1” indicates the path for the dry carrier gas (Ar) whereas “2” indicates the path for the wet gas that has passed through the liquid in the flask and then sent to the furnace. Before the use of this setup, calibration of the flowmeters is done for Ar and N₂ gases. The measured flow rate of Ar gas and the corresponding flowmeter readings are shown in Figure 2.4. During the corrosion tests, mostly the flowmeter reading of 40 (corresponding to 192,43 mL/min Ar gas flow) was used. The water heater was set so that water in the beaker was not more than 50°C. To

check this condition, temperature of the water in the beaker was checked every 15 minutes with a thermocouple.

2.2.4 Corrosion tests

Corrosion tests of the pellets under water vapor containing atmosphere were carried out in the test setup shown in Figure 2.3. These tests were performed at 1000°C for 4 hours.

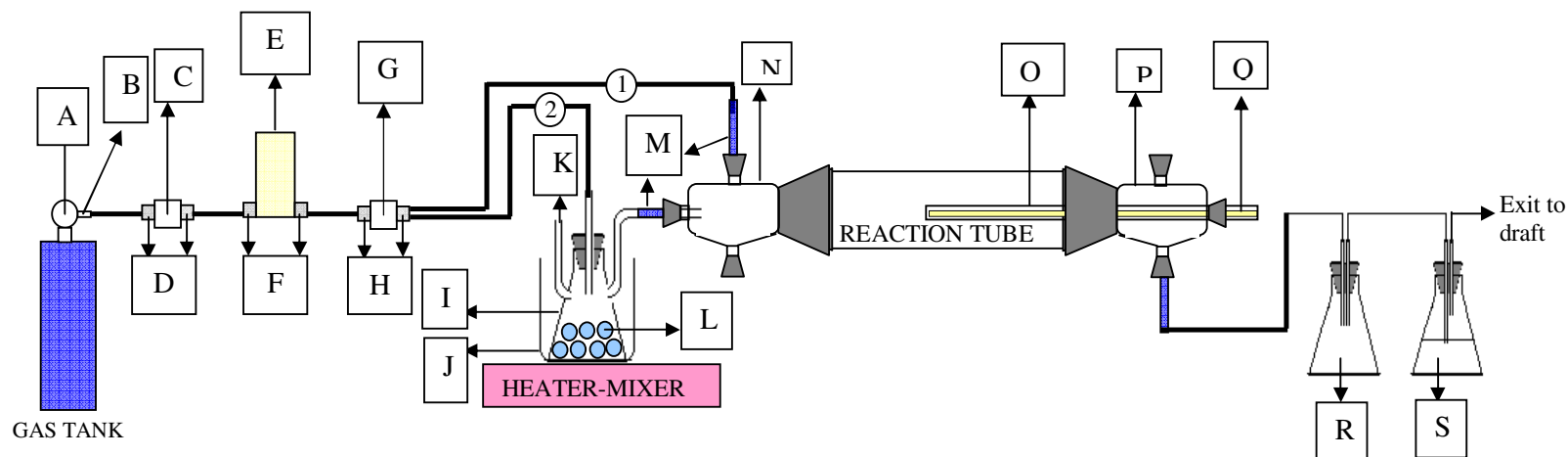
2.3 Characterization

2.3.1 Particle Size Analyses

Particle size distribution of the powder samples used in this work was determined with a Malvern Mastersizer 2000 Model Particle Size Analyzer available in the Department of Environmental Engineering at Dokuz Eylül University.

2.3.2 Specific Surface Area Measurement by Nitrogen Adsorption (BET)

The specific surface area of the powder samples were measured by using a QUANTOCHROME Nova 2200e Model Surface Area Analyzer. Analyses were performed by using nitrogen gas and carried out after degassing for 24 hours. Measurements were taken from 11 points. The specific surface area values of the powder samples were identified by the software of the analyzer.



- A: Regulator
- B: Connection parts between regulator and plastic pipe
- C: Valve
- D: Connection parts between valve and plastic pipe
- E: Flowmeter
- F: Connection parts of flowmeter
- G: Valve
- H: Connection parts between valve and plastic pipe
- I: 3-way glass flask

- J: Glass beaker
- K: Connection to acid solution
- L: Glass bead
- M: Connection parts between plastic pipe and quartz tube head
- N: Quartz tube gas entrance side
- O: Quartz tube thermocouple
- P: Quartz tube gas exit side
- Q: Pt-%13Rh Thermocouple
- R,S: Exit gas washing units

Figure 2.3 Schematic representation of the atmosphere controlled testing setup designed and used in this work

2.3.3 Scanning Electron Microscope (SEM) and Energy Dispersive Spectrometry (EDS) Analyses

Surface morphologies and microstructures of the powder samples and pellets were investigated by JEOL-JSM 6060 Scanning Electron Microscope (SEM) in the Metallurgical and Materials Engineering Department's Materials Characterization Laboratory.

EDS is an analytical technique used for the elemental analysis or chemical characterization of a sample. The technique is based on collection and evaluation of the characteristic X-ray energies emitted from the sample. Atoms in the material emit characteristic X-rays when they are ionized by high energy electrons. These X-rays are converted into electronic signals by a Si(Li) crystal in the EDS detector. The detector is attached and controlled by the SEM and cooled with liquid nitrogen.

In this work, chemical analyses of the solid oxidation products were done by the EDS technique.

2.3.4 Differential Thermal Analyses / Thermogravimetric (DTA-TG) Analyses

In order to observe the effect of temperature on their weight and/or structural changes, powder samples of the boron compounds were analyzed by a DTA-TG (SHIMADZU DTG-60H) equipment available in the Metallurgical and Materials Engineering Department. By this technique, processes such as evaporation of adsorbed water, volatilization of organic/inorganic phases and exothermic or endothermic reactions indicating phase changes can be investigated

2.3.5 X-Ray Diffraction (XRD) Analysis

X-ray diffractometer is used to determine the crystalline phases present in materials. Each crystalline material, when exposed to X-ray radiation, diffracts X-

rays to develop a unique X-ray diffraction pattern. The crystal structure of the sample is determined by comparing this pattern with those in the database of the equipment.

In this thesis work, XRD analyses were done to determine mainly the oxidation products formed on the powder and pellet samples. For this purpose, the XRD (Rigaku, D/Max-2200/PC) equipment available in the Materials Characterization Laboratory of the Metallurgical and Materials Engineering Department was used.

CHAPTER THREE

RESULTS AND DISCUSSION

3.1 Characterization of the Powder Raw Materials

3.1.1 Particle Size Analyses Results

Table 3.1 shows the particle size analyses results for the powder samples used in this study. According to d (50) values, the particle size values measured for the B₄C powder agreed well with values (22-59 μm) obtained from the supplier. As for the ZrB₂ and TiB₂ powders, analyses results were in agreement with the supplier data of -325 mesh (< 44 μm) average size for these powders. However, the experimental d(50) value of the TiB₂ powder was smaller than that of the ZrB₂ powder.

In the experimentally obtained particle size distribution graphs of the TiB₂ and ZrB₂ powders, less strong “secondary” distribution peaks were observed at higher particle sizes. It is thought that presence of such peaks was due to the agglomeration of powder grains. A “secondary” distribution peak was not observed for the B₄C powder. As the SEM pictures below showed clearly, d(50) values determined for these powders were consistent. While the ZrB₂ powder is made of grains with different sizes, B₄C powder grains almost have similar sizes.

Table 3.1 Results of the particle size analyses conducted for the boride powders.

Properties of powders	TiB ₂	ZrB ₂	B ₄ C
d(90) μm	20.839	57.983	76.994
d(50) μm	5.882	19.971	49.289
d(10) μm	2.278	5.975	31.101

3.1.2 Specific Surface Area Analyses Results

Table 3.2 shows the specific surface area values of the powder samples used in this study. Comparison between the results obtained from the BET analyses and the

particle size analyses showed that specific surface area values increased in the order $B_4C < ZrB_2 < TiB_2$.

Table 3.2 Specific surface area values obtained for the boride powder samples (m^2/g)

Specific surface area values (m^2/g)	TiB_2	ZrB_2	B_4C
Based on BET analysis	1.40	0.50	0.18
Based on particle size analysis	1.10	0.46	0.13

3.1.3 SEM Images and EDS Analyses Results

3.1.3.1 TiB_2 Powder

Two groups of samples were taken from the powder. One of them was examined in the as-received (loose powder) condition, whereas the other group was examined after embedded in a polyester holder. Scanning Electron Microscope (SEM) pictures in Figures 3.1 and 3.2 show the morphologies of the TiB_2 powder. Both rounded and sharp edged grains were present in the powder.

Elemental analysis of the powder was performed by EDS. As expected, Ti and B elements were detected in the samples (Figure 3.3). The unmarked peaks in the graph belong to the Au-Pd coating used to increase surface conductivity of the powder.

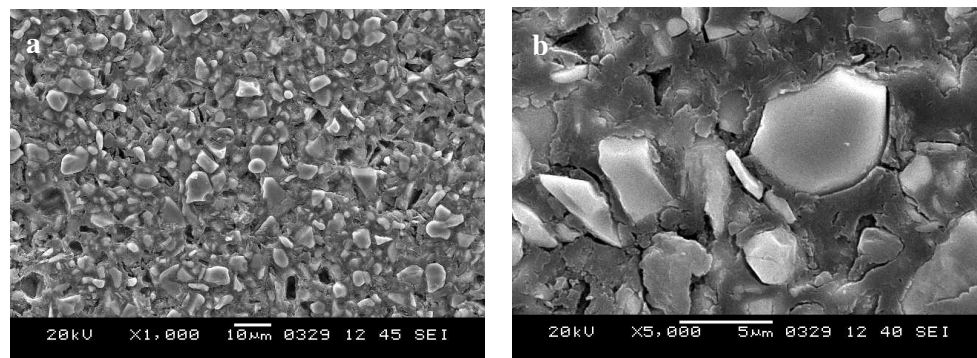


Figure 3.1 SEM images of the TiB_2 powder in the polyester holder.

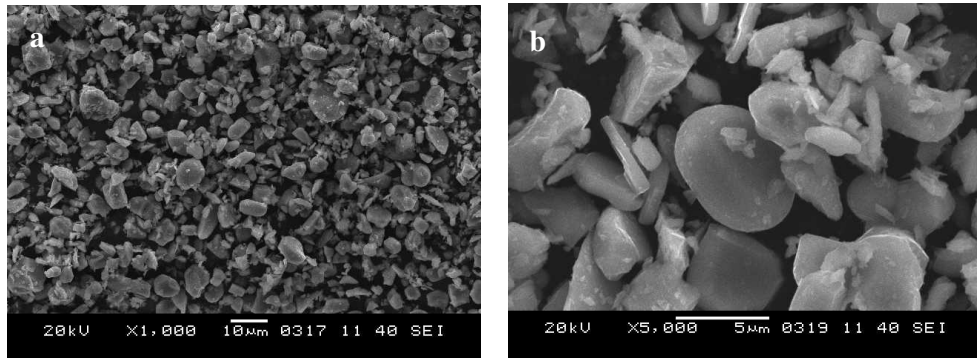


Figure 3.2 SEM images of the as received TiB_2 powder.

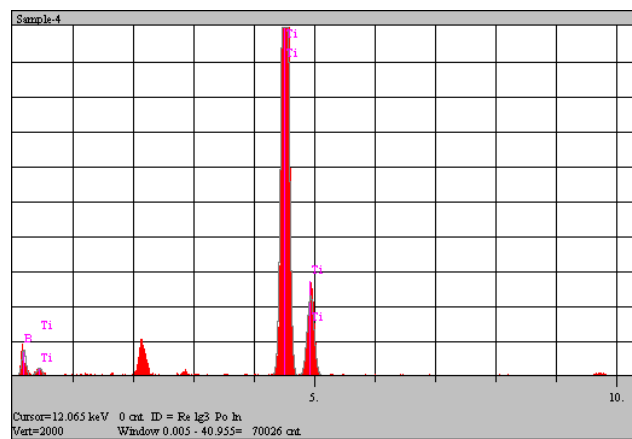


Figure 3.3 EDS analysis result of TiB_2 powder.

3.1.3.2 ZrB_2 Powder

SEM images of the “as received” ZrB_2 powder are given Figure 3.4. According to these images, ZrB_2 powder is consisted of grains with various sizes. Some grains are larger and have sharp edges. Smaller grains are seen as agglomerated to form larger particles.

3.1.3.3 B_4C Powder

Figure 3.5 shows the SEM images of the as-received B_4C powder sample. The grains appear to have similar sizes. Also almost all the grains are observed to have sharp edges.

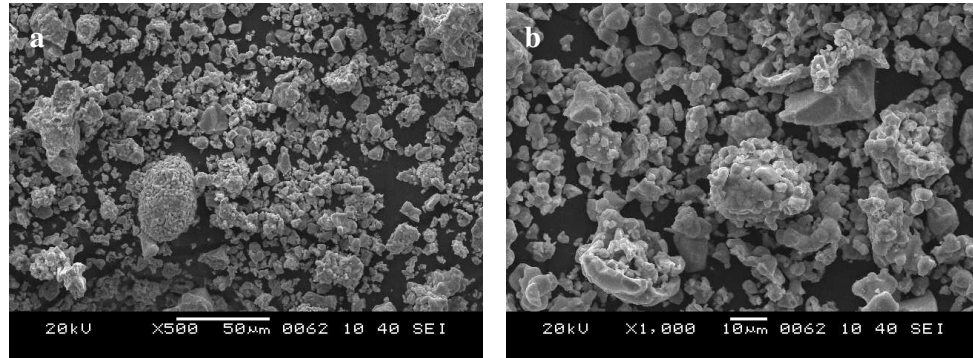


Figure 3.4 SEM images of as received ZrB_2 powder.

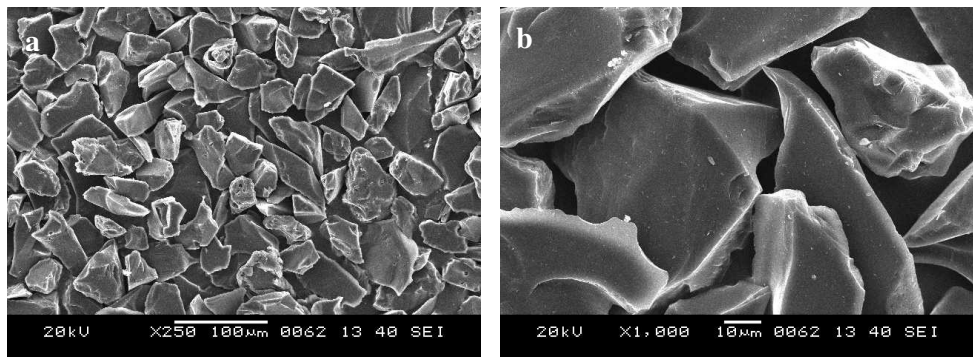


Figure 3.5 SEM images of as received B_4C powder.

3.1.4 XRD Analyses Results

3.1.4.1 TiB_2 Powder

XRD analysis result for the TiB_2 powder is shown in Figure 3.6. All the reference peaks reported in the literature for the TiB_2 compound are observed to match the peaks presented by the as-received powder.

3.1.4.2 ZrB_2 Powder

XRD analysis of the as-received powder showed that the observed peaks matched those of the zirconium diboride phase whose ICDD catalogue number is 034-0423 (Figure 3.7).

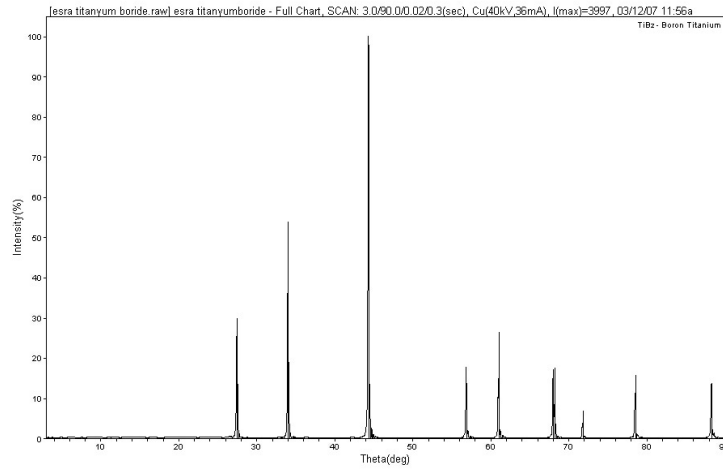


Figure 3.6 XRD analysis result for the as-received TiB_2 powder.

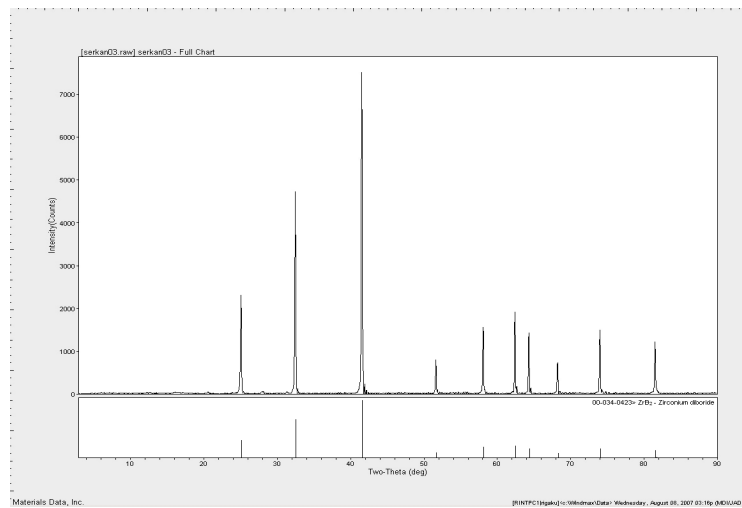


Figure 3.7 XRD analysis result for the as-received ZrB_2 powder

3.1.4.3 B_4C Powder

XRD analysis of the B_4C powder can be seen in Figure 3.8. XRD data matched well to that of the boron carbide phase registered as 035-07983 in the ICDD database.

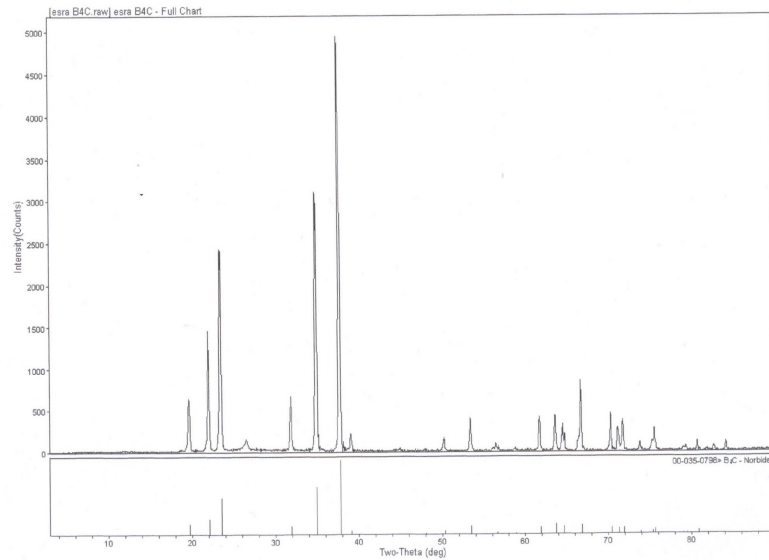


Figure 3.8 XRD analysis result for the as received B₄C powder.

3.1.5 DTA-TG Analyses Results

3.1.5.1 TiB₂ Powder

DTA-TG analysis was done in order to observe the thermal behavior of the compound (Figure 3.9). Small exothermic peaks were observed approximately at 438^oC with the increase in weight. Increase in weight continued until the end of the measurement and the total weight gain was observed to be 4.44%.

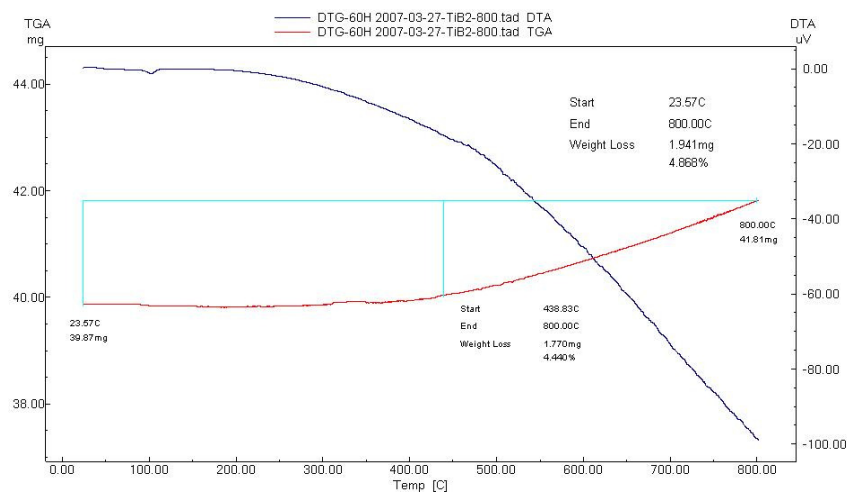


Figure 3.9 DTA/TGA analyses results for the TiB₂ powder

3.1.5.2 ZrB₂ Powder

Figure 3.10 shows the results of the DTA/TGA characterization of the as received ZrB₂ powder sample. Small exothermic peaks were observed at 400°C. According to the TGA data, weight gain started around 650°C. The total weight gain of the sample was 38.6%. The same analysis also suggested that some structural changes took place for the powder at about 950°C.

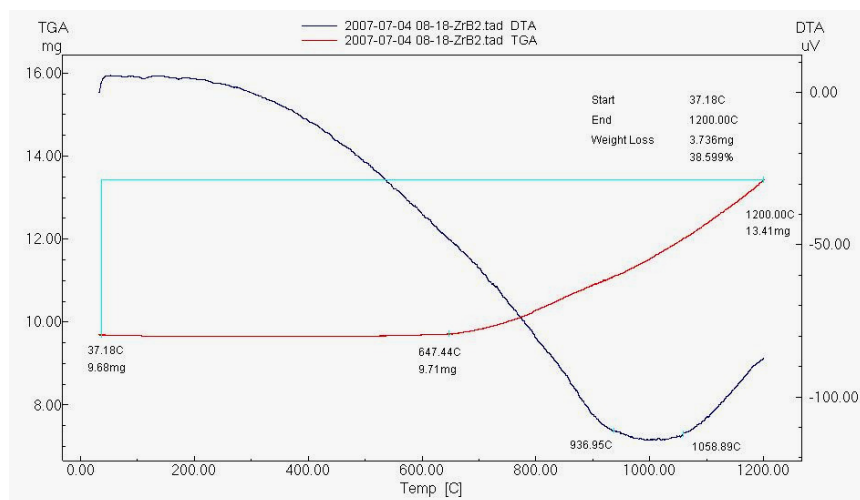


Figure 3.10 DTA/TGA analyses results for the ZrB₂ powder

3.1.5.3 B₄C Powder

Figure 3.11 shows the results of the DTA/TGA test conducted on the as received B₄C powder sample. According to the TGA analysis, no weight gain was observed up to 600°C. The analysis ended at 800°C and the total weight gain of the sample was 2.3%. DTA data, on the other hand, showed no reaction or phase change during heating.

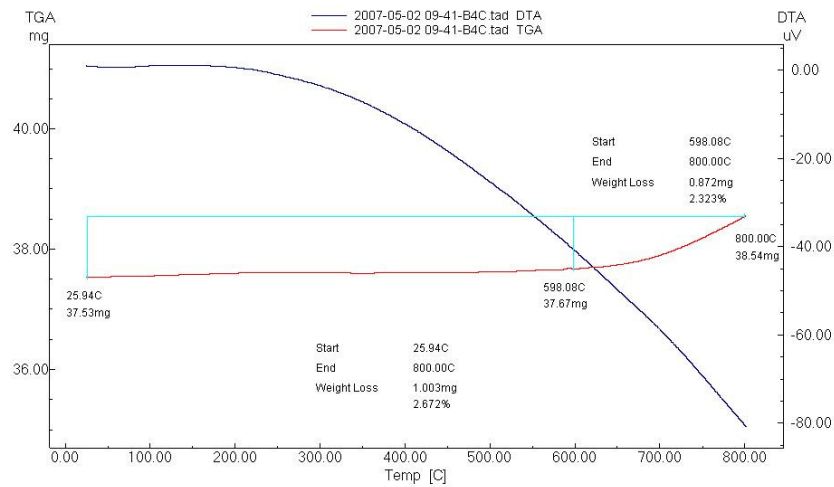


Figure 3.11 DTA/TGA analyses results for the B₄C powder

3.2 Oxidation Test Results for Powder Raw Materials

3.2.1 Oxidation Test Results for TiB₂ Powder

In this group of tests, air oxidation of the powder samples was investigated. First, TiB₂ powder was put inside a ceramic boat which was covered with another boat. The sample was heated to 800°C at a heating rate of 10°C/min. The test lasted for 6 hours at 800°C in a box furnace.



Figure 3.12 Appearances of the TiB₂ powder sample (a) before oxidation, (b) after oxidation.

After the test, two important observations were made. First one was the change in the color of the powder from black to white (Figure 3.12 b). Second observation was that the powder became rigid and adhered also to the walls of the ceramic boat. While trying to remove the powder from it the boat broke and the rigid powder mass had to be cut with a diamond saw.

Figure 3.13a shows the SEM image of the TiB_2 powder sample whose color turned to white after oxidation at $800^{\circ}C$ for 6 hours. Compared to the as-received TiB_2 powder, the oxidized powder grains were difficult to be separated from each other. It was clear some kind of bonding took place among the grains. Because the melting point of TiB_2 was much higher than the oxidation temperature and because the test period was relatively short, it was not possible for the powder grains to join through solid state diffusion (sintering). Therefore, the reason for the observed low temperature sintering is thought to be the reaction of powder with the oxidizing gas. EDS analysis of the area seen in Figure 3.13a indicated that approximately 20% (by weight) oxygen besides Ti and B elements were present there (Figure 3.13b).

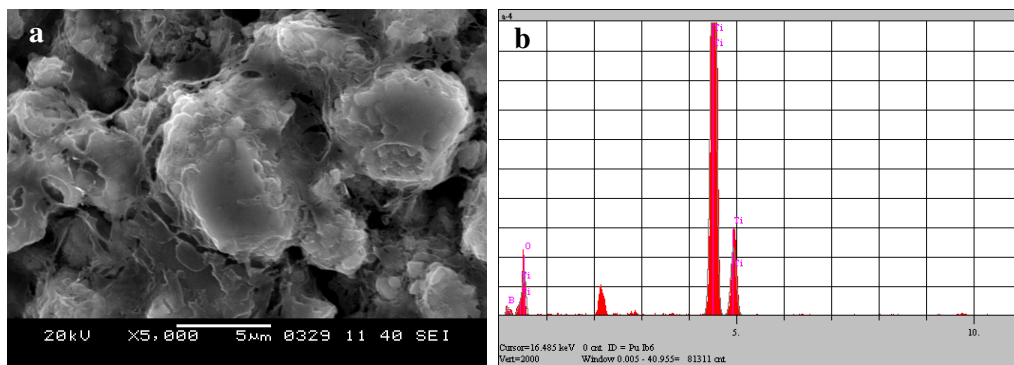


Figure 3.13 (a) SEM image and (b) EDS analysis of the area in the SEM image after oxidation at $800^{\circ}C$ for 6 hours in air.

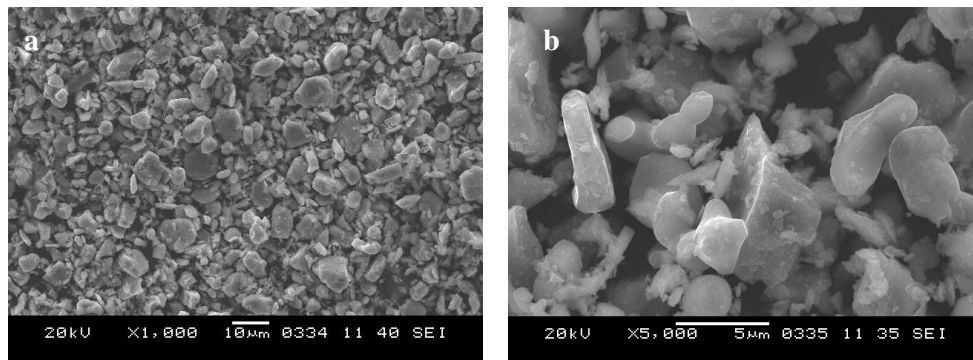


Figure 3.14 SEM images of TiB_2 powder after oxidation at $350^{\circ}C$ for 6 hours in air.

Another tests were done to observe the change of the color of TiB_2 powder from black to white during oxidation. In these tests, TiB_2 powders were exposed to temperatures between $350-800^{\circ}C$ for different times.

Figure 3.14 shows the SEM images of TiB_2 powder oxidized at 350°C for 6 hours in air. In these pictures smaller grains were observed over larger TiB_2 grains. The color of the powder did not change after this low temperature test. Also, the powder was not rigid.

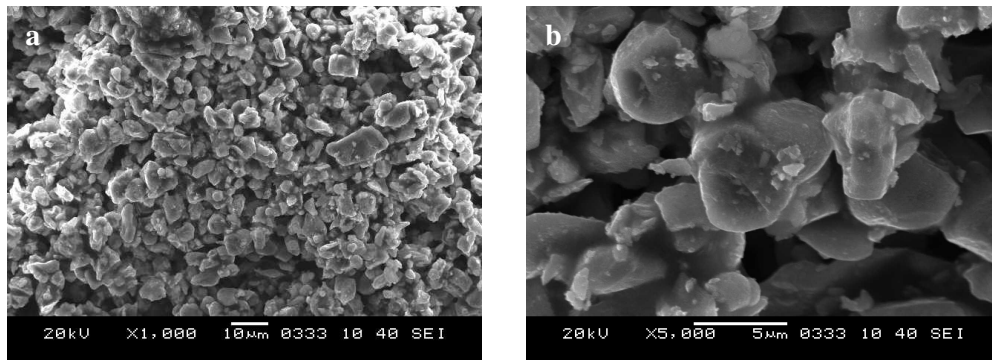


Figure 3.15 SEM images of TiB_2 powder after oxidation at 550°C for 2.5 hours.

Figure 3.15 shows SEM images of the powders oxidized at 500°C for 2.5 hours. This was the same powder that had been used in the previous oxidation test. According to the EDS analysis, the amount of oxygen at the surface of the grains increased during the test. Additionally, the powder was not mixable. Later, the same powder sample oxidized more, this time at 800°C for an hour. SEM images of the powder after this final test are shown in Figure 3.16.

In Figure 3.16c, development of layers is seen over the TiB_2 powder surfaces. Also whisker-like structures were present among the grains (Figure 3.16a and b). It was observed that, at the end of the earlier low temperature tests, the powder had a yellow color and was easy to mix after taken out of the furnace. However at the end of the last test at 800°C , the color of the powder was white and the powder was more rigid. Thus, it is concluded that the whisker-like structures formed during oxidation and connected the grains to each other. Figure 3.17 shows the SEM images of the powder after oxidation at 800°C for 3 hours in air.

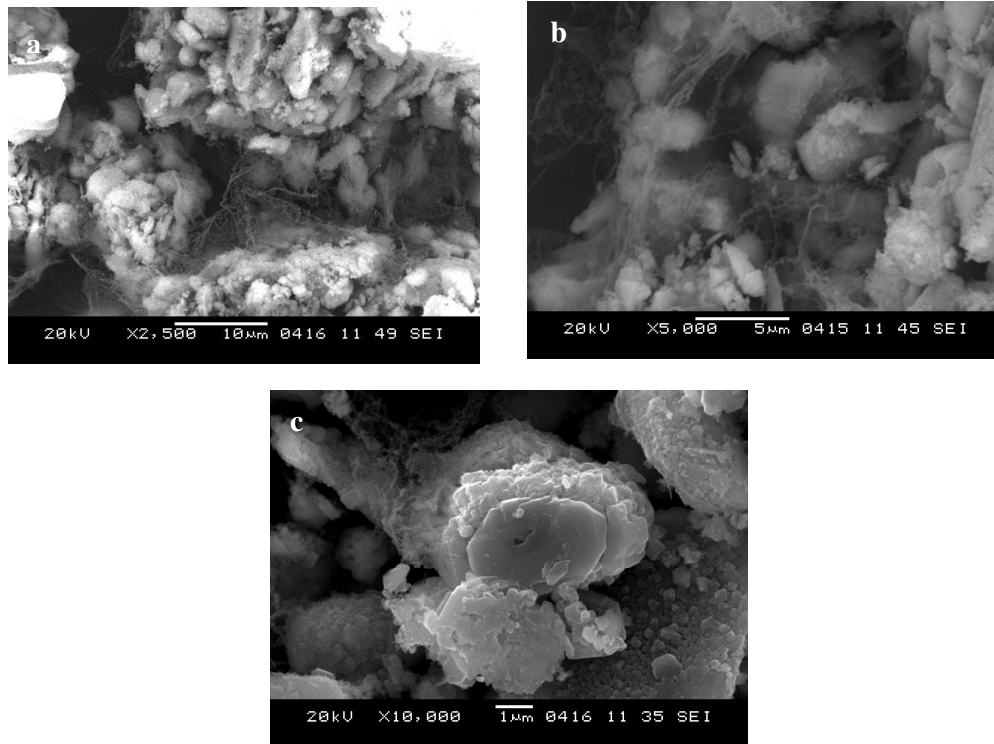


Figure 3.16 SEM images of TiB_2 powder after oxidation at 800°C for 1 hour.

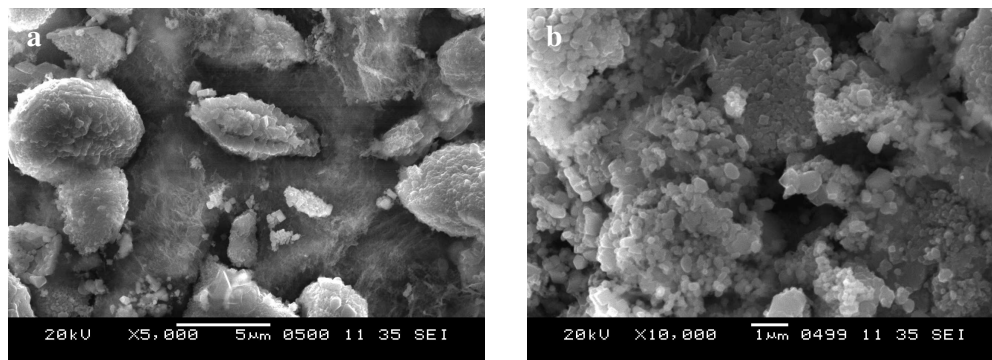


Figure 3.17 SEM images of the TiB_2 powder after oxidation at 800°C for 3 hours

Figure 3.18 shows the XRD analysis results of the TiB_2 powder that was oxidized first, at 350°C for 6 hours and then at 550°C for 2.5 hours. It was clear that TiO_2 phase formed on the surfaces of the powder grains. This result is consistent with the results of the SEM/EDS analyses conducted on the same powder sample.

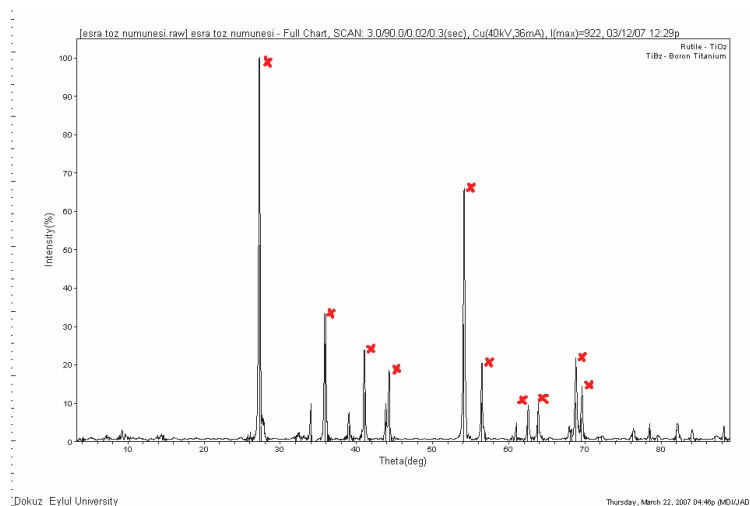


Figure 3.18 The XRD analysis of the TiB_2 powder after oxidation at 550°C for 2.5 hours.

3.2.2 Oxidation Test Results for Powder ZrB_2

Oxidation tests on this material were performed also in a box furnace at 550, 800 and 1000°C . Powder sample was first placed in a ceramic boat and oxidized at 550°C for 2.5 hours in air. During this test the boat containing the powder was removed from the furnace after every 30 minutes and the powder was stirred. As the exposure time increased, it was observed that stirring became difficult. Thus, the ZrB_2 powders became less mixable after oxidation at 550°C as was the case for TiB_2 powder.

After the oxidation test at 800°C for 1 hour, weight gain of about 6% was observed for the ZrB_2 powder sample. Even after this short exposure time, the color of the powder turned from black to white. Furthermore, powder became rigid and adhered to the ceramic boat.

Figure 3.19 shows the SEM images of the ZrB_2 powder after oxidation at 550°C for 2.5 hours. It can be seen that grains adhered to each other during the test and formed lumps. Also, the appearance of the outer surfaces of these lumps (Figure 3.19b) suggested that they formed by the “fusion” of the grains. Thus, formation of a liquid phase during oxidation was a possibility.

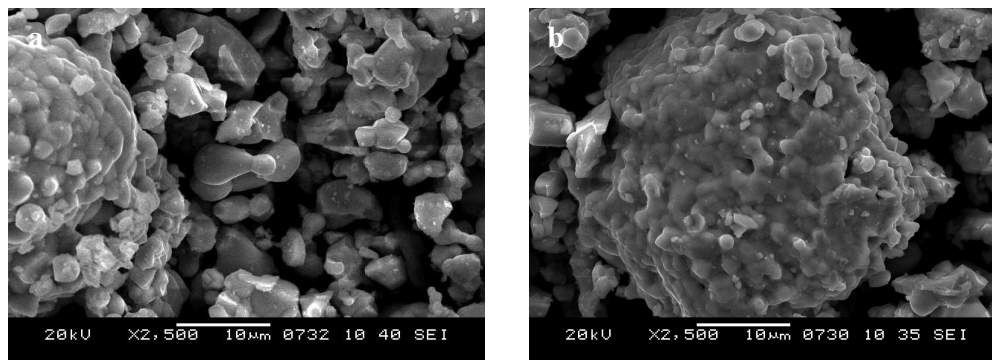


Figure 3.19 SEM images of the ZrB_2 powder after oxidation at $500^{\circ}C$ for 2.5 hours.

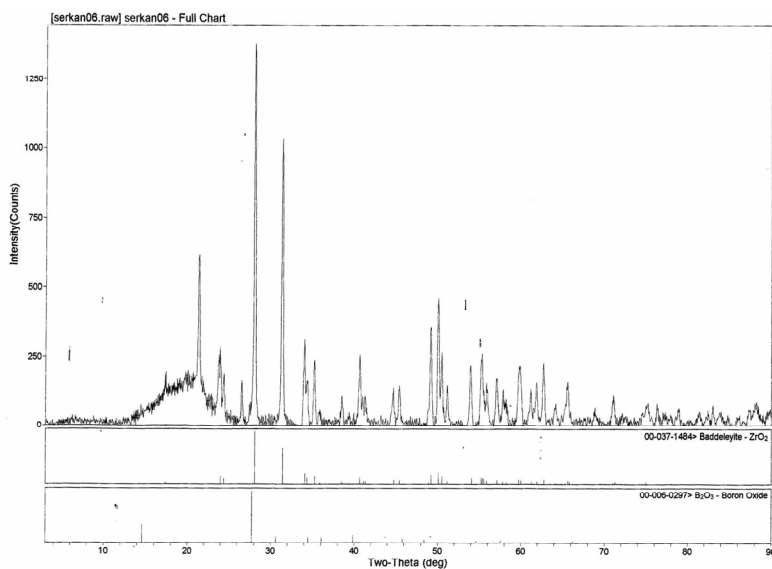


Figure 3.20 XRD graph of the ZrB_2 powder after $1000^{\circ}C$ for 30 minutes.

XRD analysis of the ZrB_2 powder after oxidation at $1000^{\circ}C$ for a short time is given in Figure 3.20. The presence of peaks belonging to the ZrO_2 phase confirms that this oxide phase formed during oxidation. Thus, the change in the color of the powder from black to white must have been the result of oxide formation. Also, features observed in the XRD graph at low angles suggested the formation of amorphous structure in the powder. It was possible that amorphous oxide products containing boron (B_2O_3) formed during oxidation of the boron-containing powder. This result is supported also by the thermodynamic data. Other researchers reported

the formation of phases such as B_2O_3 after the oxidation of ZrB_2 (Monteverde et al, 2003; Lee et al., 2001). Formation of low-melting and amorphous products can also explain the observation that powders were not mixable after the tests at $550^\circ C$ and $800^\circ C$. During cooling of the powder, the liquid B_2O_3 phase that was molten at about $400^\circ C$ must have solidified and thus made the powder not mixable. It may be that this mechanism is also responsible for the formation of the whisker-like structures observed in the TiB_2 powder that was oxidized at $800^\circ C$ for 1 hour.

3.2.3 Oxidation Test Results for B_4C Powder

Oxidation tests on B_4C powder were done at $800^\circ C$ and also at lower temperatures in air. Powder sample was first oxidized at $300^\circ C$ and then at $400^\circ C$ in two consecutive 15- minute long tests for a total of 30 minutes. At the end of these tests, the powder was still mixable and its color did not change. The same powder sample was later oxidized at $550^\circ C$ for 2 hours. After this test, its color was still the same but its mixability was lower. After oxidation at $800^\circ C$ for 30 minutes, the color of the powder sample did not change.

SEM images in Figure 3.21a and b show that B_4C powder grains did not interact with each other during oxidation at $300^\circ C$ and $500^\circ C$. But after the oxidation test at $800^\circ C$ grains lost their original sharp edges and joined with each other (Figure 3.21c). In the same SEM image it is clearly observed that the regions where the grains touched each other appeared “white” in color.

Figure 3.22 shows the high magnification SEM images of the powder after oxidation at $800^\circ C$. EDS analyses showed that oxygen contents of the “white” regions is higher. Since carbon does not form liquid or solid oxidation products, the oxygen-rich boron oxide phase must have been formed in these regions. It is known that materials with no or low electrical conductivity appear “white” in the SEM pictures due to electron charging at the sample surface. It is, therefore, probable that B_4C grains lost their sharp edges as a result of the formation of liquid and volatile oxidation products. Such products were present in the “white” appearing areas since

they had low electrical conductivities. Elements like Al and Si detected in these white regions could have originated from the ceramic boat used to hold the powder samples. They could also be impurities introduced into the powder from outside unintentionally.

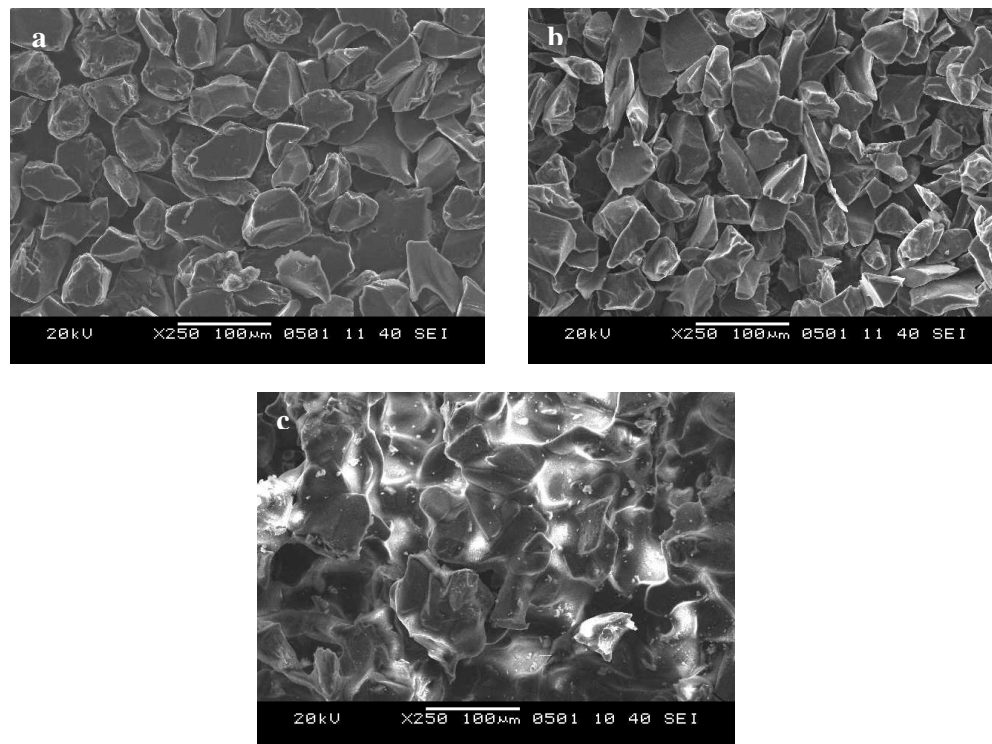


Figure 3.21 SEM images of B_4C powder after oxidation (a) at $300^\circ C$, (b) $550^\circ C$ and (c) $800^\circ C$.

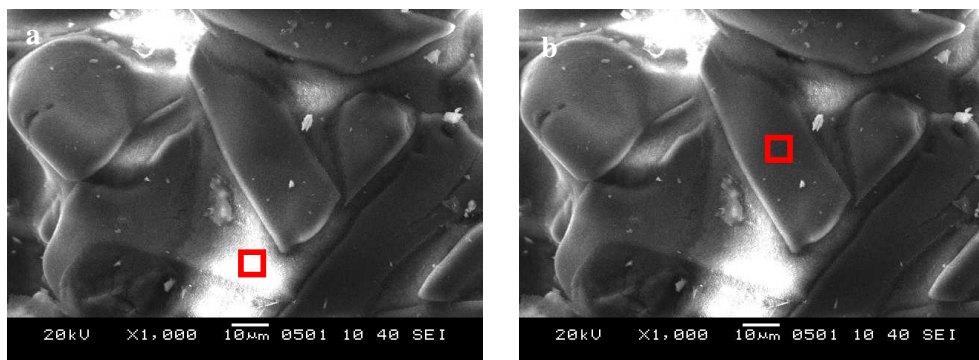


Figure 3.22 EDS analysis regions for the B_4C powder oxidized at $800^\circ C$ in air.

Table 3.3 EDS analyses results of the red squares in Figure 3.22.

Element concentration (w/o)					
Analyzed region	B	C	O	Al	Si
Figure 3.27a	54.1	21.0	19.1	2.7	2.4
Figure 3.27b	55.3	37.5	7.2	-	-

3.3 Oxidation Test Results for Pellets under Static Air

3.3.1 Oxidation Test Results for TiB_2 pellets

The oxidation test results for the pellet samples are discussed in this section. One of the TiB_2 pellets was oxidized at $300^{\circ}C$ for 4 hours in the box furnace in air. At the end of the test the color of the pellet turned gray (Figure 3.23).

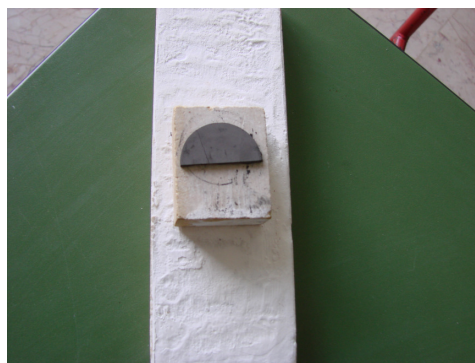


Figure 3.23 The TiB_2 pellet after oxidation at $300^{\circ}C$ for 4 hours.

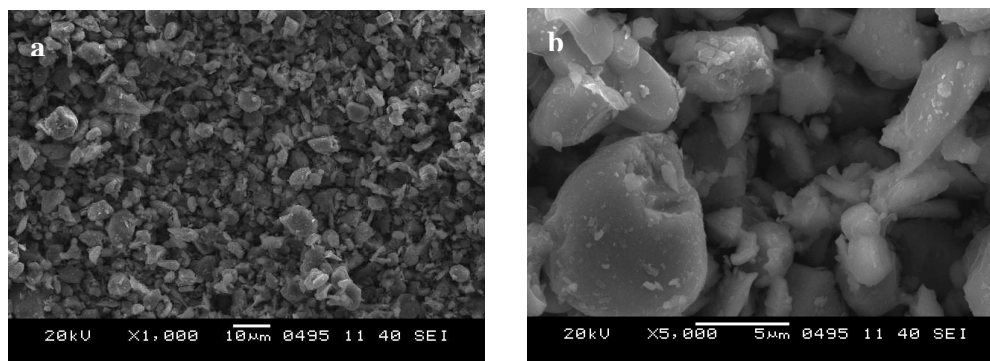


Figure 3.24 SEM images of the TiB_2 pellet after oxidation at $300^{\circ}C$ for 4 hours.

In the SEM images no significant oxidation was observed for this pellet when compared to the powder sample of the same boride. Also the EDS analysis results for the area seen Figure 3.24 (a) was 78,1% B, 20,6% Ti and 1,2% O indicating low oxygen content at the surface of the pellet.

After the oxidation test at 500°C for 5 hours, the color of the pellet was blue (Figure 3.25). The color change was thought to be an evidence for the beginning of oxidation process. EDS analysis of the whole area in Figure 3.26a showed that the oxygen content of the surface increased.



Figure 3.25 TiB₂ pellet after oxidation at 500°C for 5 hours.

After these two tests where the pellets were placed on a refractory plate, oxidation of the pellets continued by suspending them inside a quartz crucible. This way total surface area of the pellet was able to interact with the air environment.

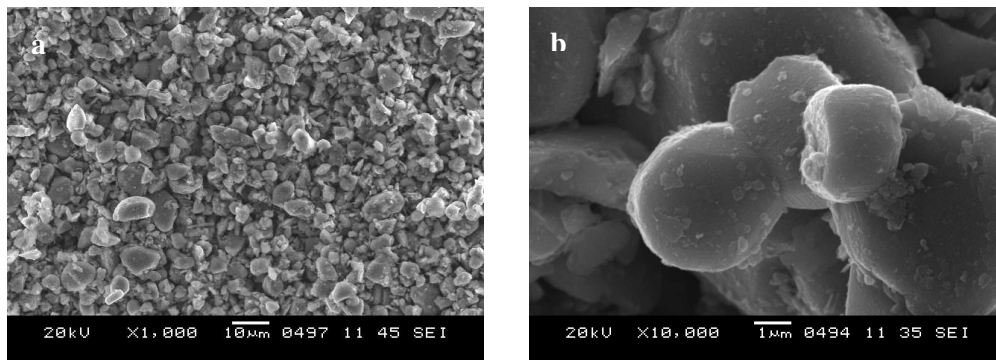


Figure 3.26 SEM images of the TiB₂ pellet after oxidation at 500°C for 5 hours.

Four groups of tests were done on the TiB_2 pellets. For each group, 4 different pellets were prepared. Weights and total surface areas of them were measured before the tests. Four samples from the same group were placed inside the furnace together using quartz crucibles. After the predetermined oxidation time, pellets removed from the furnace and their weights were measured. Based on these measurements weight changes (g/cm^2) were calculated.

The first group of tests were performed at 800°C for 1, 3, 5 and 10 hours. The weight change data for the samples are given in Figure 3.27. During the first hour of the test, a rapid weight gain was observed. But later, rate of weight gain decreased. These results suggested that during the first one hour an oxide layer formed rapidly over the sample surface. Because of this layer, the oxidation rate was lower during the rest of the test.

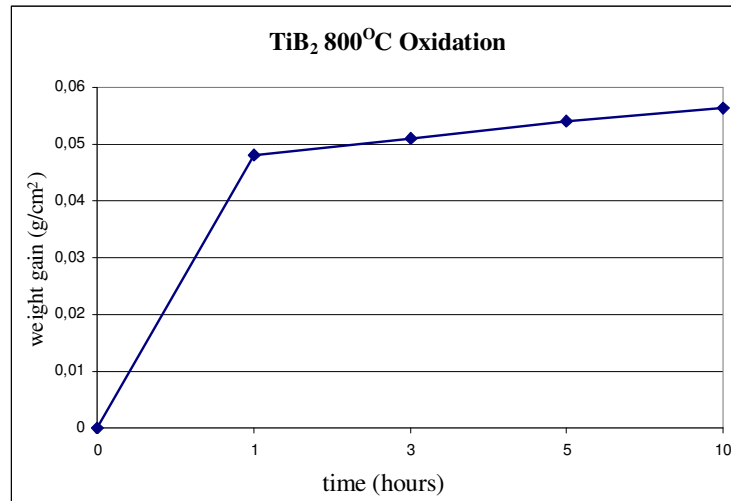


Figure 3.27 Weight changes of the TiB_2 pellets oxidized at 800°C .

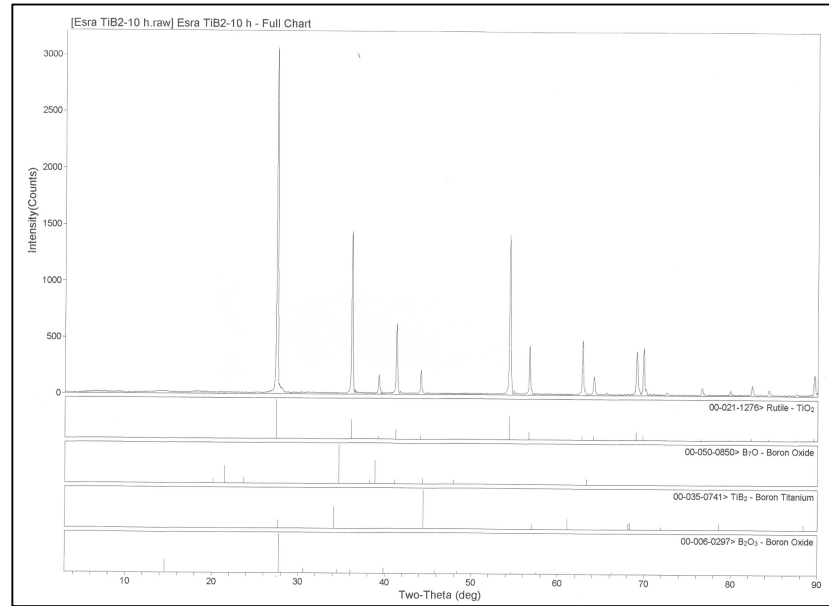


Figure 3.28 XRD analysis of the TiB₂ pellet oxidized at 800°C for 10 hours.

XRD analysis of the sample oxidized at 800°C for 10 hours showed that mainly the TiO₂ phase (rutile) developed at the pellet surface (Figure 3.28).

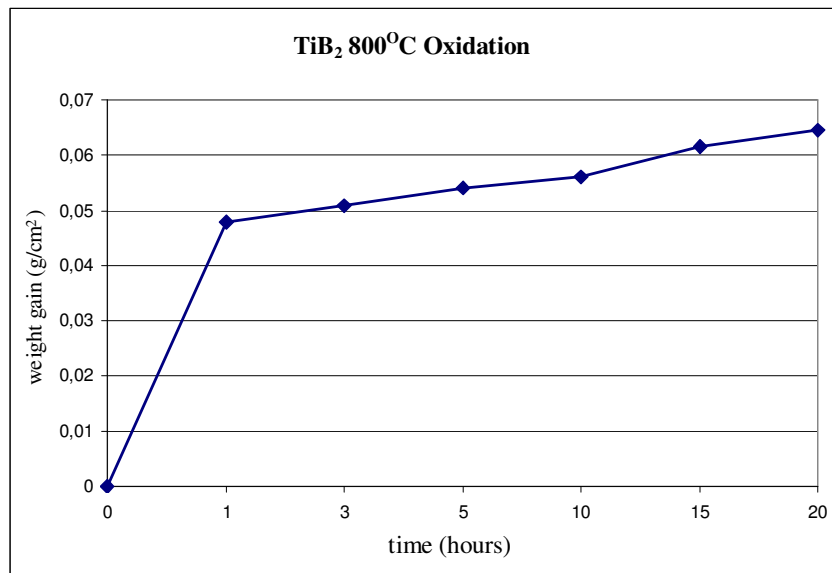


Figure 3.29 Weight changes of the TiB₂ pellets oxidized at 800°C.

In the second group of tests, four new pellets were used for tests at 800°C lasting 5, 10, 15 and 20 hours. Weight gain values observed for the 5 and 10-hour tests were

similar to those of the tests conducted previously. Weight gains for the 15 and 20-hour tests were also compatible with the previous test results at 800°C (Figure 3.29). After oxidation at 800°C, surface colors of the pellets changed from gray to yellow (Figure 3.30).

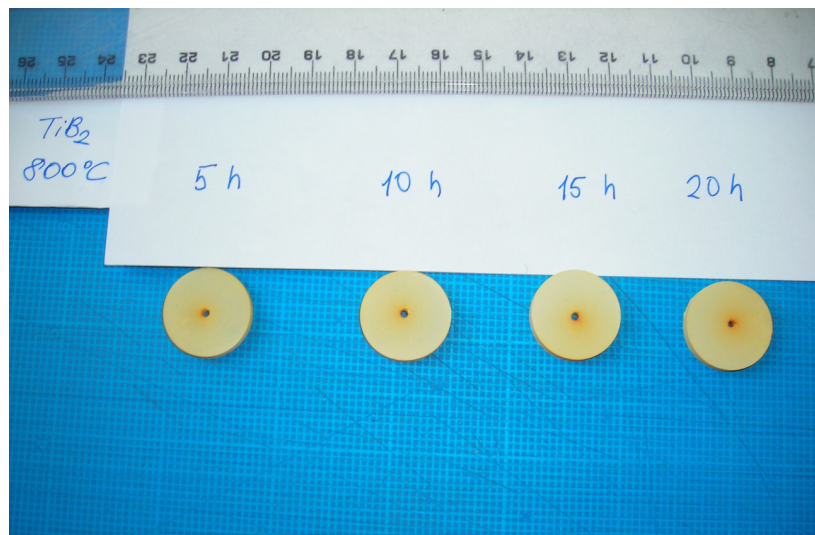


Figure 3.30 TiB₂ pellets after oxidation at 800°C.

The third group of tests on the TiB₂ pellets were conducted at a higher temperature of 1000°C for 5, 10, 15 and 20 hours. After the 5-hour test, the weight gain observed was higher than that measured at 800°C. Weight gains after 10 and 15 hours were higher. A slight weight loss was observed at the end of the 20-hour test. Weight gains after the test at 1000°C were higher than those at 800°C. During these tests at 1000°C, the color of the pellets changed from dark to yellow (Figure 3.32). After 15 and 20-hour tests, the color of the pellets became lighter. This change in color seems to be related to the weight loss observed after the 20-hour test. However, it is not clear why the pellets oxidized for 5 and 10 hours were darker.

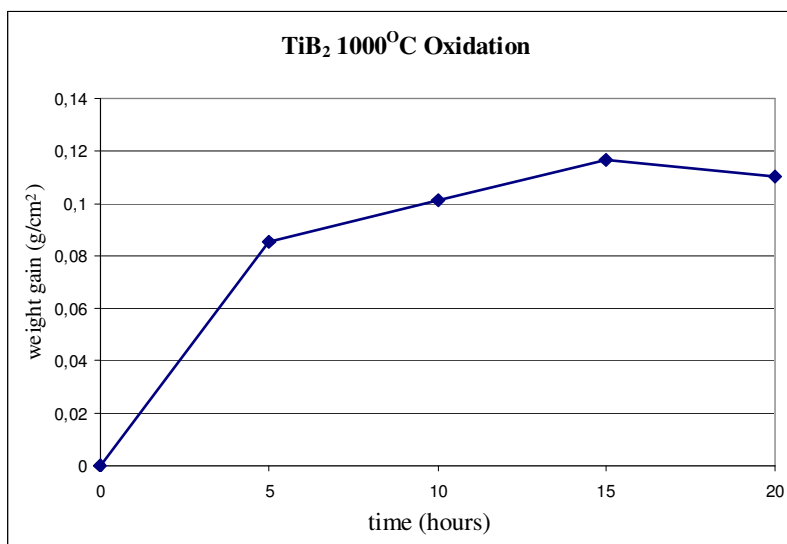


Figure 3.31 Weight changes of the TiB₂ pellets oxidized at 1000°C.



Figure 3.32 TiB₂ pellets after oxidation at 1000°C.

In the fourth group of tests, TiB₂ pellets were oxidized at 1200°C for 5, 10, 15 and 20 hours. Similar to the previous tests, a rapid weight gain was observed after the 5-hour test. Later, the rate of weight gain decreased slightly. In Figure 3.33 weight changes for the three groups of tests are shown together. It is clear that weight gains increased with the duration and temperature of the test. Pellets after oxidation at 1200°C are shown in Figure 3.34.

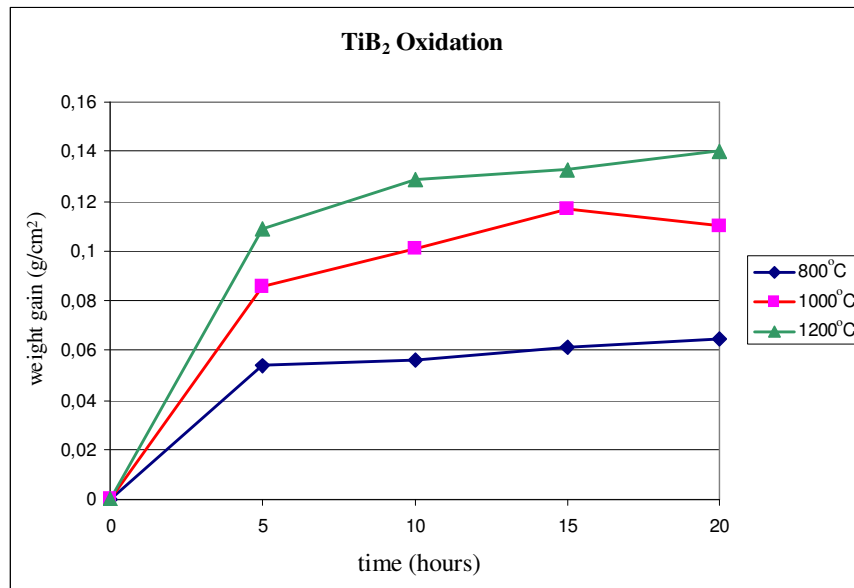


Figure 3.33 Relative weight changes of the TiB₂ pellets oxidized at 800°C, 1000°C and 1200°C.

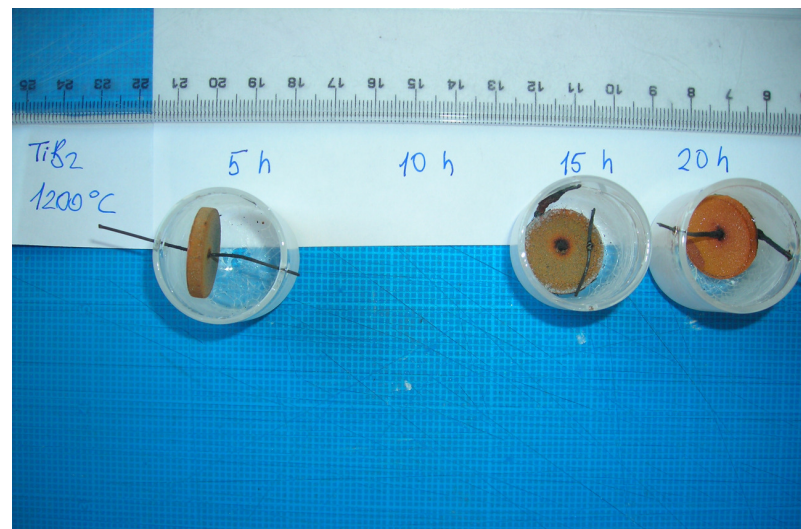


Figure 3.34 TiB₂ pellets after oxidation at 1200°C.

In Figure 3.35 SEM pictures from the TiB₂ pellet oxidized at 1200°C for 10 hours are shown. It is difficult to distinguish the powder grains in the pellet. A matrix structure seems to connect the grains with each other as seen in the high magnification image. It is possible that the matrix structure is of a glassy phase since cracks were observed in these SEM pictures.

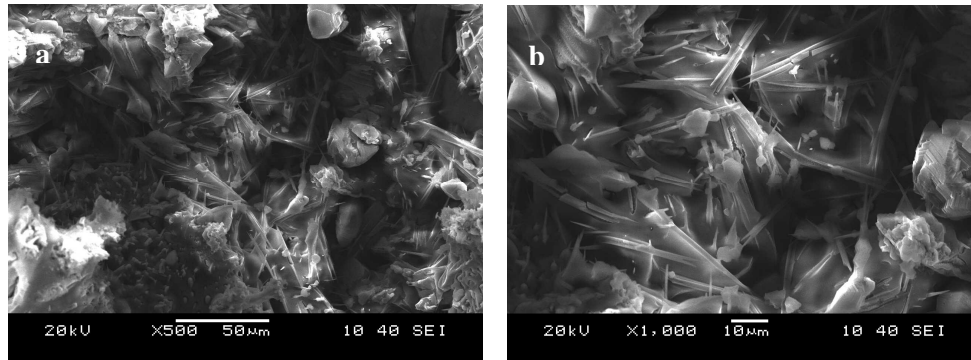


Figure 3.35 (a)-(b) SEM images of the TiB_2 pellet oxidized at 1200°C for 10 hours.

3.3.2 Oxidation Test Results for ZrB_2 Pellets

Pellet samples of ZrB_2 were used in this group of oxidation tests. Experimental conditions of these tests were similar to those explained for the TiB_2 pellets above. In the first group of tests, ZrB_2 pellets were placed on a ceramic plate and were oxidized at 1000°C for 1 and 2 hours under stagnant air in the furnace. Figure 3.36 shows the XRD analysis result for the ZrB_2 pellet oxidized at 1000°C for 2 hours. According to this analysis ZrO_2 phase developed over the sample. Although some of the XRD peaks seemed to belong to the B_2O_3 phase, it was not clear whether such a crystalline phase was present over the pellet. However, as mentioned above, amorphous boron oxide formation was observed for the ZrB_2 powder. SEM images in Figure 3.37 clearly showed the consolidation of the oxidized ZrB_2 grains. This type of behavior was possible for the powder grains if amorphous boron oxide were present in the pellet. As mentioned above, a similar process is thought to have taken place also for the TiB_2 tablet oxidized at 1200°C

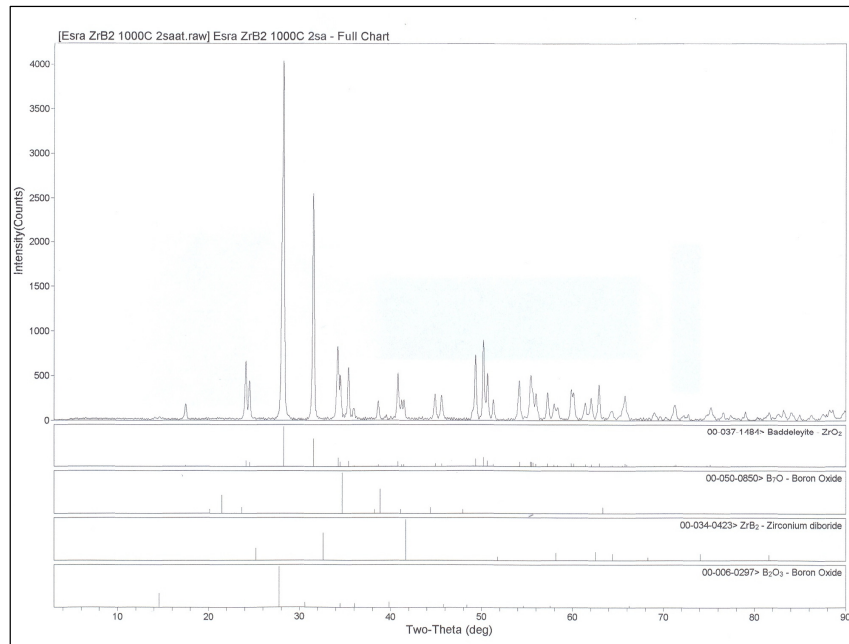


Figure 3.36 XRD analysis the ZrB_2 pellet oxidized at $1000^\circ C$ for 2 hours.

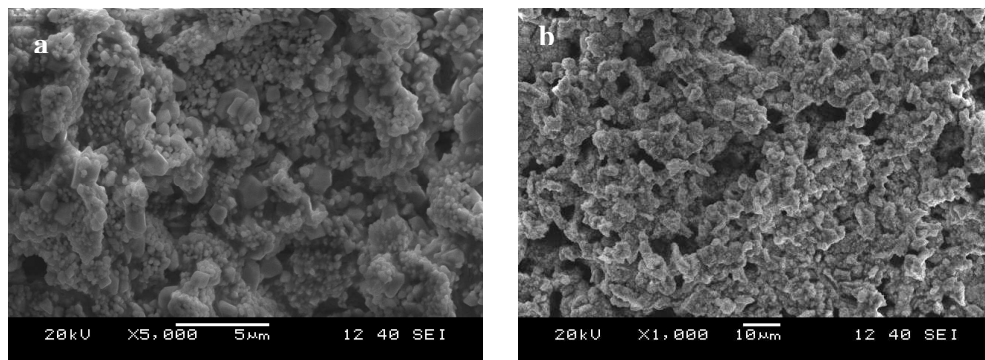


Figure 3.37 SEM images of the outer surface of the ZrB_2 pellet oxidized at $1000^\circ C$ for 2 hours.

High temperature oxidation tests on ZrB_2 pellets were conducted also in four groups. In each group, four pellets were suspended inside 4 separate quartz crucibles. The first and second group of samples were oxidized at $800^\circ C$. The third and fourth group of tests were performed at $1000^\circ C$ and $1200^\circ C$, respectively.

Weight changes measured for the samples after the oxidation test at $800^\circ C$ are shown in Figure 3.38. For the tests lasted less than 10 hours, weight changes were similar to those of the TiB_2 pellets oxidized at $800^\circ C$. Although there were small

differences between the weight change values of the first and the second group of tests conducted at 800°C , when considered together the data clearly indicated that weight gain of the ZrB_2 pellets increased with the test duration.

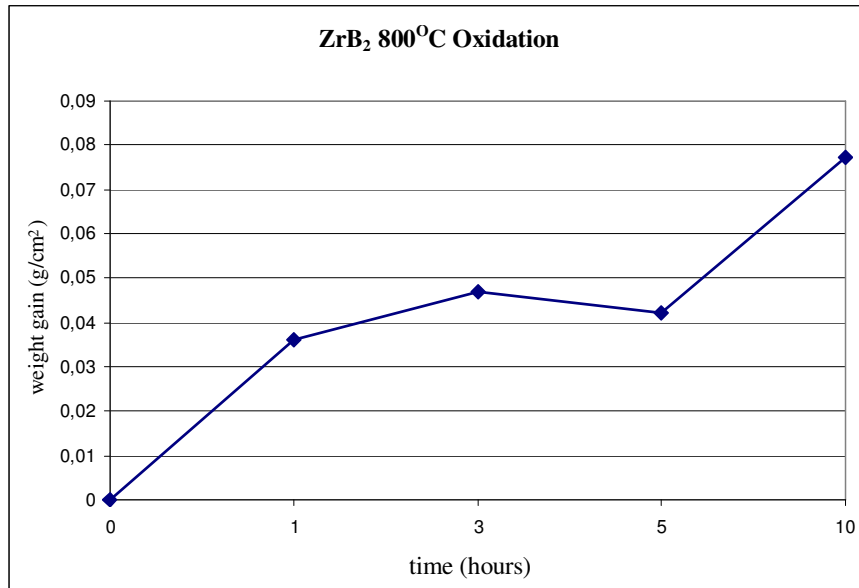


Figure 3.38 Weight changes of the ZrB_2 pellets after first group of oxidation tests at 800°C .

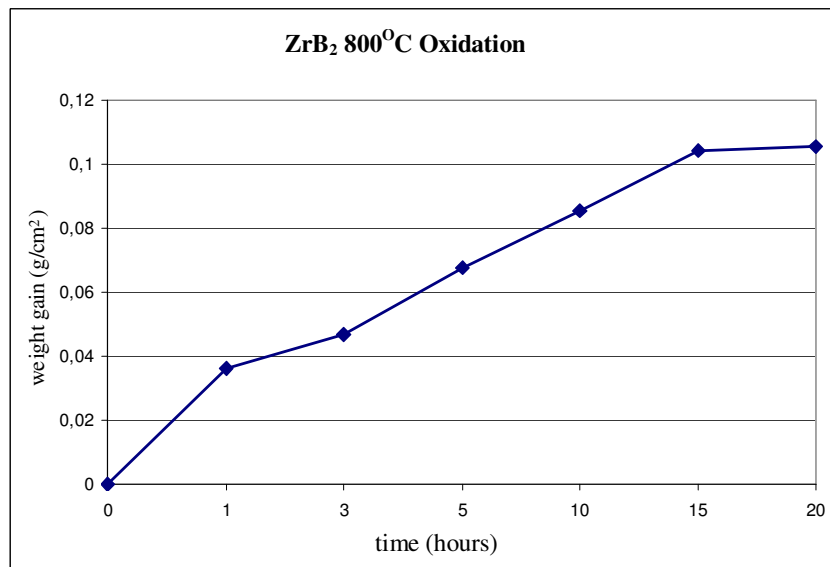


Figure 3.39 Weight changes of the ZrB_2 pellets after the first and second group of oxidation tests at 800°C .

Figure 3.40 shows the appearances of some of the ZrB_2 pellets oxidized at 800°C . All pellets had the same color. However fine cracks were present on the pellet surfaces. Samples oxidized for 15 and 20 hours were broken into pieces after the tests.

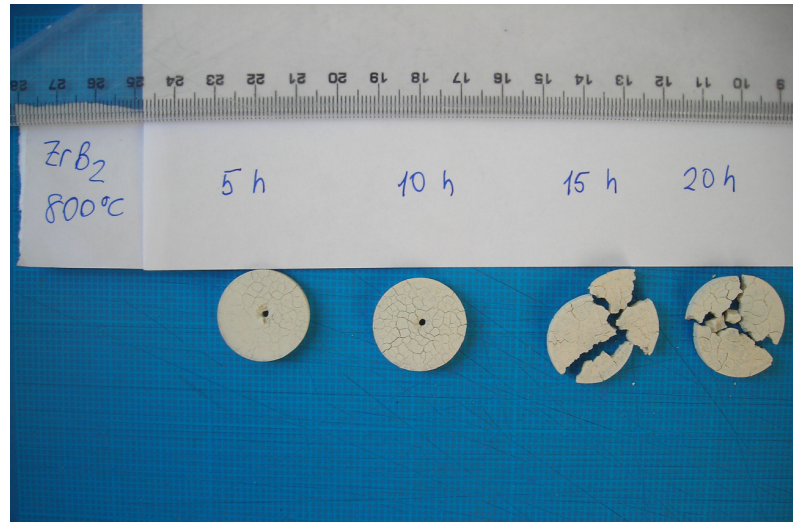


Figure 3.40 ZrB_2 pellets after oxidation at 800°C .

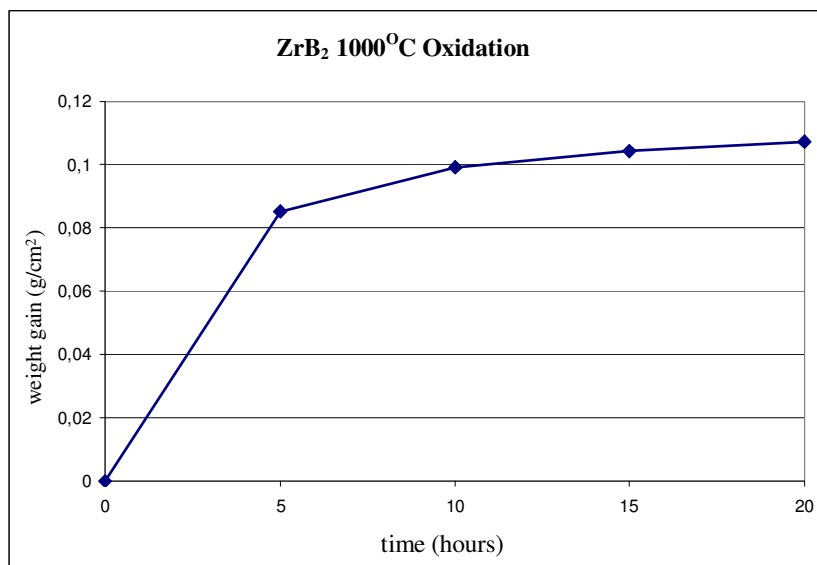


Figure 3.41 Weight changes of the third group ZrB_2 samples oxidized at 1000°C .

The third group of tests were done at 1000°C for 5, 10, 15 and 20 hours. According to Figure 3.41, after 5 hours, the measured weight gain was higher than

that measured at 800°C. Weight gain after 20 hours at 1000°C was almost the same as that of the TiB₂ pellet oxidized at the same temperature for the same duration. These ZrB₂ pellets did not change their colors during the test at 1000°C unlike the TiB₂ pellets oxidized at the same temperature (Figure 3.42).

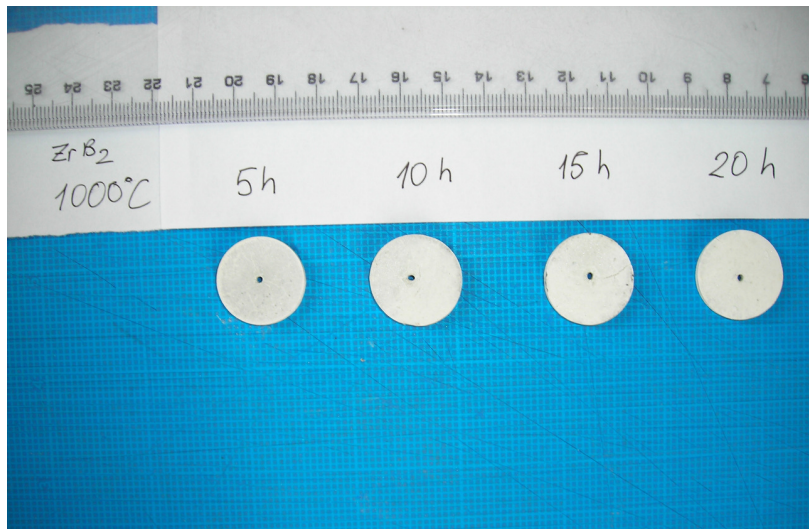


Figure 3.42 Appearances of ZrB₂ pellets after the third group of tests.

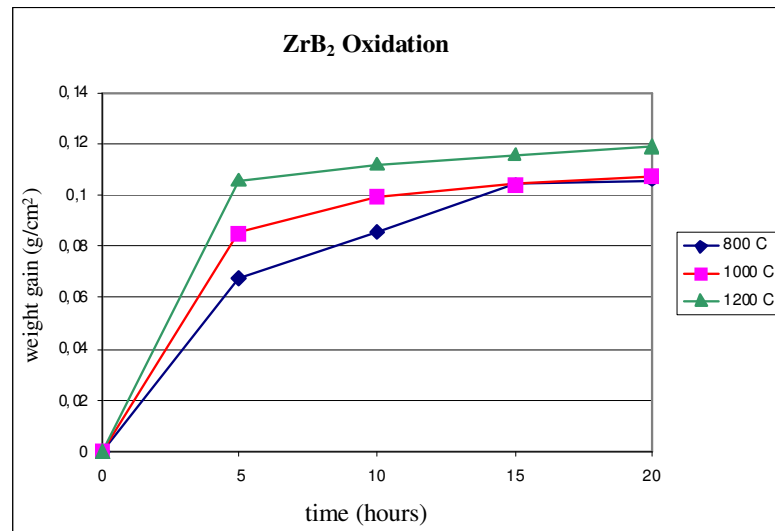


Figure 3.43 Relative weight changes of the ZrB₂ pellets.

After the fourth group of tests at 1200°C conducted for 5, 10, 15 and 20 hours, weight changes of the samples increased slowly with time. Relative weight changes of ZrB₂ pellets are shown in Figure 3.43. It is clearly seen that weight changes increased with time and temperature of the tests.

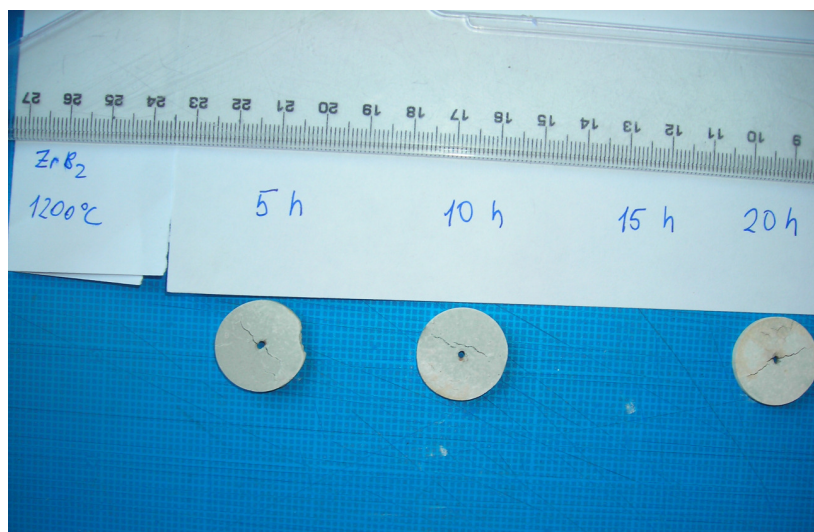


Figure 3.44 ZrB₂ pellets after oxidation at 1200°C.

In Figure 3.44, ZrB₂ pellets are seen after the oxidation test at 1200°C. Cracks were observed along the pellet diameters. However samples were not broken into smaller pieces. Figure 3.45 shows the SEM images of the ZrB₂ pellet oxidized at 1200°C for 15 hours. Grains became rounded after oxidation at this high temperature. Some coalescence of grains is observed in the SEM pictures. However, whisker-like products were not present in this microstructure.

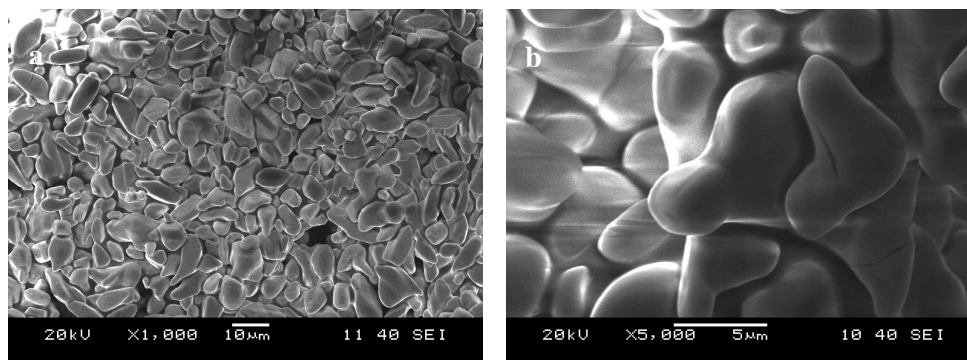


Figure 3.45 SEM images from the surface of the ZrB₂ pellet oxidized at 1200°C for 15 hours.

3.3.3 Oxidation Test Results for B_4C Pellets

Similar type of oxidation tests at $800^{\circ}C$ and $1000^{\circ}C$ were conducted on the B_4C pellets. In the first group of tests, B_4C pellets were oxidized in a box furnace at $800^{\circ}C$ for 5, 10, 15 and 20 hours. Weight changes of the samples after these tests are shown in Figure 3.46.

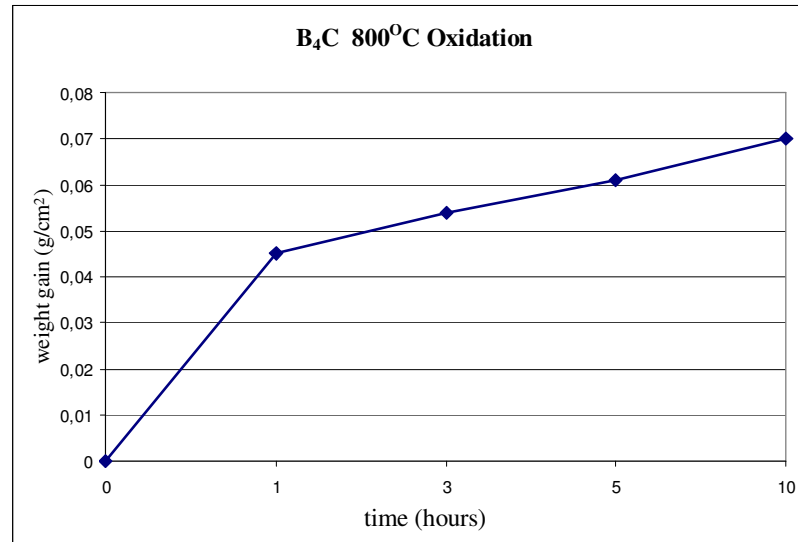


Figure 3.46 Weight changes of the B_4C pellets oxidized at $800^{\circ}C$.

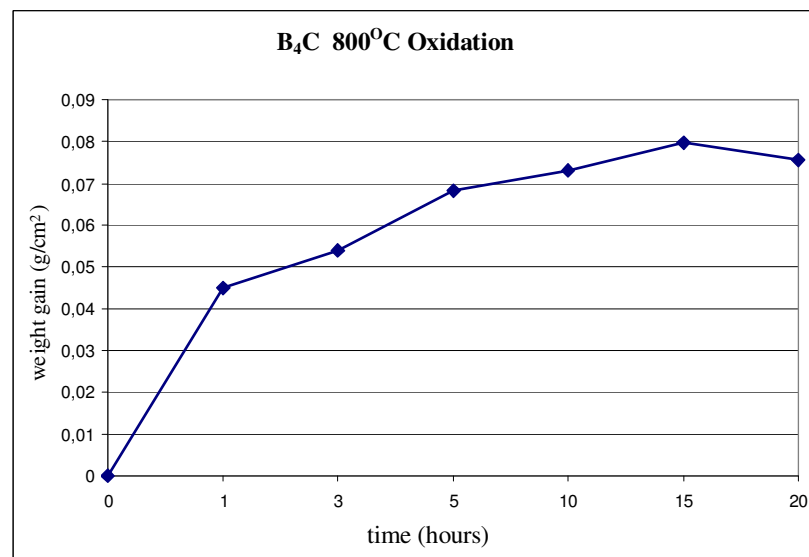


Figure 3.47 Weight changes of the B_4C pellets after the first and second group of oxidation tests at $800^{\circ}C$.

After the second group of oxidation tests, B_4C pellets gained weight at $800^{\circ}C$ after 5, 10, 15 and 20 hours (Figure 3.47). These values were similar to those measured for both TiB_2 and ZrB_2 samples oxidized at this temperature. Appearances of the B_4C pellets after the second group of tests at $800^{\circ}C$ are shown in Figure 3.48. Color changes were not observed for these samples after this test.

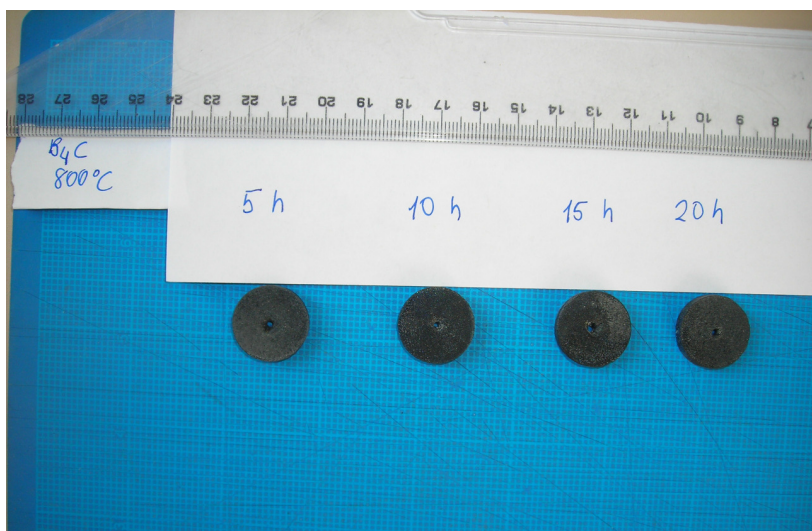


Figure 3.48 B_4C pellets after oxidation at $800^{\circ}C$.

The third group of oxidation tests on the B_4C pellets were conducted at $1000^{\circ}C$ for 5, 10, 15 and 20 hours. Weight changes of the samples are shown in Figure 3.49. It is clear that weight gains after oxidation at $1000^{\circ}C$ were slightly higher than those measured at $800^{\circ}C$. However, after 20 hours of oxidation at 800 and $1000^{\circ}C$, samples lost weight. As shown in Figure 3.50, B_4C pellets were intact after all oxidation tests. Also, no change in the color of pellets was observed.

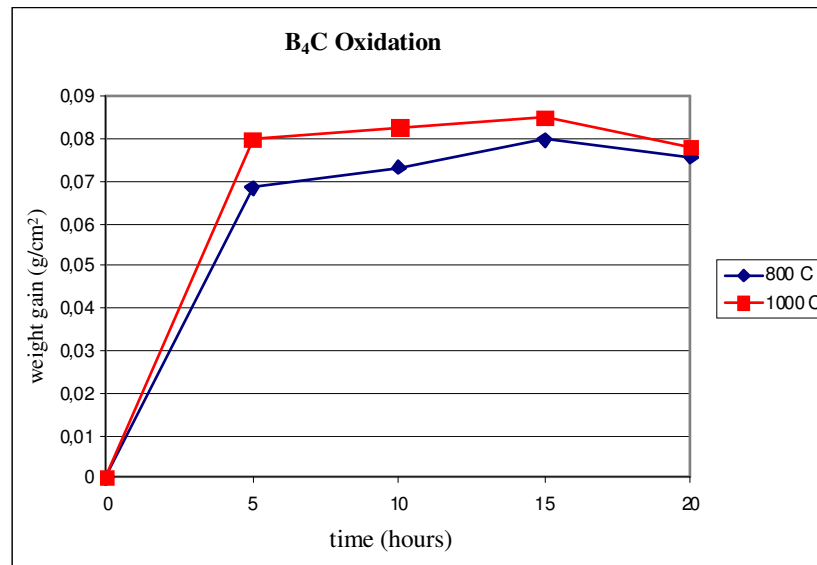


Figure 3.49 Relative weight changes of the B₄C pellets oxidized at 800°C and 1000°C.



Figure 3.50 B₄C pellets after oxidation at 1000°C.

3.4 Corrosion Test Results for the Pellets in Water Vapor Environment

In this section corrosion tests conducted on the boron compounds in water vapor containing environment are explained.

Appearances of the pellets used in this test are shown in Figure 3.51, while some of the physical properties of the samples are given in Table 3.4.

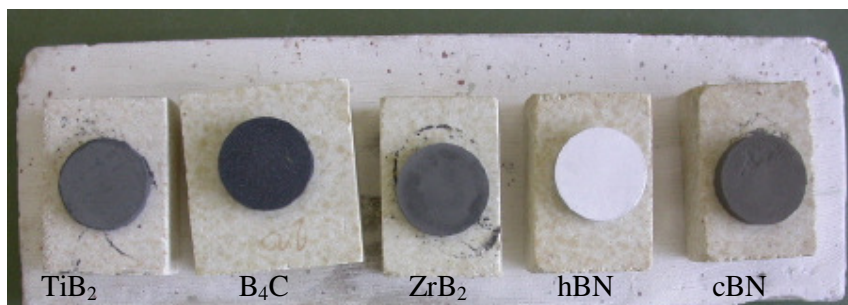


Figure 3.51 Pellets before the corrosion test in water vapor containing

Corrosion tests on TiB_2 , ZrB_2 and B_4C were conducted in the tube furnace. Each pellet was placed inside a quartz crucible and all crucibles were placed in the hot-zone of the quartz test tube as shown in Figure 3.52.

Table 3.4 Properties of the pellets used in the corrosion test under water vapor.

	Diameter (mm)	Thickness (mm)	Surface area (mm^2)
TiB_2	20.00	3.50	848.23
ZrB_2	20.00	2.60	791.68
B_4C	20.00	4.80	929.91

This test was conducted at 1000°C for 4 hours. Until reaching to 500°C , the quartz furnace tube was swept with Ar gas. Then, the gas was directed into the beaker containing distilled water. Water vapor at the water temperature was picked up and carried into the quartz tube by the flowing Ar gas. In order to prevent condensation of the vapor at the entrance to the furnace tube, the gas inlet side of the tube was covered with glass wool

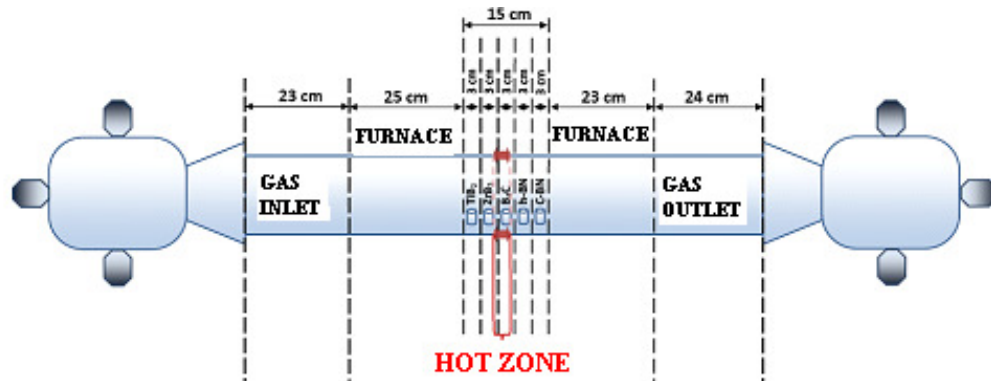


Figure 3.52 Schematic illustration of the placement of samples inside the quartz tube.

During the test, both white and black-colored deposits were observed to form closer to the hot-zone as well as the gas outlet side of the quartz reaction tube. Figure 3.53 shows, schematically, the locations and appearances of the deposits. Samples from the deposits were taken for chemical analyses.

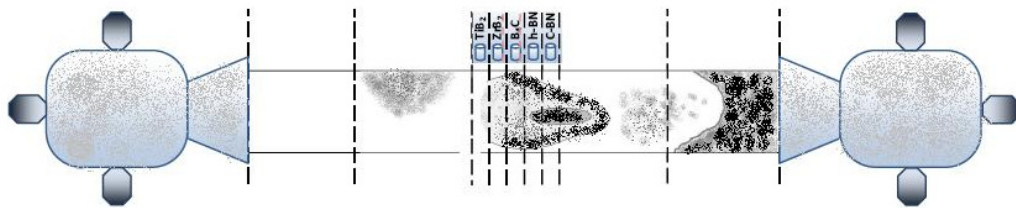


Figure 3.53 Locations of the white and black deposits developed over the internal surfaces of the quartz reaction tube.

Color of the TiB_2 pellet was observed to change during the test. Cracks were present on the surface of this pellet. Cracks were observed also on the surface of the ZrB_2 pellet. B_4C pellet, however, was free of cracks. Also its color did not change during the test.

3.4.1 Mass Changes of the Pellets

Figure 3.54 shows the relative weight changes for the pellets of the three different boride compounds. It can be seen that all pellets gained weight after the test. The maximum weight gain was observed for the ZrB_2 pellet.

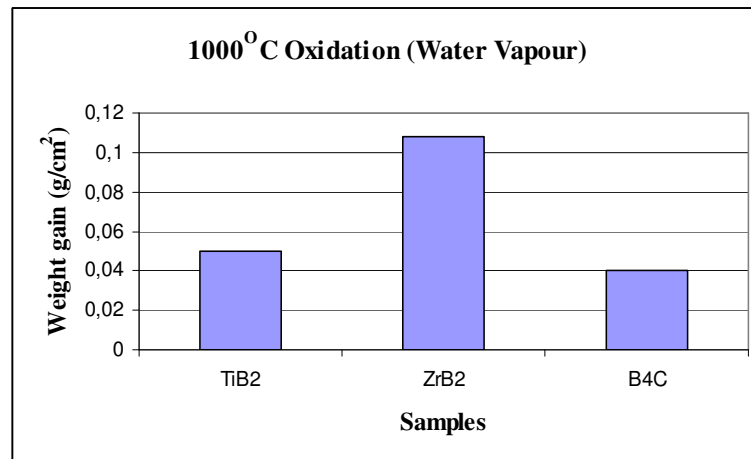


Figure 3.54 Relative weight changes of the boride pellets after oxidation at 1000°C in water vapor.

3.4.2 Analyses of the Pellets

After oxidation at 1000°C for 4 hours in water vapor, powder grains at the surface of the TiB₂ pellet had different morphologies (Figure 3.55a). EDS analyses suggested the presence of TiO₂ on this pellet. Also, powder particles in the pellet oxidized in water vapor at 1000°C were observed to be larger than grains in the pellet oxidized for 2 hours in air at the same temperature (Figure 3.55b). It is probable that the difference in the grain sizes was related to the duration of the oxidation test rather than the nature of the oxidizing environment.

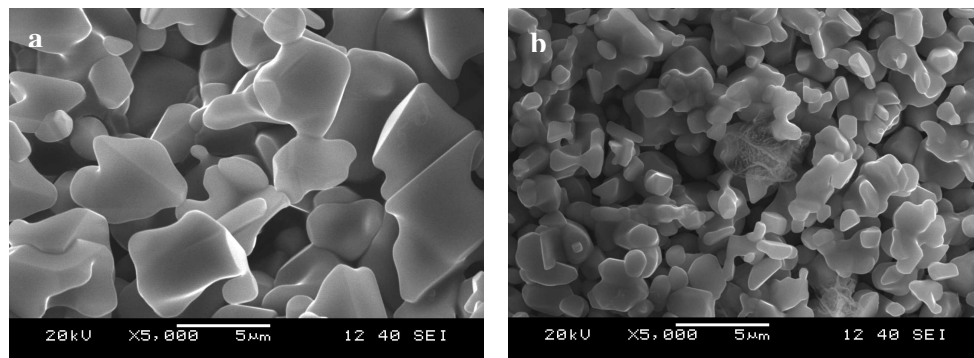


Figure 3.55 SEM images of the TiB₂ pellet oxidized at 1000°C a) for 4 hours in water vapor, and b) for 2 hours in air.

In Figure 3.56, the weight change of the TiB_2 pellet oxidized in water vapor is shown on the graph drawn for the pellets oxidized in air. It looks like the TiB_2 pellet oxidized in water vapor gained almost the same weight it would have gained if it were oxidized in air at the same temperature.

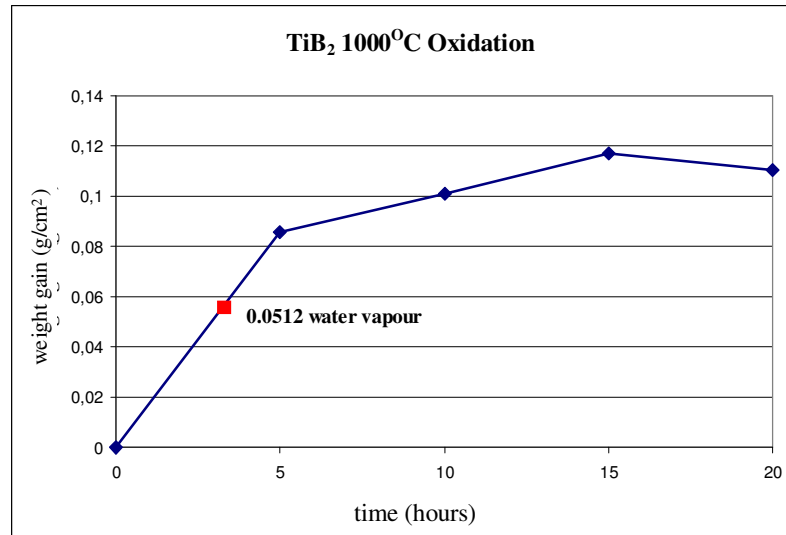


Figure 3.56 Relative weight gains of TiB_2 pellets after oxidation test in water vapor and air.

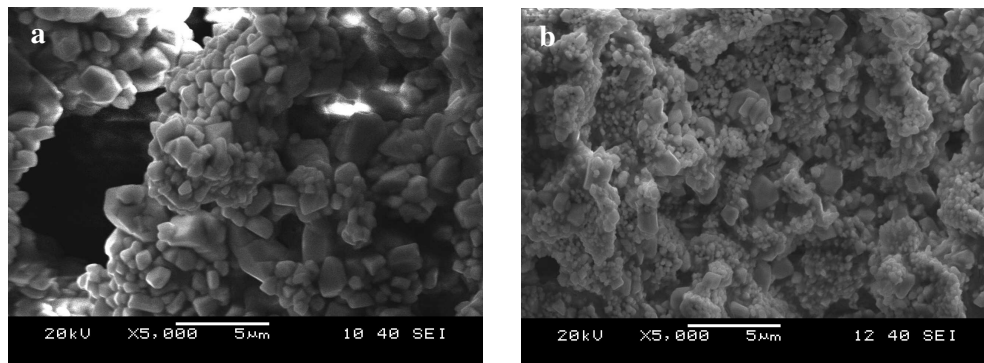


Figure 3.57 SEM images of the ZrB_2 pellets oxidized at 1000°C, a) for 4 hours water vapor and b) for 2 hours in air.

Figure 3.57 shows the SEM images of the ZrB_2 pellet that was oxidized in (a) water vapor and (b) air environments. These images suggest that the oxide particles formed in water vapor were larger than those formed under in air. According to the weight gain data in Figure 3.58, the weight change of the ZrB_2 in water vapor was

higher than it would have gained if it were oxidized 1000^o in air for the same duration. This result suggested that water vapor increased the oxidation rate of the ZrB₂ pellet.

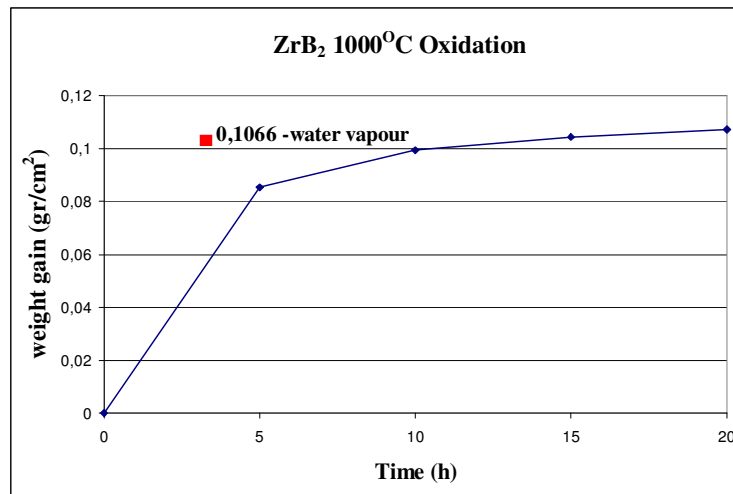


Figure 3.58 Relative weight gains of ZrB₂ pellets after oxidation tests in water vapor and air.

In Figure 3.59 the SEM images of the B₄C pellets oxidized at 1000^oC (a) for 4 hours in water vapor and (b) 5 hours in ambient air are shown. Powder grains in Figure 3.59(a) looked larger than those in Figure 3.59(b). However, the weight gain data in Figure 3.60 indicated that the weight gain of the B₄C pellet oxidized in water vapor was lower than it would have gained if it were oxidized in air at the same temperature.

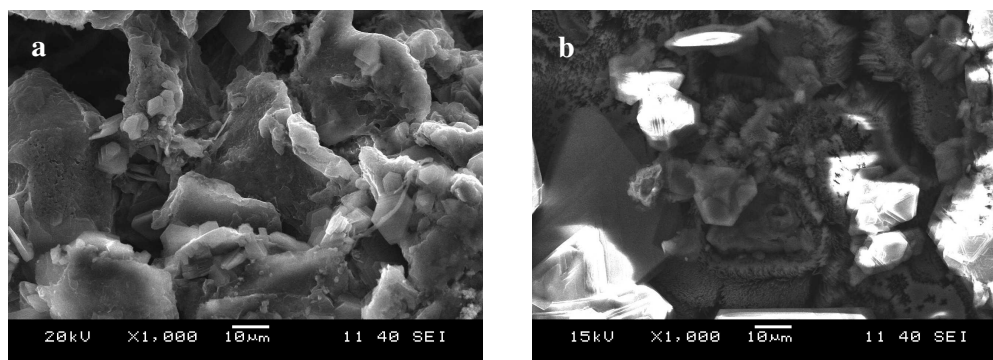


Figure 3.59 SEM images of the B₄C pellet oxidized at 1000^oC, a) for 4 hours in water vapor and b) for 5 hours in air.

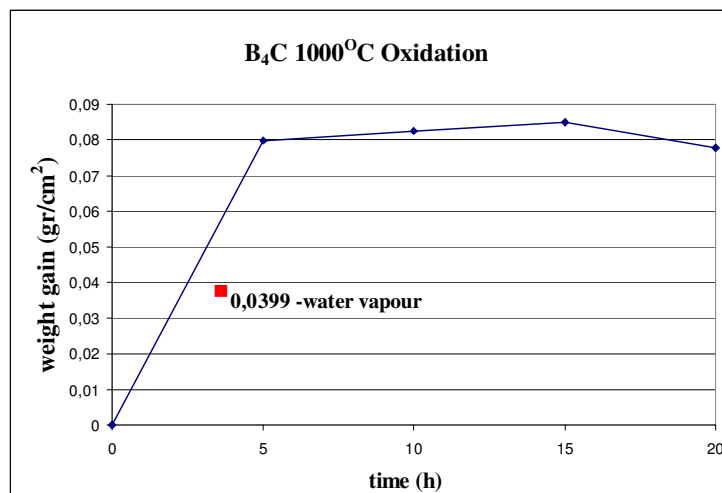


Figure 3.60 Relative weight gains of B₄C pellets after oxidation tests in water vapor and air.

3.5. Kinetic, Thermodynamic and Mechanistic Evaluations of the Oxidation Test Results

In this section, kinetic, thermodynamic and mechanistic evaluations of the oxidation behavior of the investigated boron compounds are discussed. Besides the test results, the related thermodynamic and kinetic data from the literature are used to evaluate the results.

3.5.1. Thermodynamic Properties of the Boron Compounds and Their Corrosion Products

Thermodynamic stability of the products resulting from chemical reactions of TiB₂, ZrB₂ and B₄C with oxygen can be determined by considering the Standard Gibbs Free Energy changes (ΔG°) of the oxidation reactions. Table 3.5 shows the chemical reactions and ΔG° values of these reactions calculated by using data from the literature.

ΔG° values given in Table 3.5 indicate that these oxidation reactions can take place as written at the indicated temperatures and the oxides of B, C, Ti and Zr elements are thermodynamically stable as oxidation/corrosion products. Oxidation reaction of BN and its ΔG° values are given as a reference.

Table 3.5 Oxidation reactions and Standart Gibbs Free Energy Changes (ΔG°) (Turkdoğan 1980).

Oxidation Reactions	ΔG° (kJ)		
	800 ^o C	1000 ^o C	1200 ^o C
$TiB_2(s) + \frac{5}{2}O_2(g) \Rightarrow TiO_2(s) + B_2O_3(l)$	-1492	-1419	-1345
$ZrB_2(s) + \frac{5}{2}O_2(g) \Rightarrow ZrO_2(s) + B_2O_3(l)$	-1597	-1522	-1448
$B_4C(s) + 4O_2(g) \Rightarrow 2B_2O_3(l) + CO_2(g)$	-2369	-2286	-2203
$2BN(s) + \frac{3}{2}O_2(g) \Rightarrow B_2O_3(l) + N_2(g)$	-1192	-1185	-1178

3.5.2. Physical Properties of the Corrosion Products

XRD analyses of the oxidized TiB_2 and ZrB_2 (Figure 3.18 and 3.20) showed that solid TiO_2 and ZrO_2 phases formed during the oxidation tests conducted, in air, at the indicated temperatures. The stable corrosion product; CO_2 of the B_4C compound was in the gas phase at all temperatures. Data in Table 3.5 state that N_2 gas also forms as a corrosion product of the BN compound. Formation of gaseous corrosion products like NO_2 and NO after oxidation of BN was reported by other researchers (Jacobson et al., 1999). In our work, however, chemical analyses of the gaseous oxidation products were not made. Therefore, it is not known whether carbon or nitrogen oxides formed as corrosion products or not. However, some gaseous products were observed to form during the tests conducted in the tube furnace as indicated in Figure 3.53.

The boron oxide (B_2O_3) phase is the common corrosion product for the boron compounds investigated. According to the literature, this phase is liquid over 450^oC and its boiling temperature is about 1600^oC. Thus, around 1000^oC, the vapor pressure of this phase increases significantly (Lee et al., 2001; Parthasarathy et al.,

2007). Other researchers reported that the vapor pressure of boron oxide becomes significant at temperatures 750°C (Irving & Worsley, 1968).

XRD analysis of the ZrB_2 sample oxidized at 1000°C in air suggested that amorphous corrosion products formed in this sample during the test (Figure 3.21). This was possible if B_2O_3 were present as a liquid at 1000°C and solidified in amorphous form during cooling. On the other hand, SEM/EDS analyses of the oxidized B_4C sample showed areas appearing “white” in the SEM pictures (Figure 3.22). It is known that such “white” colors indicate the presence of electrically insulating structures. Since B and O elements were detected by EDS at the same location, it was concluded that boron oxide formed in the samples during oxidation. Also, whisker-like structures observed in the SEM analyses of the powder samples oxidized over 400°C in air had both B and O elements. Furthermore, the observation that powder samples became less mixable after the oxidation tests can be explained by the presence of liquid boron oxide at the test temperatures. Presence of the liquid boron oxide in the samples also explains the observed adherence of the powder grains to each other during the oxidation tests conducted at high temperatures.

In the tests conducted in water vapor at 1000°C , deposits were observed over the furnace tube’s internal surfaces (Figure 3.53). B and O elements were also detected by EDS in these deposits. These results showed that boron oxide was able to form in water vapor-containing environments. In the same test, black colored deposits were also seen inside the furnace tube regions closer to the B_4C sample (Figure 3.53). Besides B and O elements, carbon was also present in these deposits. Based on these experimental observations, it is concluded that gaseous oxidation products expected to form according to the thermodynamical calculations in Table 3.5 did form during the tests conducted in this study.

3.5.3. Kinetic Evaluations of the Oxidation Test Results

Kinetic aspects of the oxidation reactions of boron compounds can be evaluated by considering the relationship between the measured weight changes of the samples

and the temperature and duration of the oxidation tests. Also, nature and properties of the oxidation products need to be considered because they have significant effects on the weight changes. For example, if the oxidation products were all solid and did not spall (fall off) from their substrates (powders or pellets), then the substrates would only have weight increases. However, if the corrosion products were gases, only weight losses would be observed. On the other hand, in the case of liquid corrosion products, either weight gains or weight losses could be expected. However, corrosion products in different forms can also form simultaneously during chemical reactions as observed in this study.

In order to understand the kinetics of the oxidation reactions, generally, weight changes calculated per unit surface area of the sample $[(\Delta m/A)]$ are reported. In Figure 3.61, $[(\Delta m/A)]$ values measured for the boride pellets after oxidation are plotted as a function of both the time and temperature.

These graphs show that TiB_2 and ZrB_2 samples gained weight during oxidation at all temperatures. This result is consistent with XRD analyses which showed the formation of solid oxide products; TiO_2 and ZrO_2 in these samples. There was evidence also for the formation of liquid boron oxide during the same tests. Although the liquid phase was expected to be volatile at high temperatures such as $1200^\circ C$, the observed weight gains for these samples suggested that the amount of the solid oxide formed must have been higher than the amount of volatile boron-containing products. The same graphs also show that weight gains of the ZrB_2 pellets decreased as the test temperature increased. Since the amount of volatile products increases with temperature, it is possible that the decrease in the weight gain of ZrB_2 was related to the formation and evaporation of boron oxide from ZrB_2 pellets. TiB_2 had higher weight gains at $1200^\circ C$ suggesting the development of protective oxide surface layers.

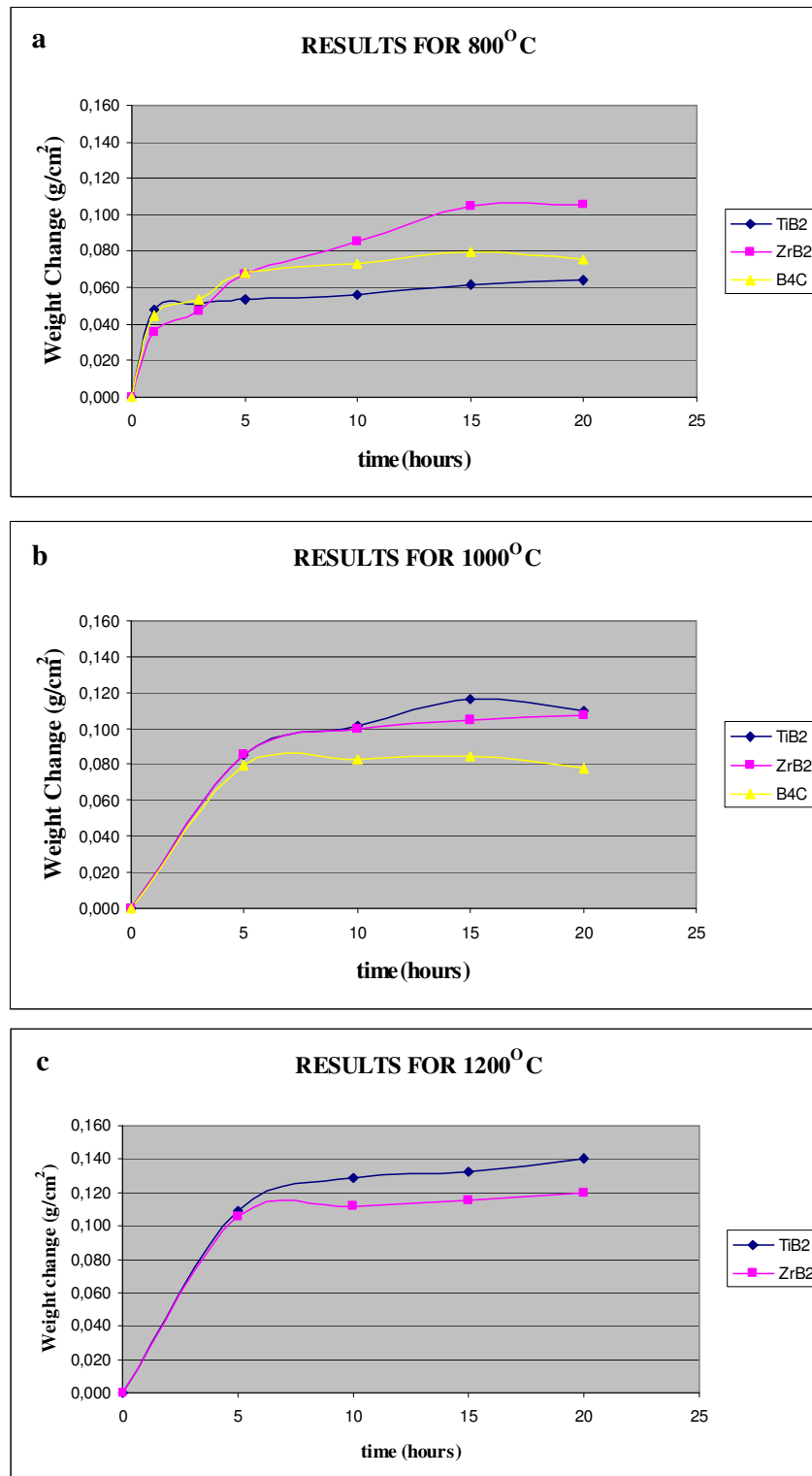


Figure 3.61 Weight changes of TiB₂, ZrB₂ and B₄C compounds oxidized at (a) 800°C, (b) 1000°C and (c) 1200°C in this study.

Carbon in the B_4C compound could form only gaseous products during the tests. However, weight gains were observed for this compound at $800^\circ C$ and $1000^\circ C$. However, the rate of weight gain was lower at $1000^\circ C$. After 20 hours of oxidation, weight losses were observed for B_4C . These results can be explained by proposing that the initial weight increase at low temperatures was caused by boron oxide formation. At higher temperatures, volatilization of boron oxide and formation of the gaseous oxidation products of carbon must have increased the weight loss of this material. It is necessary to remember that black-colored deposits were observed near the B_4C pellet during its oxidation in water vapor.

In Figure 3.61, it is also observed that weight changes of the borides increased with temperature. This increasing rate of oxidation with increasing thermal energy suggested that the behavior is of an Arrhenius type. Since the corrosion products are formed by the reaction of the elements in the borides with the oxygen in the environment, the rate of the reaction is controlled by the diffusion of the elements involved. Thus, diffusion process is expected to be the mechanism that controlled the kinetics of the oxidation of boron compounds.

Kinetic behavior of the scale forming materials can be described by the following expression, discussed earlier as Equation 1.9, where "X" is the weight change of the

$$X^n = k t$$

material per unit surface area ($\Delta m / A$) or the thickness of the scale layer, "t", the time (experiment duration) and "k" the kinetic coefficient of the relationship between (X) and (t). In other words, "k" indicates the "rate" of the reaction, "n" is an exponential coefficient related to the mechanism of the reaction. The coefficient "n" can take values such as 1, 2, 3, indicating that the dependence of ($\Delta m / A$) on (t) is linear, parabolic or cubic, respectively.

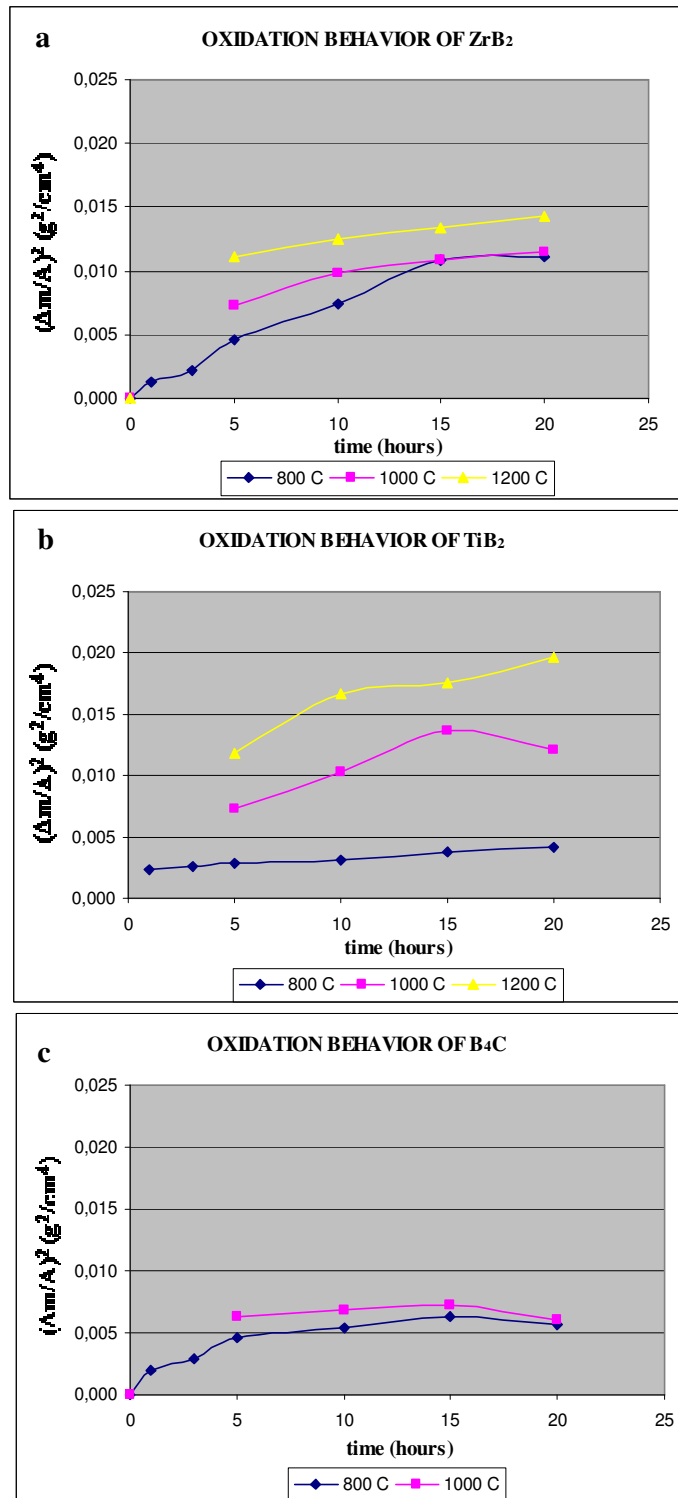


Figure 3.62 Weight change per unit area squared $[(\Delta m/A)^2]$ vs experiment duration(t) for (a) ZrB₂, (b) TiB₂ and (c) B₄C.

In many high temperature oxidation studies, it has been observed that if the corrosion products formed on the substrate are solids with low vapor pressure, thicknesses of the solid product (scale) increase with time according to the “parabolic” kinetics (Kofstad, 1988). In order to examine the kinetic behavior of TiB_2 , ZrB_2 and B_4C samples, the weight change data in Figure 3.61 are rearranged to plot graphs so that the kinetic coefficient is 2. These new graphs are shown in Figure 3.62.

In Figure 3.62, the squared values of the specific weight changes $[(\Delta m/A)^2]$ are plotted as a function of the experiment duration(t). Thus, if the weight gains are “parabolic”, the lines in these graphs should be linear. For the oxidation tests at 800°C in which experimental data were collected for less than 5 hours, it can be said that TiB_2 samples showed a parabolic behavior. A similar behavior for ZrB_2 samples was observed approximately after 15 hours at 800°C . B_4C samples which did not form solid oxide phases showed a limited parabolic behavior at 800°C for a shorter time period of about 5 hours. The rate of weight gain of the B_4C samples also decreased with increasing time as can be seen from the slopes of the lines in the graphs.

Experimental data obtained at 1000 and 1200°C showed that the amount of corrosion products increased with the increasing temperature. After similar test times, weight gains of TiB_2 were higher than those of ZrB_2 and B_4C . At these temperatures, kinetics of the oxidation reactions did not seem to be parabolic. As the rate of weight gain with time decreased, after long term oxidation, net weight losses were observed. This type of oxidation behavior can be explained by the removal of a gaseous product, probably the boron oxide vapor from the samples. Such a behavior was possible since vapor pressure of a liquid increases with temperature. In other studies, similar kinetic and mechanistic behaviors were reported for TiB_2 and ZrB_2 (Irving & Worsley, 1968). For B_4C , besides volatilization of boron oxide, C containing gaseous products are also believed to play an important role in the weight loss of B_4C .

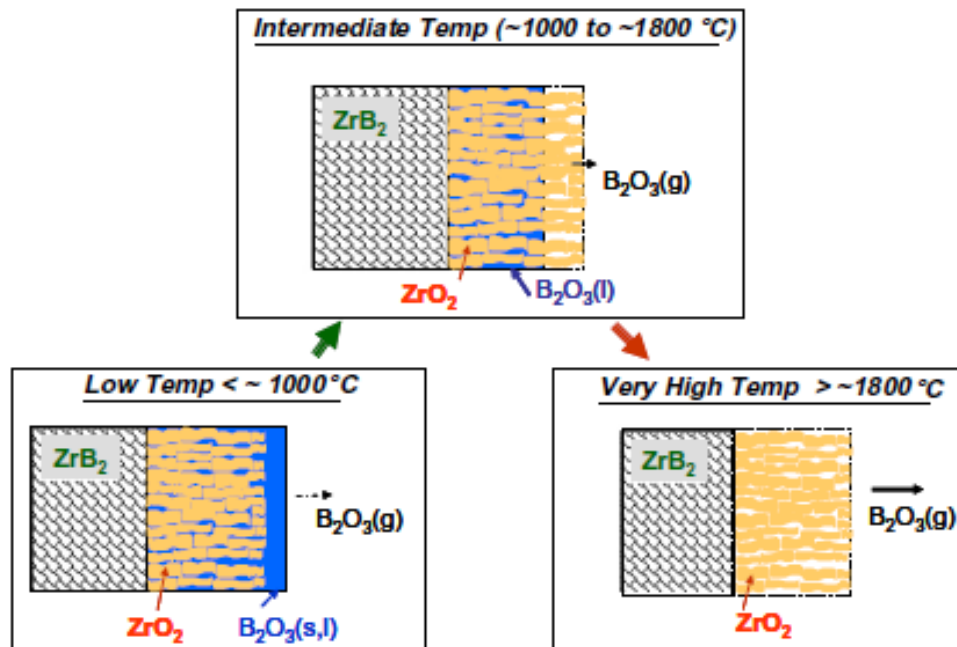


Figure 3.63 Schematic representation of the suggested mechanistic model for the oxidation of ZrB₂ between 1000 – 1800°C in air (Parthasarathy, 2007).

Recently, mechanistic and kinetic modeling studies for the so called “high-temperature ceramics” (TiB₂, ZrB₂ and HfB₂) have been reported in the literature. In one such study, Parthasarathy et al proposed an oxidation model for some borides using the experimental data in the literature. Figure 3.63 shows the corrosion products and microstructures of the borides proposed in the study (Parthasarathy et al., 2007).

According to this model, solid ZrO₂ and liquid boron oxide phases formed after the oxidation of ZrB₂ as indicated in Table 3.9. Oxide layers are thought to grow as “columnar” grains while the liquid boron oxide is present in the lower part of the pores between this columnar structure. It is proposed that at temperatures below 1000°C, pores will be completely filled with liquid boron oxide and at temperatures higher than 1800°C the pores will be completely empty due to the volatilization of boron oxide. This model is considered only for the intermediate temperature zone in detail with the assumption that the oxidation rate of the samples depend on the diffusion rate of oxygen through the pores and liquid boron oxide.

In order to compare the experimental data obtained in our study to those of this proposed model, cross sectional views of the oxidized TiB_2 samples were examined with SEM and EDS. Figures 3.64-66 show the microstructures of the samples after oxidation. It is observed that different microstructures were formed at different experimental temperatures. For example, after oxidation at 800°C for 5 hours, the developed microstructure contained some porosity at about a depth of $70\ \mu\text{m}$ from the sample surface (Figure 3.64). Ti, B and O elements were determined in the EDS analyses in this region. Closer to the outer surface of this region, a layer containing boron and oxygen is observed. In other studies, formations of similar microstructures were also reported (Koh et al, 2001). Moreover, this observed microstructure is similar to the proposed “intermediate temperature” model structure in Figure 3.63 for $T < 1000^\circ\text{C}$. But, in Figure 3.64 no “columnar” structure was observed at the oxidized region. This can be due to the short oxidation time used for this sample

In our study microstructures of the TiB_2 pellet samples changed with increasing temperature and time. The sample shown in Figure 3.65 was oxidized at 1000°C for 20 hours. Here, columnar grains which joined each other were observed in the region down to a depth of about $300\ \mu\text{m}$ from the sample surface. Polishing has made the pores between the columns more visible.

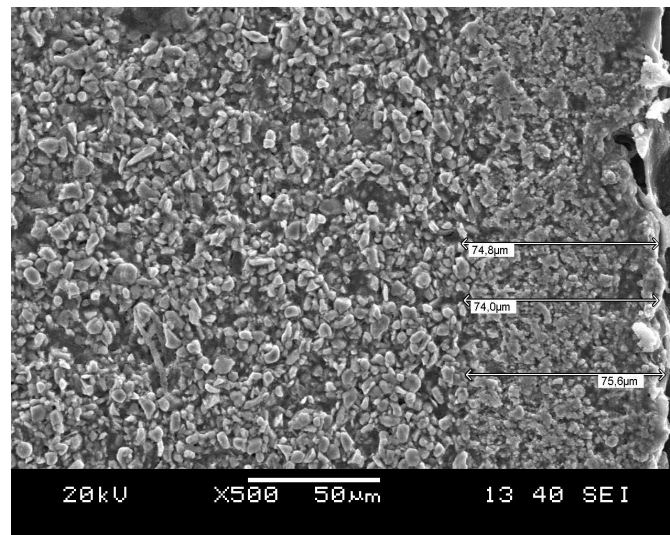


Figure 3.64 SEM image of the TiB_2 pellet oxidized at 800°C in air for 5 hours.

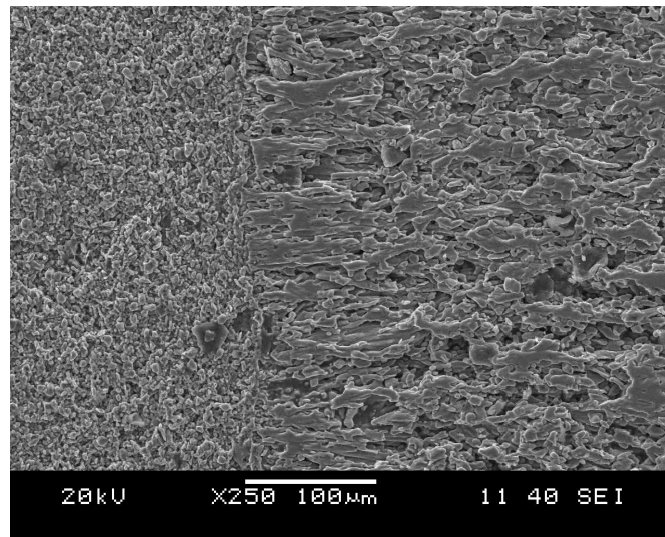


Figure 3.65 SEM image of the TiB₂ pellet oxidized at 1000°C in air for 20 hours.

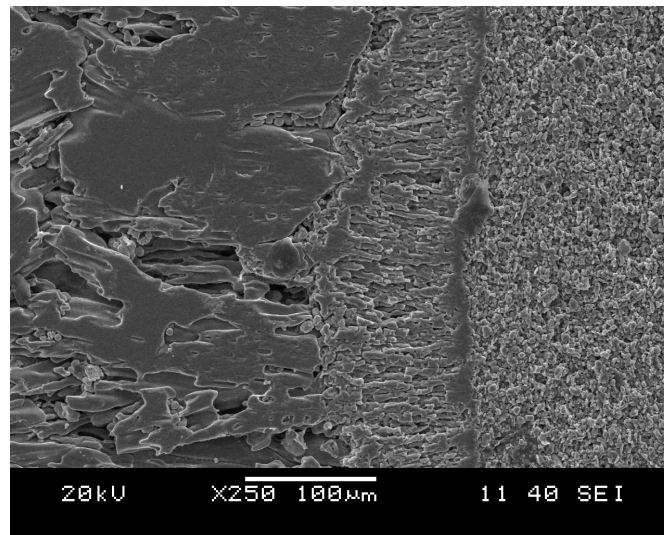


Figure 3.66 SEM image of the TiB₂ pellet oxidized at 1200°C in air for 10 hours.

TiB₂ pellets that were oxidized at 1200°C for 10 hours had large amounts of columnar grains which had grown closer to each other. Thus, after polishing, these interconnected grains caused the formation of the wide and planar areas in the microstructure as seen on the left side in Figure 3.66. Porous regions can also be seen in this SEM image. However, boron oxide was not observed between these pores. Evaporation of the liquid boron oxide during the experiment must have caused this

lack of liquid there. Also in the same SEM picture, a region which separates the oxidized and the unoxidized regions of the sample was present. The depth of the oxidized region is around 600 μm and this value is twice the oxidized zone developed at 1000°C for the same oxidation time.

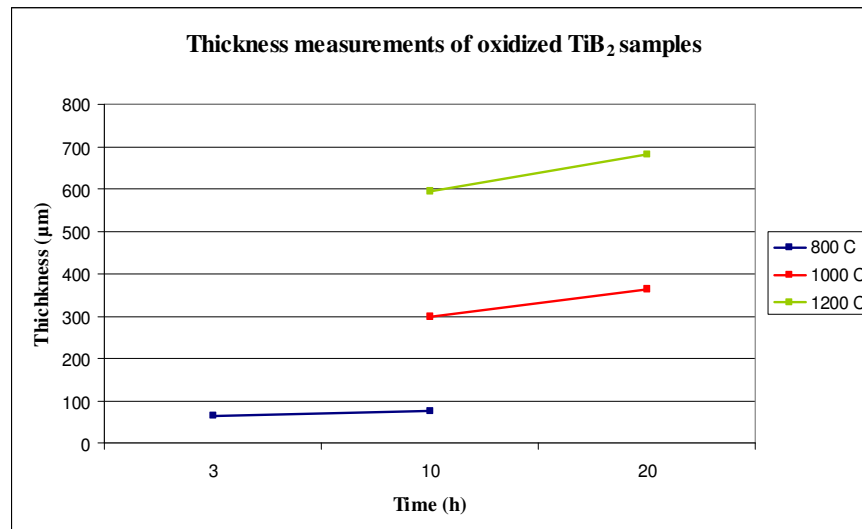


Figure 3.67 Thickness measurements for TiB₂ samples after oxidation at ambient air conditions.

Figure 3.67 shows thicknesses of the oxidized zone measured from the above cross-sectional SEM micrographs for the TiB₂ pellets. Although the experimental data are limited, it is observed that the change in oxide thicknesses with time and temperature is similar to the change in weight gains shown in Figures 3.61 and 3.62.

When we compare our experimental data (sample weight changes) with those of the modeling study referenced above, it is observed that our ($\Delta m/A$) values for TiB₂ and ZrB₂ were higher. It is thought that such discrepancies are the result of differences between the physical properties of the samples used in different studies. The tablet samples used in our studies were obtained by cold pressing of the compound powders. Also, sintering for the densification of the samples was not practiced. Consequently, the amounts of porosity in our samples were higher as observed in the microstructure pictures given above. During oxidation, oxygen in the

environment used the open pores in the structure for diffusion thus bringing about a higher oxidation rate for the test samples.

3.6 Applications of Boron Containing Materials

3.6.1 Production Metal Added TiB₂ Pellets

In the previous chapters, it is mentioned that titanium diboride (TiB₂) is an attractive material and has a wide range of applications because of its excellent physical and chemical properties (Lotfi, 2010). However, applications of TiB₂ are limited mainly because of its low sinterability and poor mechanical properties, such as flexural strength and fracture toughness (Li et al., 2002). Besides, TiB₂ has covalent bonding thus high melting temperature. Also Ti and B have low self-diffusion coefficients so sinterability of TiB₂ is rather poor (Khanra et al., 2007). Therefore, densification of TiB₂ requires high temperatures (≥ 2000 °C) (Li et al., 2002). As a result, most of the research in this area is focused on using various sintering additives to attain maximum densification of the composite (Venkateswaran et al., 2006).

On the other hand different strategies have been developed for brittle materials such as ceramics to increase their strength toughness. The use of a metal matrix has been the most studied route for improving not only the mechanical properties but also sinterability of titanium diboride. For this purpose metals like iron, cobalt and nickel have been used as additives to promote liquid phase sintering of TiB₂. By following this route, several TiB₂ cermets were produced with different metallic binders (Sánchez et al., 2000).

In this study, few attempts were made to produce metal-added TiB₂ pellets by using the Vacuum Arc Melting (VAM) process. Below, these studies are summarized.

3.6.1.1 Production of the pellet samples

VAM process is generally used for melting of metallic materials. It has a water-cooled copper hearth and uses non-consumable tungsten electrode for heating the charge by striking an arc between the electrode and the charge. This is done in an inert gas environment to prevent oxidation of the charge materials. The VAM equipment used in this study is shown in Figure 3.68.

3.6.1.2 Tests conducted on the samples

Initially, a TiB_2 pellet was used to observe the effect of arching on the boride pellet. The 70 Ampere (A) arc was observed to be non-uniform at the pellet surface. The pellet broke into several pieces and one of them turned red under the 50A arc indicating heating of the pellet (Figure 3.69).



Figure 3.68 Vacuum arc melting equipment.

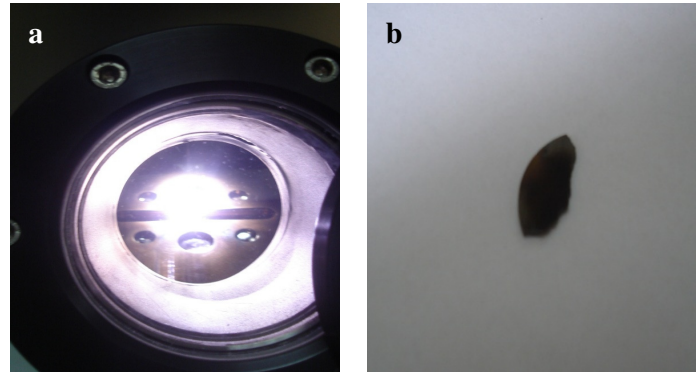


Figure 3.69 (a) arc formation in VAM, (b) broken pellet.

In an other test, TiB_2 pellet containing 20 w/o Al was used. The 58A arc formed over this sample was uniform. This result suggested that the conductivity of the pellet was increased by the Al powder. Figure 3.70a shows the SEM image of the TiB_2 -20%Al pellet surface. Besides a crack, areas appearing either bright or dark were observed at the sample surface. EDS analysis indicated 96 % Ti and 3 % Al in the dark area. In the bright area, oxygen was detected besides Al and Ti. These results suggested the oxidation of the pellet surface.

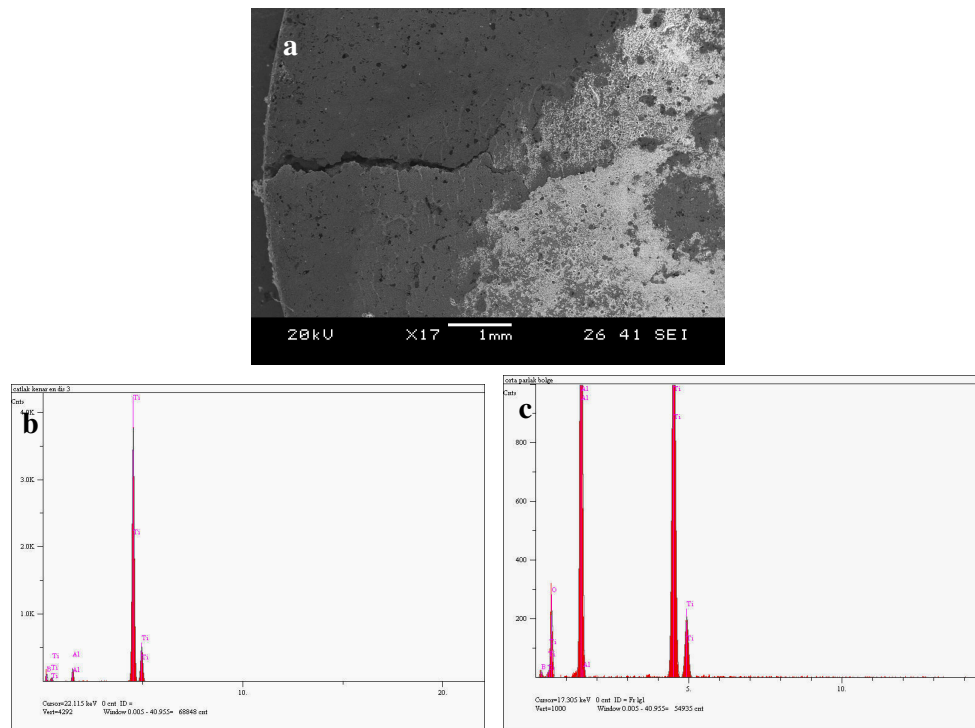


Figure 3.70 (a) SEM image of the TiB_2 -20%Al pellets after heating in VAM, (b) EDS result for the dark area (c) EDS result for the bright area on the pellet surface.

After these preliminary tests, TiB₂ pellets containing 316L-type stainless steel (abbreviated as “316” below) were made and their heat treatment in VAM was investigated. Table 3.6 lists the compositions and measured weight changes of the pellets as well as the other test conditions.

Table 3.6 The compositions of the pellets, measured weights and applied arc currents.

Test no	Composition by volume (%)	Weight before test (gr)	Weight after test (gr)	Weight change	Applied arc current (A)
1	100% 316L	2.43	2.40	-0.03	40
2	100% 316L	2.64	2.56	-0.09	60-80
3	100% 316L (heat treated)	2.84	2.85	+0.01	60
4	100% 316L (heat treated powder)	1.66	1.51	-0.15	60
5	90% 316L-10%TiB ₂	2.36	2.13	-0.23	40-50
6	70% 316L-30%TiB ₂	1.63	1.61	-0.03	60-80
7	50% 316L-50%TiB ₂	2.16	2.11	-0.05	40-60
8	30% 316L-70%TiB ₂	1.56	1.54	-0.02	40-50
9	10% 316L-90%TiB ₂	1.27	1.26	-0.01	40-50
10	100%TiB ₂	1.51	1.68	+0.16	60-80

In Test 1 (T1), a pellet with 100% 316 was used. 40 A arc was formed over the pellet surface but arcing was non-uniform on the pellet surface and volatilization was observed. Changing the current and decreasing the distance between the sample and the electrode did not improve the arc condition. Consequently, melting of the pellet did not take place. In T2, a pellet with the same composition was used at 80A. Although the arc was still not uniform, the pellet completely melted at this higher current.

In T3, another 100% 316 pellet was prepared but it was, first, heat treated in a tube furnace. The aim of the heat treatment was to burn away the organic materials used during the production of the pellet. The furnace was heated up to 650^oC at a heating rate of 10^oC/min. and the sample was kept inside for 30 minutes. Then the

pellet placed inside the VAM. The arc formed at 58A current was uniform. Pellet surface turned red and melting was observed. The test clearly showed that the volatilization observed earlier was due to the organic material left in the pellet and that the gas emission disturbed the arcing process. In test T4, pretreatment of the powder was conducted by keeping it in the furnace before forming into a pellet. Then the pellet was processed in the VAM at 60A arc current. The arc formation was again uniform and the pellet melted completely.

Starting with T5, TiB_2 -added pellets were used. Under 40A and 50A currents, arc formation was not uniform and melting of the pellet was not achieved. Interestingly, the maximum weight loss was observed for this sample during the tests. In the next test (T6), a pellet with 70%316 and 30% TiB_2 was used. Melting of the sample started at 60A arcing. Before the melting, sample surface became red and gas evolution from the pellet was observed.

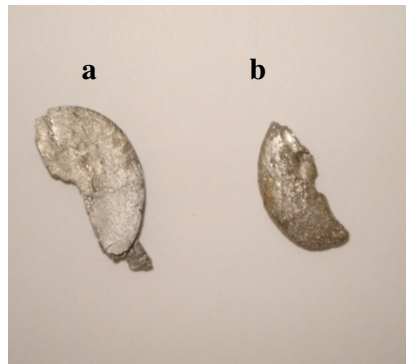


Figure 3.71 Broken pellets after (a) test T7 and (b) test T1.



Figure 3.72 Broken pellets prepared for micro-sectional analysis (a) pellet from T1, (b) pellet from T7.

In the case of the 50%316-50%TiB₂ mixture (T7), melting of the sample was at 40A under a uniform arc. When the current increased to 55A, melting at the surface was observed. By using the manipulator arm in the metler, the sample was turned over and the other surface of the pellet was process under the same arcing condition. However, the sample cracked during this operation. When it was removed from the VAM, both the outer and inner surfaces of the pellet were observed to be shiny. In Figure 3.71, broken pellets used in tests T7 and T1 are shown. In Figure 3.72, pieces from the pellets used in tests T7 and T1 are shown before their cross-sectional analyses. In the tests conducted on the TiB₂-rich pellets T8 – T10, it was difficult to obtain uniform arcing even under different current values.

Three different regions in T1 sample and two different regions in T7 sample were investigated with an optical microscope. According to the images in Figure 3.73, layered structures with longitudinal spaces between them are present in regions 1 and 3 of the T1 sample. This result indicates that melting of the 316 powder grains did not take place in these regions. However, the microstructure in region 2 showed that melting took place in this region of the pellet.

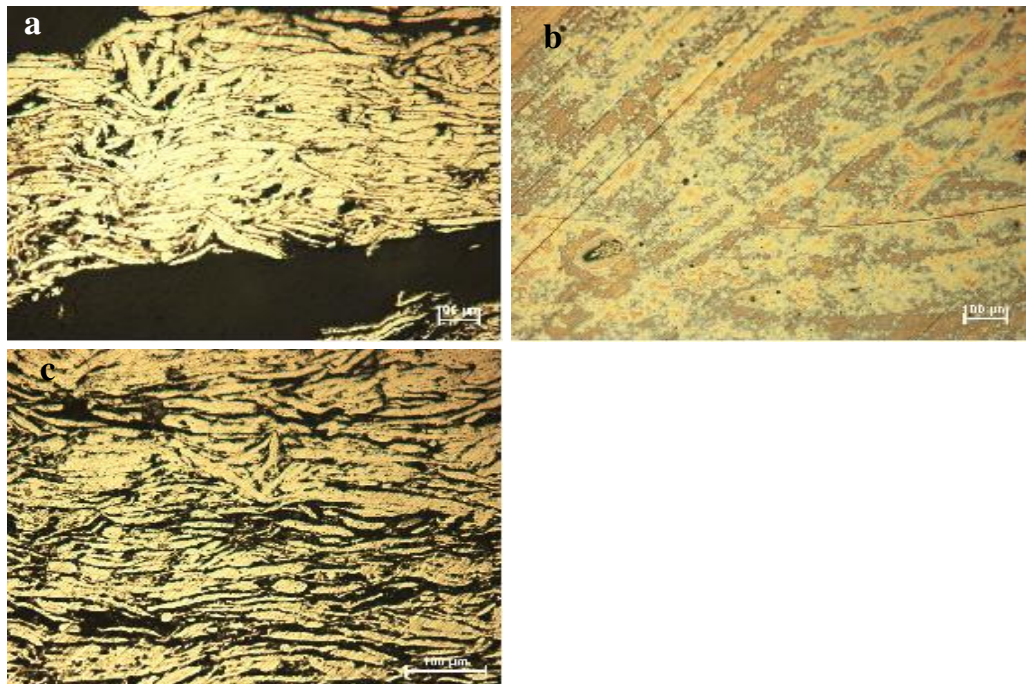


Figure 3.73 Optical microscope images (X200) for T1 sample from (a) region 1, (b) region 2, (c) region 3.

In Figure 3.74, it is clearly seen that melting did take place in both regions of the T7 sample. Porosity in the microstructure can be due to different reasons such as temperature variation in the pellet, incomplete flow (high viscosity) of the molten metal and low metal content compared to that of the boride phase.

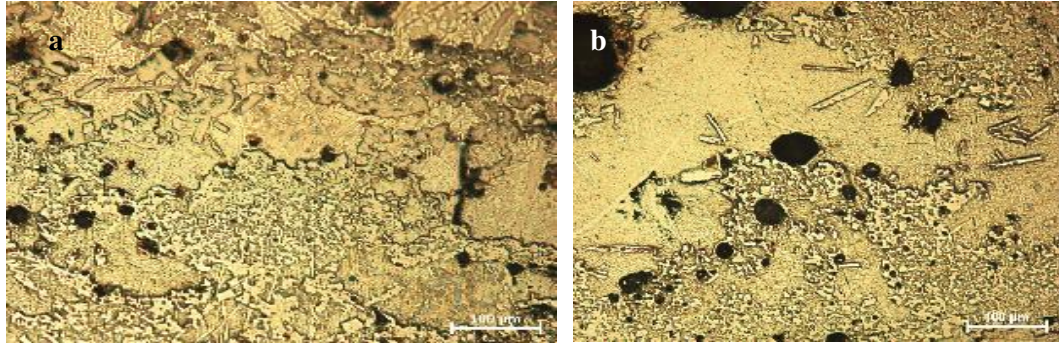


Figure 3.74 Optical microscope images of different parts of the sample used in test 7 at 200x magnification: (a) region 1, (b) region 2.

Figure 3.75 shows the SEM images of the T7 sample. In Figure 3.75.(b), bright regions contain the metal phase whereas dark regions contain TiB_2 powder since light atoms such as B appear darker in the BE image mode of the SEM. It is clear that the stainless steel powder surrounded TiB_2 powder grains showing that the ceramic phase is wetted by the metal phase. SEM images taken from the TiB_2 -rich pellet used in T9 also confirms this conclusion (Figure 3.76).

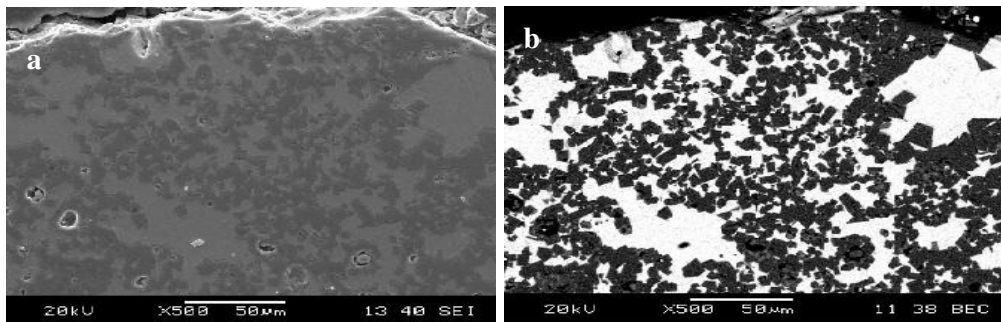


Figure 3.75 Cross-sectional SEM images (a) in SE mode and (b) BE mode for the sample T7.

This study conducted on the production of TiB_2 -base composites showed that the use of 316L-type stainless steel as the metallic phase was a proper choice because it

was able to wet the ceramic particles which are important requirement for the densification of composite materials. The tests also showed that VAM processing of composite pellets would be difficult because of the complex interactions among the material composition, arc current, electrode distance and electrical properties such as resistivity of the components. Furthermore, at high arc currents, volatilization of the metallic phase is a possibility because of its relatively lower melting temperature. Also organic additives used in the preparation of the pellets are an other source of volatilization, thus affecting the soundness of the final product.

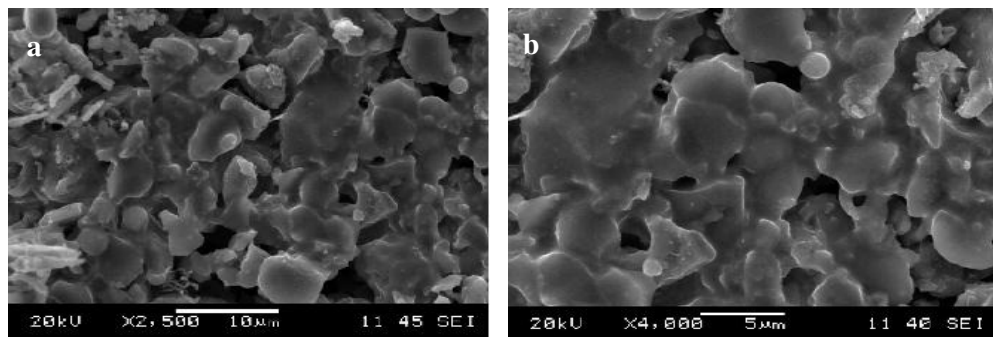


Figure 3.76 (a-b) SEM images taken from the pellet used in T9

Nevertheless, some degree of densification was achieved for a few pellets in this study. It was also observed that pretreatment of pellets before processing can lessen the negative effect of the additives. Therefore, it is necessary to plan future tests on the VAM processing of the composites after a detailed understanding of the relationship among the above mentioned variables. Also, using this processing technique for the surface modification of materials can be considered as an alternative route.

3.6.2 Production and Oxidation of Boron-Containing Ceramic Layers on Metal Substrates

In this section, experimental studies conducted on an other application of the boron compounds; namely the modification of metal surfaces by boron-containing layers is discussed. However, boron compounds studied in this section of the Thesis

work are compositionally different from the 3 boron compounds (TiB_2 , ZrB_2 , B_4C) considered in the previous sections.

Boron compounds discussed here are produced as a result of the diffusion of B from an outside source into the metal, thus forming the compound layer “in-situ” over the metal. This process is also known as “boronizing” or “boriding” as explained below. For the experimental work described in this section, stainless steel substrates were used. Thus, the boron-compounds formed over the metallic substrates during the tests were the thermodynamically stable borides of the constituent elements of the substrate alloy.

3.6.2.1 Boronizing Process

Boronizing is a thermochemical surface treatment by which boron atoms diffuse into a metal substrate to form borides at its surfaces. This process has been applied to both ferrous and non-ferrous materials including superalloys, mainly to improve their wear resistance (Jain & Sundararajan, 2002; Özbek & Bindal, 2002; Mu & Shen, 2010). Although the boronizing process can be carried out using different boron-containing mediums, pack-boronizing is the frequently used method where the substrate is embedded inside a solid powder mixture containing a boron source in a sealed container. The container is heated to the process temperature for predetermined periods to allow B diffusion into the substrate before cooling (Jain & Sundararajan, 2002).

Compared to those of the pure metals, boronizing of multicomponent alloys have been shown to be a complex process since the nature of the boride layers are determined by the thermodynamic properties of the alloying elements. While pure and single-phase borides form over the pure metals, multi-phase layers can form over the alloy substrates.

3.6.2.2 Formation of boron-containing layers

In this work, stainless steel substrates (AISI 304 grade) were used to form the boride layers. For this purpose, surfaces of the steel samples measuring 15x15x1,5 mm were polished, first with 400 and 800 grade emery papers, then with acetone ultrasonically. The boron source used was the commercial Ekabor 2 powder which has a nominal composition of 90% SiC, 5% B₄C and 5% KBF₄.

Steel samples were covered with the Ekabor 2 powder inside a metallic crucible. Then the crucible was placed inside a box furnace and heated to 950^oC to start the boronizing process. Two separate tests were conducted for 4 hours and 8 hours. After the tests two boronized samples, one from each group, were investigated by a scanning electron microscope; SEM (JEOL-JSM 6060) equipped with an energy dispersive spectrometer; EDS (IXRF System 500) and by a X-ray diffractometer; XRD (Rigaku D/Max-2200/PC) to determine the nature of the boron-containing phases developed.

The other boronized samples and samples which are not boronized were oxidized at 800^oC, in air, for a total of 20 hours in 4 cycles each lasting 5 hours. After each cycle, samples were cooled to room temperature and their weight changes were recorded. SEM and XRD analyses were conducted also on the oxidized samples.

3.6.2.3 Test Results

XRD analysis result for the steel sample boronized for 8 hours is shown in Figure 3.77. Mostly, peaks belonging to Fe₂B and FeB phases are observed. A few peaks thought to belong to the CrB phase whose formation was thermodynamically possible at the test temperature are also present. Although EDS analyses indicated Ni element in the boronized zone, it is most likely that Ni did not react with B since its boride phase has relatively lower stability.

In Figure 3.78, a cross-sectional view of the same sample is shown. As a result of B diffusion into the steel substrate, the Fe_2B phase must have formed first inside the sample. Upon thickening of this boride layer, the B-richer phase; FeB formed, as the outer layer, closer to the sample surface. Beyond the Fe_2B layer, a diffusion zone which extends into the grain boundaries, was also present. This microstructure must be the result of faster diffusion of B as well as the alloying elements such as Cr along the grain boundaries.

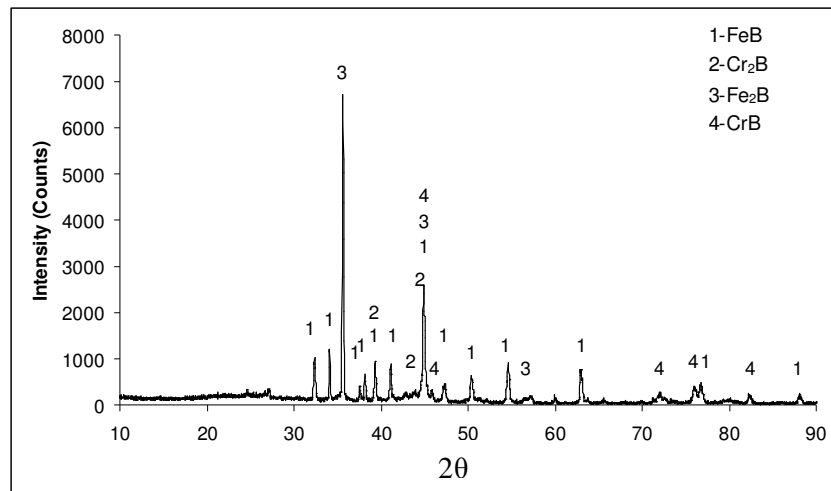


Figure 3.77 XRD analysis result for the 304 sample boronized at 950°C for 8h.

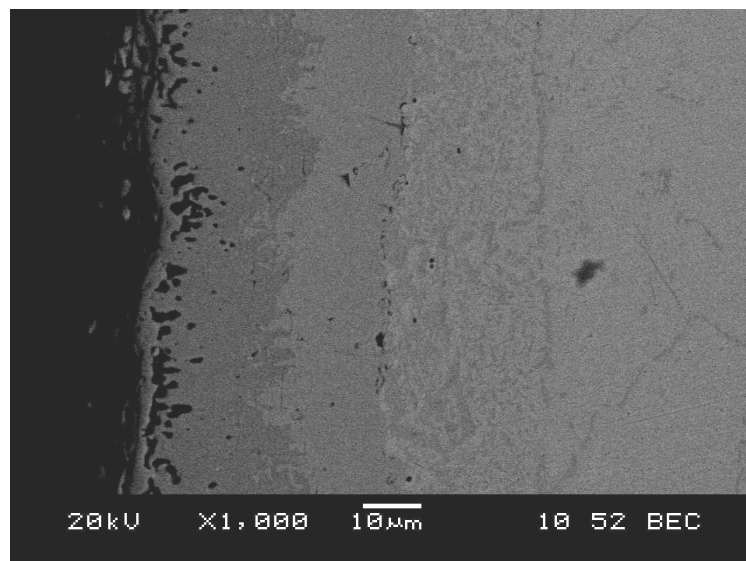


Figure 3.78 Cross-sectional SEM image of the 304 steel sample boronized at 950°C for 8 h.

In accordance with the earlier studies reported in the literature, the interface between the boronized zone and the metallic zone was flat (Campos et al, 2006; Campos-Silva et al, 2010; Yoon 1999). In an other study, Petrova et al concluded that the high alloy content of the 304 steel slows the diffusion rate of boron atoms causing the formation of a smooth interface. (Petrova et al., 2008).

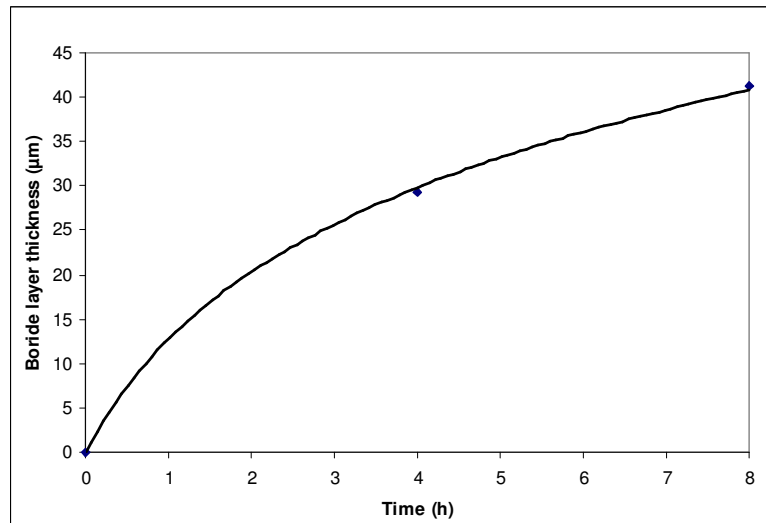


Figure 3.79 Changes in the boride layer thickness with boronization time.

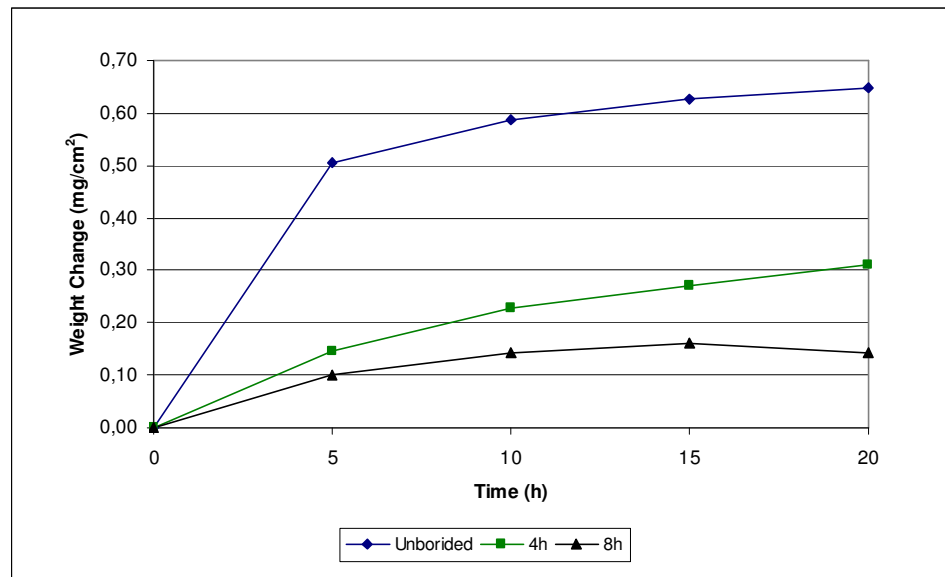


Figure 3.80 Weight changes of boronized and nonboronized samples after oxidation at 800°C.

The dependence of the boride layer thickness on the test duration is shown in Figure 3.79. Thickness values increased from 29 μm after 4 hours to 41 μm after 8 hours of boronizing as expected for a diffusion-controlled process.

Results of the cyclic oxidation tests conducted at 800°C, in air, on both boronized and non-boronized steel samples are given in Fig. 3.80. All samples were observed to have gained weight with time during oxidation. However, weight gains of the non-boronized samples were relatively higher. As for the boronized samples, those with thicker boride layers seemed to have gained less weight during oxidation. Although spallation of oxide products were observed from some of the samples during these tests, the amount was not significant compared to the amount of weight gains measured. However, weight loss of the long-term boronized sample was significant after 20-hour of oxidation.

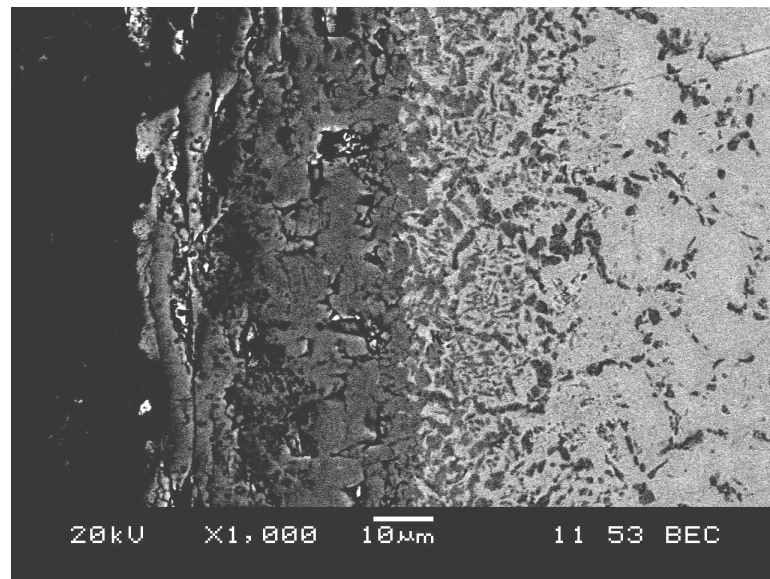


Figure 3.81 Cross-sectional SEM image of the steel oxidized at 800°C for 20 hours after boronizing for 8 hours.

Figure 3.81 shows the cross-sectional SEM image of the steel sample which had been oxidized at 800°C, in air, for 20 hours after boronizing for 8 hours. When this SEM image is compared to that in Figure 3.78, it can be seen that microstructures of both the outer FeB and the inner Fe₂B layers were modified by the oxidation of the

sample. Porosity and fine cracks were observed in this modified zone. However, oxidation product spallation from this zone did not take place. This observation supports the above mentioned experimental result that spallation from the samples during oxidation were not significant.

Another conclusion that can be reached by considering the SEM images in Figures 3.81 and 3.78 is that the thickness of the diffusion zone in the boronized samples did not change significantly after the oxidation of the samples. However, its morphology after oxidation changed indicating compound formation both inside the grains and along the grain boundaries. Such a process was possible in the case of oxygen arrival to the diffusion zone. Oxidation of alloying elements such as Cr and even borides of this and other alloying elements in the alloy would have taken place because of the higher thermodynamic stabilities of metal oxides than those of metal borides (Garrett, 1998).

The XRD analysis result in Figure 3.82 shows that the main oxidation product in the oxidation tests was the oxygen-rich Fe_2O_3 phase. This was not unexpected since the boride layers over the steel samples would have oxidized to form oxides of all components of the borides, simultaneously, as discussed in Section 3.7.

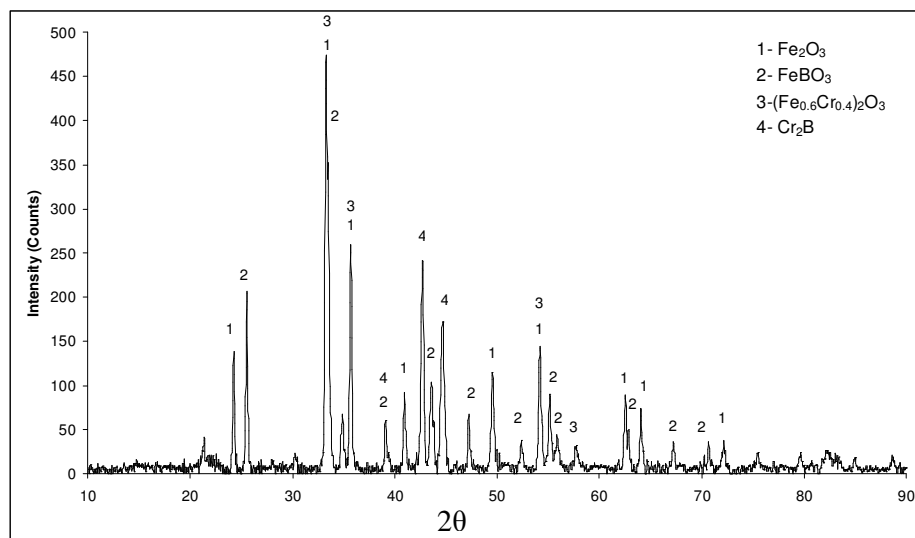


Figure 3.82 XRD graph of the steel oxidized at 800°C for 20 hours after boronizing at 950°C for 8h.

Consequently, the B_2O_3 phase, too, must have been formed during the same oxidation tests. This phase was liquid during the tests conducted at $800^\circ C$ because it melts above $400^\circ C$. Besides this study, others showed that liquid B_2O_3 can act as a protective coating against oxidation (Rizzo, 1960; Sen et al, 2006). In the oxidation modeling proposed by Parthasarathy, diffusion of oxygen through the liquid boron oxide is considered as the rate determining step for the oxidation of the borides (Parthasarathy et al., 2007) study.

Furthermore, it is reasonable to think that liquid boron oxide present among the oxidation products at the test temperature of $800^\circ C$ solidified during cooling of samples in the cyclic oxidation tests. The solid boron oxide phase might have prevented spalling of the oxidation products by acting as glue among the oxidation products. This type of a behavior was observed during the oxidation of the boride powders, mixing of which became difficult after oxidation tests conducted, in this study, at high temperatures in air.

Some of the XRD peaks in Figure 3.82 suggested that the iron borate phase; $FeBO_3$ also formed during the oxidation tests conducted. Petrova et al, discussed that at about $550^\circ C$, iron borates; $Fe_2B_4O_7$, FeB_2O_4 , and $FeBO_3$ are stable. At temperatures above $800^\circ C$, only $FeBO_3$ was the stable phase but it later dissociated into liquid B_2O_3 and solid Fe_2O_3 (Petrova et al., 2008).

CHAPTER FOUR

CONCLUSIONS

In this Thesis, high temperature oxidation behavior of three different boron-containing compounds; TiB_2 , ZrB_2 and B_4C were studied. Additionally, two applications of borides were investigated. Main conclusions of this study are presented below:

1. Boride powders obtained from commercial sources and used in “as-received” condition had different properties. TiB_2 powder had both rounded and edged grains whereas B_4C powder contained only edged grains with uniform dimensions. ZrB_2 powder had differently sized grains which are agglomerated to form larger particles. Analyses showed that specific surface area values were in the order $\text{TiB}_2 > \text{ZrB}_2 > \text{B}_4\text{C}$ and their average particle sizes were in the order $\text{TiB}_2 < \text{ZrB}_2 < \text{B}_4\text{C}$. XRD analyses of the boride powders did not show other phases.
2. During high temperature oxidation (300-800°C) in air, color changes were observed for TiB_2 and ZrB_2 powders but not for the B_4C powder. This was due to the formation of solid oxidation products such as TiO_2 and ZrO_2 over TiB_2 and ZrB_2 powders whose surface colors were different than those of the oxides. Since B_4C does not have solid oxidation products, its color did not change.
3. After oxidation between 300-500°C in air, TiB_2 , ZrB_2 and B_4C powders became less mixable. Based on the SEM/EDS and XRD analyses as well as the related thermodynamic data, it is concluded that liquid oxidation products such as boron oxide formed around the powder grains and caused to adhere to each other during cooling. Thus, mixing of powder grains become difficult.
4. During the oxidation tests conducted at 800°C in air, pellet samples of all three borides gained weight. This result indicated TiO_2 and ZrO_2 formation for TiB_2 and ZrB_2 , respectively. Weight gains of these borides increased also with time indicating a parabolic-type kinetic behavior. Since B_4C could not

form solid reaction products, its weight gain is thought to be the result of formation of liquid boron oxide which was stable at this temperature.

5. Weight gains of TiB_2 and ZrB_2 pellets increased with temperature as well as with time. However, B_4C pellets did not show a similar behavior. Furthermore, B_4C pellets lost weight after 20 hours at 1000°C . These results support the view that high temperature oxidation of B_4C is controlled by the formation and evaporation of liquid boron oxide. Oxidation tests at 1200°C could not be conducted on B_4C pellets because of their unstability at this temperature.
6. After the oxidation test in the water vapor-containing environment at 1000°C , B_4C pellet gained much lower weight than it would have in air. This was because of the large amount of gaseous products evolved from this boride. ZrB_2 pellet gained more weight than it would have after oxidation in air. The TiB_2 pellet, on the other hand, gained almost the same weight as it would have gained in air at 1000°C . These results and the SEM observations suggested that growth rate of ZrO_2 may be dependent on the humidity of the oxidizing environment.
7. The application-oriented study related to TiB_2 -based composite production, showed that stainless steel was a proper choice as the metallic phase. However, complex interactions observed among the equipment operation and the material properties indicate that VAM processing of the composites will be difficult for bulk products. However, the process can be developed for applications to surfaces of materials.
8. In the other applied study, it was observed that the iron boride layer, thermochemically formed over stainless steel samples, decreased the weight gain of steel during its oxidation at 800°C . The boride layer is thought to have slowed down the access of oxygen to the steel by forming protective oxidation products which possibly contained glassy phases.

REFERENCES

- Baik, S., & Becher, P.F. (1987). Effect of Oxygen Contamination on Densification of TiB₂. *Journal of American Ceramic Society*, 70 (8), 527–30.
- Barandika, M.G., Sanchez, J.M., Rojo, T., Cortes, R., & Castro, F., (1988) Fe–Ni–Ti Binder Phases for TiB₂-based Cermets: A Thermodynamic Approach. *Scripta Materiala*, 39 (10), 1395–400.
- Barin I. (1995). *Thermochemical Data of Pure Substances*, vol.2. (3rd ed). Weinheim: VCH
- Birks, N., & Meier, G.H. (1983). *Introduction to the High-Temperature Oxidation of Metals*. London:Edward Arnold (Publishers) Ltd.
- Campos, I., Palomar, M., Amador, A., Ganem, R., & Martinez, J. (2006). Evaluation of the corrosion resistance of iron boride coatings obtained by paste boriding process. *Surface & Coatings Technology*, 201, 2438–2442.
- Campos-Silva, I., Ortiz-Domínguez, M., Bravo-Bárceñas, O., Doñu-Ruiz, M.A., Bravo-Bárceñas, D., Tapia-Quintero, C., et al. (2010). Formation and kinetics of FeB/Fe₂B layers and diffusion zone at the surface of AISI 316 borided steels. *Surface & Coatings Technology*, 205, 403–412.
- Chen, L., Gu, Y., Yang, Z., Shi, L., Ma, J., & Qian, Y. (2004). Preparation and Some Properties of Nanocrystalline ZrB₂ Powders. *Scripta Materiala*, 50, 959–961.
- Dokumacı, E. (2006). Investigation of High and Low Temperature Corrosion Behaviour of Nickel-Base Alloys, Master of Science Thesis, Dokuz Eylül University, Department of Metallurgical and Materials Engineering.

- Fahrenholt, W.G. (2007). Thermodynamic Analysis of ZrB₂-SiC Oxidation: Formation of a SiC-Depleted Region. *Journal of American Ceramic Society*, 90 (1), 143–148.
- Garrett, D.(1998). *Borates Handbook of Deposits, Processing, Properties, and Use*. California: Academic Press.
- Guo, S., Mizuguchi, T., Ikegami, M., & Kagawa, Y. (2011). Oxidation behavior of ZrB₂-MoSi₂-SiC composites in air at 1500°C. *Ceramics International*, 37, 585–591.
- Han, J., Hu, p., Zhang, X., Meng, S., & Han, W. (2008). Oxidation-resistant ZrB₂-SiC composites at 2200°C. *Composites Science and Technology*, 68, 799–806.
- Hu, P., Guolin, W., & Wanga, Z. (2009). Oxidation mechanism and resistance of ZrB₂-SiC composites. *Corrosion Science*, 51, 2724–2732.
- Irving, R. J., & Worsley, I. G. (1968). The Oxidation of TiB₂ and ZrB₂ at High Temperatures. *Journal of Less Common Metals*, 16, 103-112.
- Jacobson, N., Farmer, S., Moore, A., & Sayir, H. (1999). High-Temperature Oxidation of Boron Nitride:I, Monolithic Boron Nitride. *Journal of American Ceramic Society*, 82 (2), 393–398
- Jain, V., & Sundararajan G. (2002). Influence of the pack thickness of the boronizing mixture on the boriding of steel. *Surface and Coatings Technology*, 149, 21–26.
- Kang, E.S., Jang, C.W., Lee, C.H., Kim, C.H., & Kim, D.K. (1989). Effect of Iron and Boron Carbide on the Densification and Mechanical Properties of Titanium Diboride Ceramics. *Journal of American Ceramic Society*, 72 (10), 1868–72.

- Karlsdottir, S., N., & Halloran, J., W. (2009). Oxidation of ZrB₂-SiC: Influence of SiC Content on Solid and Liquid Oxide Phase Formation. *Journal of American Ceramic Society*, 92 (2), 481–486.
- Khanna, A.S. (2002). *High Temperature Oxidation and Corrosion*, USA: ASM International.
- Khanra, A.K., Godkhindi, M.M., & Pathak L.C. (2007). Sintering behaviour of ultra-fine titanium diboride powder prepared by self-propagating high-temperature synthesis (SHS) technique. *Materials Science and Engineering A*, 454–455, 281–287.
- Koh, Y.H., Lee, S.Y., & Kim, H.E. (2001). Oxidation Behavior of Titanium Boride at Elevated Temperatures. *Journal of American Ceramic Society*, 84 (1), 239–241
- Kofstad, P.(1998). *High Temperature Oxidation Corrosion*. England:Elsevier Applied Science Publishers.
- Konigshofer, R., Furnsinn, S., Steinkellner, P., Lengauer, W., Haas, R., Rabitsch, K., et al. (2005). Solid-State Properties of Hot-Pressed TiB₂ Ceramics. *International Journal of Refractory Metals and Hard Materials*, 23, 350–7.
- Kuşoğlu, İ. M. (2004). *İleri Teknik Seramik Üretimi*, Dokuz Eylül University, Metallurgical and Materials Engineering, Master of Science Thesis, İzmir.
- Lee, D.B., Lee, Y.C., & Kim, D.J. (2001). The Oxidation of TiB₂ Ceramics Containing Cr and Fe. *Oxidation of Metals*, Vol. 56, 177-189.
- Li, L.H., Kim, H.E., & Kang, E.S. (2002). Sintering and Mechanical Properties of Titanium Diboride with Aluminum Nitride as a Sintering Aid. *Journal of European Ceramic Society*, 22, 973–7.

- Li, Y.Q., & Qiu, T. (2007). Oxidation behaviour of boron carbide powder. *Materials Science and Engineering A*, 444, 184–191.
- Lotfi, B. (2010). Elevated temperature oxidation behavior of HVOF sprayed TiB₂ cermet coating. *Transactions of Nonferrous Metals Society of China*, 20, 243-247.
- Matkovich, V.I. (1977). *Boron and Refractory Borides*, New York: Springer-Verlag.
- Monteverde, F., Guicciardi, S., & Bellosi, A. (2003). Advances in Microstructure and Mechanical Properties of Zirconium Diboride Based Ceramics. *Materials Science and Engineering A*, 346, 310-319.
- Moricca, M.D.P. (2009). *High Temperature Oxidation Characteristics Of Nb-10W-XCr Alloys*. Doctor of Philosophy Thesis, The University of Texas at El Paso, Department of Metallurgical and Materials Engineering.
- Mu, D., & Shen, B. (2010). Oxidation resistance of boronized CoCrMo alloy, *International Journal of Refractory Metals & Hard Materials*, 28, 424–428.
- Muolo, M.L., Ferrera, E., Novakovic, R., & Passerone, A. (2003). Wettability of Zirconium Diboride Ceramics by Ag, Cu and Their Alloys with Zr. *Scripta Materialia*, 48, 191–196.
- Murthy T.S.R.Ch., Basu, B., Balasubramaniam, R., Suri, A.K., Subramanian, C., & Fotedar, R.K. (2006). Processing and Properties of TiB₂ with MoSi₂ Sinter-Additive: A First Report, *Journal of American Ceramic Society*, 89 (1), 131–8.
- Murthy, T.S.R.Ch., Balasubramaniam, R., Basu, B., Suri, A.K., & Mungole, M.N. (2006). Oxidation of Monolithic TiB₂ and TiB₂-20 wt.%MoSi₂ Composite at 850°C. *Journal of the European Ceramic Society*, 26, 187–192

- Özbek, I., & Bindal, C. (2002). Mechanical properties of boronized AISI W4 steel. *Surface and Coatings Technology*, 154, 14–20.
- Parthasarathy, T.A, Rapp, R.A., Opeka, M., & Kerans, R.J. (2007). A Model for the Oxidation of ZrB₂, HfB₂ and TiB₂. *Acta Materialia*, 5, 5799–6010.
- Pekin, Ş. (1992). *Hekzagonal Bor Nitrür Sentezinde Reaksiyon Hızını Kontrol Eden Aşamalar ve Turbostratik-Hekzagonal Yapı Geçişi*, İ.T.Ü. Fen Bilimleri Enstitüsü, Yüksek Lisans Tezi, İstanbul.
- Peng, F., & Speyer, R.F. (2008). Oxidation Resistance of Fully Dense ZrB₂ with SiC, TaB₂, and TaSi₂ Additives. *Journal of American Ceramic Society*, 91(5), 1489–1494.
- Petrova, R.S., Suwattananont, N., & Samardzic, V. (2008). The Effect of Boronizing on Metallic Alloys for Automotive Applications, *JMEPEG*, 17, 340–345.
- Pierson, H.O. (1996). *Handbook of Refractory Carbides and Nitrides*, William Andrew Publishing / Noyes.
- Rezaie, A., Fahrenholtz, W.G., & Hilmas, G.E. (2007). Evolution of structure during the oxidation of zirconium diboride–silicon carbide in air up to 1500°C. *Journal of the European Ceramic Society*, 27, 2495–2501.
- Rizzo, H.F. (1960). Oxidation of boron at temperature between 400 and 1300 °C in air J.A. Kohn, W.F. Nye, G.K. Gaule (Eds.), *Boron: Synthesis, Structure and Properties* (I Ed.)(175-189). Plenum Press Inc, New York
- Roskill. (1999). *The Economics of Boron: Roskill Information Services Ltd.*, London: England.

- Sánchez, J. M., Azcona, I., & Castro, F. (2000). Mechanical properties of titanium diboride based cermets, *Journal of Materials Science*, 35, 9– 14.
- Sekizinci Beş Yıllık Kalkınma Planı. (2001). *Madencilik Özel İhtisas Komisyonu Raporu, Endüstriyel Hammaddeler Alt Komisyonu, Kimya Sanayi Hammaddeleri, Cilt 2, (Bor Tuzları-Trona Kaya Tuzu-Sodyum Sülfat-Stronsiyum)*, Ankara.
- Sen, S., Sen, U., & Bindal, C. (2006). Tribological properties of oxidised boride coatings grown on AISI 4140 steel. *Materials Letters*, 60, 3481–3486.
- Steinbrück, M. (2005). Oxidation of boron carbide at high temperatures. *Journal of Nuclear Materials*, 336, 185–193.
- Steinbrück, M., Veshchunov, M.S., Boldyrev, A.V., & Shestak, V.E. (2007). Oxidation of B₄C by steam at high temperatures: New experiments and modelling. *Nuclear Engineering and Design*, 237, 161–181.
- Subramanian, C., Murthy, T.S.R.Ch., & Suri, A.K. (2006). *Synthesis and Consolidation of Titanium Diboride*, Bhabha Atomic Research Centre, Mumbai, India.
- Talmy, I.G., Zaykoski, J.A., & Opeka, M.M. (2008). High-Temperature Chemistry and Oxidation of ZrB₂ Ceramics Containing SiC, Si₃N₄, Ta₅Si₃, and TaSi₂. *Journal of American Ceramic Society*, 91(7), 2250–2257.
- Thevenot, F. (1990). Boron Carbide – A Comprehensive Review. *Journal of European Ceramic Society*, 6, 205- 225.
- Töre İ., & Ay N. (2002). Borlu Seramiklerin Karakterizasyonu, 1. Uluslar arası Bor Sempozyumu Bildiriler Kitabı, 26-33.

- Turkdoğan, E.T. (1980). *Physical Chemistry of High Temperature Technology*, Academic Press, 1-26.
- Venkateswaran, T., Basu, B., Raju, G.B., & Kim, D.Y. (2006). Densification and properties of transition metal borides-based cermets via spark plasma sintering. *Journal of the European Ceramic Society*, 26, 2431–2440.
- Wang, W., Fu, Z., Wang, H., & Yuan, R. (2002). Influence of Hot Pressing Sintering Temperature and Time on Microstructure and Mechanical Properties of TiB₂ Ceramics. *Journal of European Ceramic Society*, 22, 1045–9.
- Weast, R.W. (Ed.). (1982). *CRC Handbook of Chemistry and Physics* (62th. Ed.). CRC Press.
- Yoon, J.H., Jee, Y.K., & Lee S.Y. (1999). Plasma paste boronizing treatment of the stainless steel AISI 304. *Surface and Coatings Technology*, 112, 71–75.